BRNO UNIVERSITY OF TECHNOLOGY
VYSOKÉ UČENÍ TECHNICKÉ V BRNĚ

FACULTY OF CHEMISTRY
FAKULTA CHEMICKÁ

INSTITUTE OF MATERIALS SCIENCE
ÚSTAV CHEMIE MATERIÁLŮ

STUDY OF ELECTRIC AND DIELECTRIC PROPERTIES OF IONIC LIQUIDS

STUDY OF ELECTRIC AND DIELECTRIC PROPERTIES OF IONIC LIQUIDS

DOCTORAL THESIS
DIZERTAČNÍ PRÁCE

AUTHOR — Ing. Jakub Altšmíd
AUTOR PRÁCE

SUPERVISOR — prof. RNDr. Stanislav Nešpůrek, DrSc.
ŠKOLITEL

BRNO 2019

BRNO FACULTY UNIVERSITY OF CHEMISTRY OF TECHNOLOGY

Specification Doctoral Thesis

Department:	Institute of Materials Science	Academic year:	2018/19
Student:	**Ing. Jakub Altšmíd**		
Study programme:	Chemistry, Technology and Properties of Materials		
Study field:	Chemistry, Technology and Properties of Materials		
Head of thesis:	**prof. RNDr. Stanislav Nešpůrek, DrSc.**		

Title of Doctoral Thesis:

Study of Electric and Dielectric Properties of Ionic Liquids

Doctoral Thesis:

1) Characterisation of basic properties of chosen ionic liquids, study of their electric and dielectric properties
2) Preparation of an experimental NO2 sensor
3) Study of prepared sensor's properties
4) Evaluation of measured electric and dielectric properties

Deadline for Doctoral Thesis delivery: 22.8.2019:

Ing. Jakub Altšmíd Student	prof. RNDr. Stanislav Nešpůrek, DrSc. Head of thesis	doc. Ing. František Šoukal, Ph.D. Head of department

In Brno dated 16.9.2018

prof. Ing. Martin Weiter, Ph.D.
Dean

ABSTRACT

Presented thesis is focused on study of electric and dielectric properties of ionic liquids (ILs). ILs may find its use in wide spectre of applications, namely in electrotechnics. Thesis is divided into theoretical and experimental part. The theoretical part is dedicated to description of basic properties of ILs and possibility of use in capacitors and electrochemical gas sensors. The experimental part describes used methods of characterisation of physical properties and evaluation of measured data. The results are divided into two main parts. The first part deals with the study of properties of ILs for their use as capacitors. The second part is dedicated to the study of prepared experimental NO_2 sensor, namely to influence of ILs properties to commonly studied properties.

ABSTRAKT

Dizertační práce je zaměřena na studium elektrických a dielektrických vlastností iontových kapalin. Iontové kapaliny mohou nacházet uplatnění v široké škále aplikací, především pak v elektrotechnice. Teoretická část se věnuje popisu základních vlastností iontových kapalin a možností jejich uplatnění v kondenzátorech a elektrochemických senzorech plynů. Experimentální část se věnuje použitým metodám charakterizace vlastností iontových kapalin, jsou zde popsány teoretické poznatky o dielektrické spektroskopii včetně metod stanovení fyzikálních vlastností a vyhodnocení experimentálních dat. Experimentální část je rozdělena na dvě základní části. První se věnuje studiu iontových kapalin pro použití jako elektrolytu v kondenzátorech, druhá část se věnuje studiu vlastností připravených experimentálních senzorů na NO_2, zejména vlivem vlastností iontových kapalin na sledované parametry senzoru.

KEY WORDS

Ionic liquids, impedance spectroscopy, amperometric NO_2 sensor, capacitor, electrolyte

KLÍČOVÁ SLOVA

Iontové kapaliny, impedanční spektroskopie, amperometrický NO_2 senzor, kondenzátor, elektrolyt

ALTŠMÍD, Jakub. *Study of Electric and Dielectric Properties of Ionic Liquids.* Brno, 2019. Dostupné také z: https://www.vutbr.cz/studenti/zav-prace/detail/122391. Dizertační práce. Vysoké učení technické v Brně, Fakulta chemická, Ústav chemie materiálů. Vedoucí práce prof. RNDr. Stanislav Nešpůrek, DrSc.

PROHLÁŠENÍ

Prohlašuji, že jsem dizertační práci vypracoval samostatně a že všechny použité literární zdroje jsem správně a úplně citoval. Dizertační práce je z hlediska obsahu majetkem Fakulty chemické VUT v Brně a může být využita ke komerčním účelům jen se souhlasem vedoucího dizertační práce a děkana FCH VUT.

……

Podpis studenta

Poděkování:
Děkuji vedoucímu dizertační práce prof. RNDr. Stanislavu Nešpůrkovi, DrSc. za odborné rady, trpělivost a vstřícný přístup při sepisování této práce a také za vedení v průběhu doktorského studia. Dále děkuji svým kolegům a spolupracovníkům za sdílení svých zkušeností a bez jejichž účasti by tato práce nemohla vzniknout.

Contents

Contents 5
1 Introduction 7
2 Ionic liquids 9
2.1 Properties of ionic liquids 9
2.1.1 Conductivity 9
2.1.2 Viscosity 9
2.1.3 Influence of temperature on conductivity 10
2.1.4 Dielectric polarization 11
2.1.5 Electrolyte conductance and dissociation 12
2.1.6 Role of dielectric constant and donicity 12
2.2 Electrochemical window of room temperature ionic liquids 13
2.2.1 Evaluation of the reduction and oxidation potential of the room temperature ionic liquids by voltammetry 14
2.2.2 Reference electrode 15
2.2.3 Effect of residual water on voltammetry 15
2.2.4 Effect of the scan rate on the voltammetry 16
3 Double-layer capacitors 17
3.1 Breakdown theory 18
4 Sensors, basic parameters and principles of detection 23
4.1 Infrared sensors 25
4.2 Sorption sensors 26
4.3 Thermocatalytic sensors 27
4.4 Electrochemical sensors 28
4.4.1 Potentiometric sensors 29
4.4.2 Amperometric sensors 29
4.4.3 Electrochemical sensors with solid and liquid electrolytes 30
4.4.4 Electrodes and their topology 31
5 Description of basic mechanisms in amperometric gas sensors 33
6 Experimental part 36
6.1 Properties of ionic liquids 36
6.1.1 Impedance spectroscopy 37
6.1.2 UV-VIS, IR measurements 38
6.1.3 TGA measurements 43
6.2 Ionic liquids for use in capacitors 44

6.2.1 Impedance measurements 44
6.2.2 Temperature dependence of C-V properties 46
6.2.3 Dependence of BDV on conductance of the electrolyte 50
6.3 Ionic liquid-based amperometric NO_2 sensor 55
6.3.1 Influence of the polymer electrolyte conductivity on sensor sensitivity 55
6.3.2 Influence of the polymer electrolyte morphology on sensor sensitivity 58
7 Conclusions 69
8 Used symbols 71
9 List of tables 73
10 List of figures 74
11 References 76
12 List of publications and other activities 83

1 Introduction

Ionic Liquids (ILs), often also called „liquid salts“, are such substances with melting point usually lower than room temperature. As their predecessors „low-melting“ mixtures of inorganic salts (e.g. NaCl/$AlCl_3$ with melting point 107 °C) were used. ILs usually consist of organic kation and organic or inorganic anion. In order to have ionic character and low melting point, it is necessary that the compound consists of large anion and/or kation. Such ions shouldn't be coordinated and they should have delocalized charge. These requirements are fullfiled by compounds with quaternary atom of nitrogen (e.g ammonium, imidazolium, pyridinium and pyrrolidine salts), phosphorus (phosphonium salts), or sulfur (sulfonium salts) [1-3]. As an anions tetraflouroborate [BF_4], hexafluorophosphate [PF_6], trifluoromethane-sulfonate [OTf], tetrachloroaluminate [$AlCl_4$] or tris(perfluoroalkyl)trifluorophosphate [FAP] are usually used (see Fig. 1).

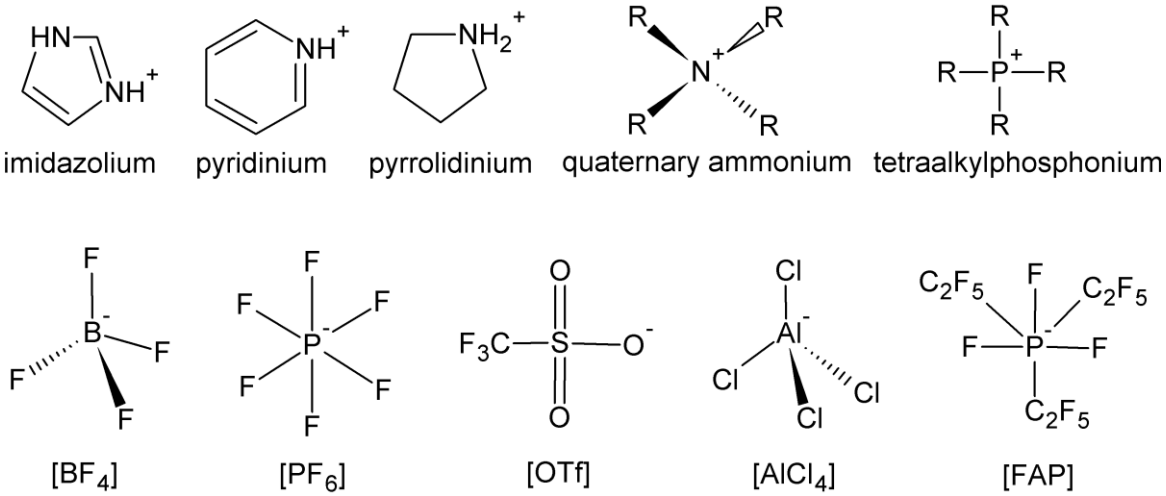

Fig. 1 Cations and anions used in ionic liquids

Ionic liquids (ILs) are substances, which have received great interest lately because of their different properties from those of ordinary molecular liquids. The properties of ionic liquids which are liquid at room temperature (so-called Room temperature ionic liquids –RTILs), their synthesis, purification and charge carrier transport were published in many papers, e.g., in refs. [4-8]. The basic characteristic of ILs are:

- Low melting point.
- Non-volatility.
- High thermal stability.
- Good electrochemical stability.
- Non-flamability.
- Low toxicity.
- Ionic composition - high ion density and high ion conductivity.
- Mostly organic substances, they are designable, they have almost unlimited range of combinations

From above mentioned properties non-volatility and high ion conductivity are most important. These properties are considered to be crucial when developing advanced electrolyte solutions for outdoor-used energy devices. These days the safety is as important issue as the performance and is taken into account when developing materials for practical use. Devices with non-volatile electrolyte solution are expected to change the performance of electronic

and ionic devices. Such devices would become safer and will have considerably longer life time [4]. All these properties allow the use of ILs in wide application spectre like as in electrochemical capacitors (replacement of volatile electrolytes and electrolytes with low thermal stability) [9], batteries and fuel cells (development of new electrolytes) [9], sensing technique (research in field of development of new sensing layers) [10] etc.

For use in electrochemistry water-based solutions are mostly used today. But due to water volatility, devices using these electrolytes have several limitations in use – main and most crucial limitation is quite narrow temperature range in which it is possible and safe to use them. In order to overcome this limitation water as a solvent was replaced by polar organic solvents and polymer conductors. But all used solvents had more or less same drawbacks as water. In case of non-volatile organic conductors the main drawback was also their low thermal stability [3,11,12]. Ionic liquids can be used without any limitations at temperatures around 300 - 400 °C [13].

2 Ionic liquids

2.1 Properties of ionic liquids

2.1.1 Conductivity

According to [3] specific conductivities σ of a number of representative ionic liquids at ambient temperature are within a broad range of 0.1 – 18 mS/cm. Generally, conductivity of the order of 10 mS/cm is typical of ionic liquids based on $[EMIM]^+$. On the other hand, ionic liquids based on tetraalkylammonium, pyrrolidinium, piperidinium and pyridinium cations are characterised by considerably lower conductivities, in the range between 0.1 and 5 mS/cm. However, in comparison with conventional aqueous solutions applied in electrochemistry, specific conductivity of ionic liquids is much lower. For example, the specific conductivity of aqueous KOH (29.4 wt.%) solution is 540 mS/cm and 30 wt.% aqueous H_2SO_4, shows a conductivity at the level of ca. 730 mS/cm [14].

A dilution of neat ionic liquids with molecular liquid solvents (often with high dielectric constant) can increase the conductivity. For example, the specific conductivity of neat $[EMIM][BF_4]$ is 14 mS/cm, while its 2 mol/dm^3 solution in acetonitrile shows the conductivity of 47 mS/cm and one of the most conductive $[EMIM][BF_4]$ solutions, in acetonitrile, for application in double-layer capacitors, is characterised by σ = 60 mS/cm [15]. This effect goes along with fact, that mixture of ionic liquid and molecular liquid is a solution of a salt in a solvent and its ions are separated by solvent's neutral molecules. However at high salt concentrations these solutions may show properties rather characteristic for ionic liquids than for typical solvent solutions. In this case the specific conductivity of the system increases with increasing amount of salt, reaches its maximum and then starts to decrease.

In Fig. 2 is schematic representation of cell for ionic conductivity measurement by impedance spectroscopy.

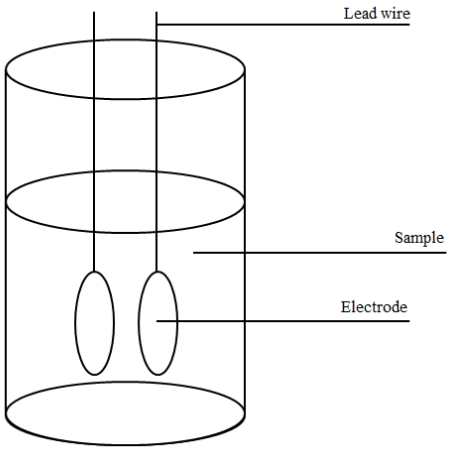

Fig. 2 Scheme of cell for measurement of conductivity by impedance spectroscopy

2.1.2 Viscosity

Viscosity of ILs is mainly caused by van der Waals forces. In comparison to „classical" molecular solvents is viscosity of ILs twice or three times higher and their values lie in range of 30 – 450 mPa·s (at 25 °C) [16], which can be disadvantageous for some applications. Viscosity of ionic liquids with same anion icreases with the lenght of the alkyl chain.

Viscosity of ILs is highly dependent on the temperature. Okoturo and VanderNoot studied in their work [17] 23 different ionic liquids in temperature range of 10 – 70 °C. Authors are describing, that only some aprotic ionic liquids behave according to Arrhenius equation (1). Behavior of group of the chloroaluminate based ionic liquids, containing small symmetrical cation with lower molar weight, corresponds better to Vogel-Tammann-Fulcher equation (2). Last group which didn't correspond with its behaviour to either of these equations was characterised by having small cation with bigger molar weight. However all studied liquids showed trend of decreasing of viscosity with increasing temperature.

$$\eta = \eta_0 \cdot \exp\left(-\frac{E_a}{RT}\right), \tag{1}$$

$$\eta = \eta_0 \cdot \exp\left(-\frac{E_a}{R(T-T_g)}\right), \tag{2}$$

where T is the temperature R is the ideal gas constant, η is the viscosity, E_a is activation energy and Tg is the glass transition temperature.

The influence of the viscosity η on the ionic liquid conductivity (expressed as the molar conductivity Λ) may be illustrated by a $\Lambda\eta$ value. Inspection of the $\Lambda\eta$ values, collected in [3] shows, that they are typically contained within a relatively narrow range of $50 \pm 20 \cdot 10^{-7}$ Ns/Ωmol, while the specific conductivities are within a broad range of 0.1 to 14 mS/cm. This indicates that the viscosity plays an important role in the conductivity of ionic liquids.

In a description of classical electrolyte solutions, the mobile charge carrier is related to its diffusion coefficient D through the Nernst–Einstein equation:

$$\Lambda = \frac{z^2 e_0 F D}{k_B T} = \frac{z^2 N_A e_0^2 D}{k_B T}, \tag{3}$$

where z represents the valence of the charge carrier, e_0 is the elementary charge, N_A the Avogadro number, k_B the Boltzmann constant and F the Faraday constant. In addition, the diffusion coefficient D of a model spherical species of an effective radius r_e depends on the medium viscosity, η, according to the Stokes–Einstein equation:

$$D = \frac{k_B T}{6\pi r_e \eta}. \tag{4}$$

By combination of the equations (3) and (4) and taking into account that $\sigma = \Lambda c = \Lambda n/V$ and $N = nN_A$ is number of charge carriers present in the volume V we get following equation:

$$\sigma = \frac{z^2 e_0^2}{6V\pi r} \frac{N}{\eta}. \tag{5}$$

It is clear that conductivity of classical electrolytes is proportional to the number of the charge carriers N and inversely proportional to the medium viscosity η. The model of ionic liquids consisted entirely from the ions causes a conceptual problem. It is difficult to determine number of charge carriers, because of ion-ion interactions (between ions with opposite sign), that can lead to formation of relatively stable aggregates. These aggregates may be regarded as a neutral species which can't be the charge carriers.

2.1.3 Influence of temperature on conductivity

In classical salt solutions ions are separated by molecules of solvent. The thermodynamic properties of such solutions are described by ion–solvent, ion–ion and solvent–solvent interactions. In case of neat ionic liquids, ions aren't separated, and hence, they are still in

contact. Their thermodynamic properties are usually described by ion-ion interactions, London interactions and in the case of some ILs by hydrogen bonding. According to [3] most efficient way to describe ILs conductivity is by using “free space model” also called “hole model”. The model is based on the observation of a large fusion volume, of ca. 20–30 vol%, exhibited by salts on their melting point. The model assumes that within the molten salt there are empty spaces, constantly fluctuating in size, due to thermal motions. To quantify a model, a probability of finding the hole in IL is calculated, which leads to the following expressions for the diffusion coefficient and conductivity [3]:

$$D = A \cdot \exp\left(-\frac{\mathrm{B}}{(T\text{-}T_0)}\right), \tag{6}$$

$$\sigma = \sigma_0 \cdot \exp\left(-\frac{\mathrm{B}}{(T\text{-}T_0)}\right). \tag{7}$$

Equations (6) and (7) are similar to the Vogel-Tammann-Fulcher equation (2) originally describing the temperature dependence of viscosity [18]. The reference temperature T_0 is related to a glass transition temperature (Tg): $T_0 = T\mathrm{g}$ –const. as the charge is transported in the amorphous phase of the system. The Tg value indicates the temperature at which a solid-like material changes to a liquid-like system. In different approach the reference temperature T_0 may be ascribed to the ideal vitreous transition temperature, at which segments of the system start to move. This temperature is always higher than the vitreous transition temperature according to empirical approximation $T_0/T\mathrm{g} \approx 0.75$. Temperature of the glass transition Tg can by determined by DSC measurements and T_0 is adjusted arbitrarily by subtracting ca. 50 K from the experimental Tg values close to 200 K. Generally, in the case of ionic liquids, the Tg value is usually not evaluated experimentally together with the conductivity, but it is estimated from a curve-fitting procedure, which usually leads to a reasonable fit of the experimental data. However, different procedures and/or data taken in a different temperature range may give different output parameters (T_0, B, σ_0 or A). The liquid-to-glass transition is still not theoretically well described and in addition, there is a number of glass transition temperature practical definitions [19,20]. Another problem is a possibility of ILs existence as a different type of a glass former: ‘fragile’ or ‘strong’ liquid [21], with possibility of a fragile-to-strong transition. Both types of liquids shows qualitatively different temperature dependency of the viscosity: strong liquids behave according to the Arrhenius law, while the fragile liquids show a non-Arrhenius change of viscosity. Moreover, it was found experimentally that the fragility is related to the potential of interactions between the system elementary units (van der Waals, hydrogen-bonding) [3].

2.1.4 Dielectric polarization

The fraction of salt moles, which are available as free charge carriers of electric current, is determined by dissociation quocient β. There is usually a dynamic equilibrium between free carriers and undissociated salt, the species depending on salt concentration, temperature, and the dielectric constant of the solvent molecules. Two other factors must be mentioned: the temperature dependent viscosity of the solvent and long-range electrostatic interactions between the free, dissociated ions, which are determined by the dielectric constant, ε of the solvent. For vacuum εo = 1, for non-polar liquids ε is between 1 and 3 and is approximately equal to the square of the refractive index, arising from electronic and atomic polarization. For polar non-H-bonded liquids the values are around 6 to 40, while for H-bonded liquids, it

can attain much higher values, e.g., 78 for water or 113 for HCN at room temperature. Dielectric constant ε depends strongly on the polarization of medium. We can write:

$$\frac{\varepsilon\text{-}1}{\varepsilon\text{-}2}\frac{M}{\rho} = P_{\mathrm{M}} = \frac{4}{3}\,T\,\mathrm{N_A}\left(\alpha + \frac{\mu^2}{3\mathrm{k_B}T}\right), \tag{8}$$

where M/ρ is the molar volume (ρ is the density), P_{M} is the molar polarization, N_A is the Avogadro number, α is the polarizability (including atom, ionic and distortional term), μ is the dipole moment, k_B is the Boltzmann constant and T is the temperature.

In the case of dielectric liquids composed of strongly interacting dipoles (e.g., CH_3NO_2, H_2O, CH_3OH, amides, and amino acids in zwitterion form), high dielectric constants are manifested. Water and HCN are hydrogen-bonded or so called "associated" liquids where the orientation of a given molecular dipole drags neighbouring dipoles in the same direction, especially with hydrogen-bonded solvents. Such solvents also have relatively high viscosities and long dielectric relaxation times, in the order of 10^{-11} s, in comparison with $10^{-12} - 5 \cdot 10^{-13}$ s for weakly interacting solvent molecules. Similar effects occur with other strongly dipolar not hydrogen-bonded solvents, but the resulting ε values are rather lower, e.g., 36 for CH_3NH_2, and 38 for CH_3CN and *N*,*N*-dimethylformamide. The case of water as a dielectric has, of course, special significance for many electrochemical systems, including the double layer formation and metal/water electrode interfaces [22-28].

2.1.5 Electrolyte conductance and dissociation

For maximum power performance, the electrical internal resistance must be minimized by maximizing the conductance of the electrolyte, which provides the basis for double-layer capacitance. This is achieved by using an electrochemically compatible electrolyte salt, or an acid or alkali that is strongly soluble in the solvent to be used and in the dissolved state has minimum ion pairing and maximum free mobility of its dissociated ions. For many salts and acids in water, dissociation degree $\beta \rightarrow 1$ (strong electrolytes) is important (in a negative way) that for non-aqueous, high operating voltage (3.5 - 4.0 V) supercapacitors, the extents of dissociation of many salts are substantially less than 1 owing to ion association (weak electrolytes). For the solutions employed as electrolytes for non-aqueous solvent double-layer capacitors, there is significant weak electrolyte behaviour so that β is much lower than is 1. This usually leads to larger electric series resistance (ESR) values for non-aqueous solution devices than for aqueous ones using the same electrode materials and cell geometries.

The ions are effective in conductance when the positive and negative ions are not in the intimate contacts. The ion pairing depends on the dielectric constant and donicity of the solvent. The ion pairing limits the concentration of movable ions. Beside the ion concentration the charge carrier mobility play an important role in electrical conductivity.

2.1.6 Role of dielectric constant and donicity

The dielectric constant of a solvent determines the interaction energy, U_{IE}, tending to diminish interionic free motion. When the (negative) energy U is higher than k_BT, the extent of ion pairing is substantial ($\beta << 1$). Similarly, β usually increases with rising temperature, leading to improved conductance. This is a common problem with supercapacitors, i.e., their internal

resistance increases at lower temperatures and their power delivery capability becomes substantially diminished.

In some cases, when solvated ions are paired, their solvation shells become shared (a case of solvent-shared ion pairs). In poorly solvating solvents, the plus and minus ions come into a contact situation (contact ion pairs). Then, the maximum plus/minus interaction arises electrostatically but is counterbalanced by a substantial loss of solvation energy. This close-encounter situation leads to the diminution of the conductance of an electrolyte [29,30].A summary of factors determining electrolyte conductance is given in Table 4 [31].

Table 1 Summary of factors determining the conductivity of electrolyte solution.

1. Solubility of the salt or acid.
2. Degree of dissociation or extent of cation and anion pairing in solution.
3. Dielectric constant of the bulk solvent.
4. Electron pair donicity of the solvent molecules.
5. Mobility of the free, dissociated ions.
6. Viscosity of the solvent.
7. Solvation of the free ions and the radii of the solvated ions.
8. Temperature coefficient of viscosity and of ion-pairing equilibrium.
9. Dielectric relaxation time of the solvent.

Here, the choice for supercapacitor electrolytes, for obvious reasons, is sulfuric acid or KOH for double-layer capacitors using an aqueous medium. However, the decomposition voltage limit is then theoretically 1.2 V or practically, in kinetic terms, 1.3-1.4 V. However, strong solutions of acid are much more corrosive than strong solutions of KOH or NaOH, so the latter may be preferred for some embodiments. These hydroxide electrolytes are very soluble in water and, because of the OH^- anion, have very good conductivities. Corrosion of the hardware components is an important factor to consider in design and reliability, and with regard to the self-discharge characteristics of the capacitor device [31]. For comparison, the conductivity of 3.9 M H_2SO_4 is 575 mS/cm, whereas other electrolytes do not exceed 20 mS/cm. The best value of the conductivity - 849 mS/cm - was found for the system 5.68 M HCl solution in H_2O [31].

2.2 Electrochemical window of room temperature ionic liquids

When we consider ionic liquids as an electrolyte for electrochemical devices, it is important to know their stability toward used electrodes. For this purpose, electrochemical potential ranges, where no reactions occur, are measured and estimated using two basic methods – cyclic voltammetry and linear sweep voltammetry. This potential range (and/or potential difference) is commonly called electrochemical window (denoted EW) and is calculated by subtracting the reduction potential from oxidation potential.

Main advantage of these methods is that they are easy to use. However there may be some complications encountered when comparing measured voltammograms with other reported data even of the same ionic liquid. The variability of measurement conditions is considered to be the main reason, including differences between used electrodes, differences in potential scan rates and differences in cut-off current densities. Another important parameter that

determines quality of measured data is quality (in sense of purity) of ionic liquid. Electrochemical measurements are generally very sensitive to impurities. For example water content can't be neglected even at 100 ppm, but despite all these difficulties the comparison of EW data can be important for better preparation of stable room temperature ionic liquids.

2.2.1 Evaluation of the reduction and oxidation potential of the room temperature ionic liquids by voltammetry

To estimate EW of ionic liquid one has to obtain reduction and oxidation potential toward certain electrode. The general issue is that oxidation and reduction reactions in case of ionic liquids are mostly irreversible [4], so oxidation and reduction potentials are harder to find unlike in case of reversible systems. Fig. 3 shows typically observed linear sweep voltammogram for ionic liquids.

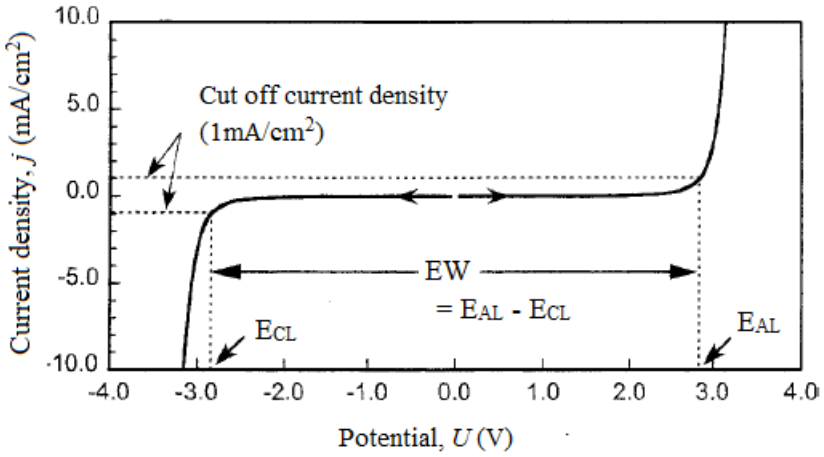

Fig. 3 Linear sweep voltammogram as typically observed. Note that two separate voltammograms are indicated here. Taken from [4]

Both reduction and oxidation current densities increase with potential sweep. Since no peak is observed even at high current density, one has to select certain value of current density to evaluate EW. Such value is called cut-off current. In this case cathodic and anodic limiting potentials E_{CL} and E_{AL} respectively were evaluated as a point when current density reached 1.0 mA/cm^2. However in many studies this value is variable between 0.1 and 1.0 mA/cm^2 and that is the reason why EW literature data of one ionic liquid may differ. In studies for capacitor application cut-off current is even selected to be below 0.1mA/cm^2 [32-34].

Ionic liquids differ from conventional electrolytes also by their viscosity. Even relatively low viscous room temperature ionic liquids possess 20 to nearly 200 mPas at 25°C, which is two or three orders of magnitude greater than that of conventional solvents. The conductivity of RTILs is not so much low (0.1 ~ 20 mS/cm at 25°C) due to its high concentration (3 ~ 6 mol/dm^3), however, it seems to be necessary to considerer the compensation of the "IR-drop" or "ohmic drop" especially in cases of highly viscous ionic liquids. However, it showed up, that this problem can be circumvented by selecting an appropriate size of working electrode to reduce the specific current [1].

2.2.2 Reference electrode

Fig. 4 shows the EW data for EMIM–BF4 obtained from voltammograms of different reference electrodes [35-37]. Note that although the range of the EW is almost the same (4.4 V), but the cathodic and anodic limiting potentials are different, even in the same RTIL. One way around this problem is to use one redox compound as the internal reference. For an organic solvent system, the IUPAC recommends the use of a redox potential of ferrocene (dicyclopentadienyliron(II)) as the reference potential regardless of the kind of solvent molecule [38].

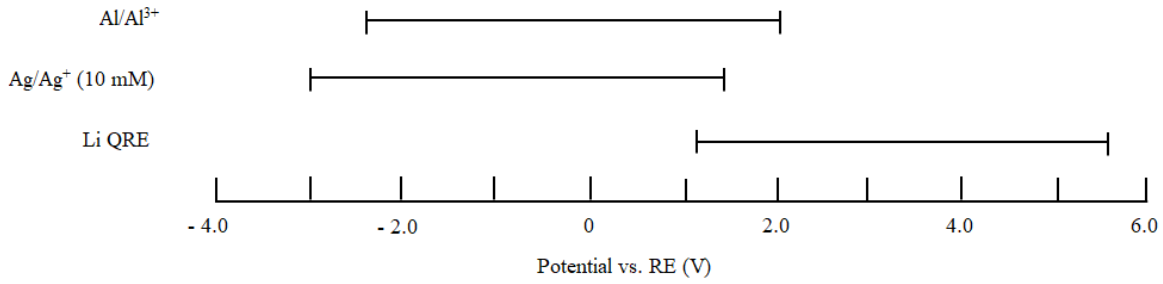

Fig. 4 Electrochemical windows of [Emim][BF_4] estimated with various reference electrodes. Taken from [4]

2.2.3 Effect of residual water on voltammetry

The major impurities contained in RTILs are water and oxygen, even in highly pure samples. This is because these molecules easily dissolve into the RTILs from air. Since these molecules are electrochemically active, the removal of these molecules is essential before any voltammetric measurement.

Effect of these impurities is influenced by three basic factors: concentration, composition of ionic liquids and by material of reference electrode. Fig. 5 shows comparison of linear sweep voltammograms of TMPA–TFSI (trimethylpropylammonium-bis(trifluoromethyl)-imide) containing various amounts of water using Pt and GC (glassy carbon) working electrodes.

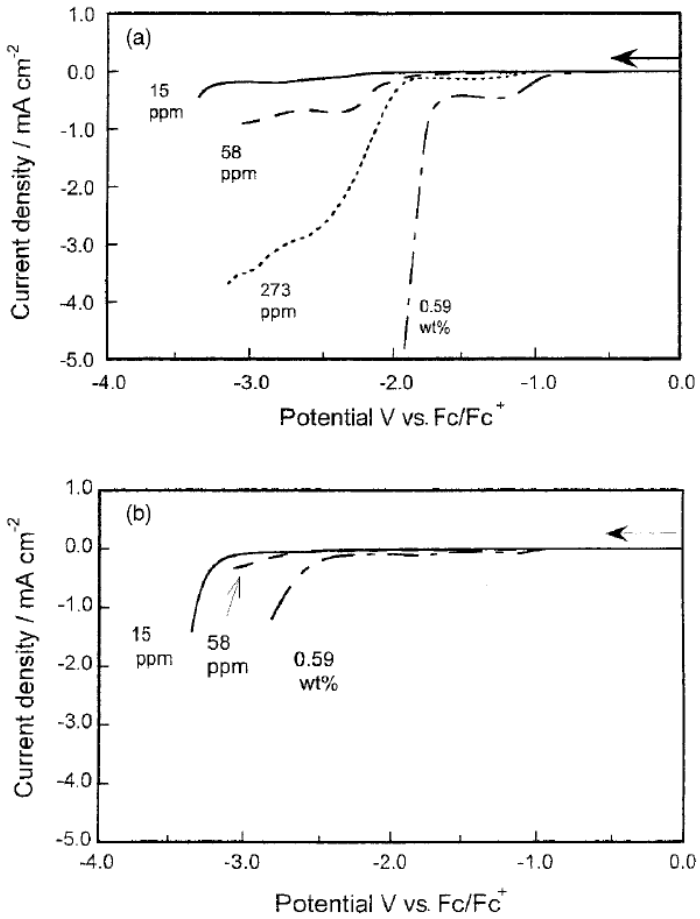

Fig. 5 Linear sweep voltammogram of TMPA-TFSI with different amount of water. Working electrodes: (a) Pt and (b) GC. Scan rate is 50mV/s. Taken from [4].

From this picture it is clear, that purification (dehydration) process before measurements is crucial. Fortunately, thanks to non-volatile nature of ionic liquids, the water can be easily removed by vacuum drying. For example after vacuum drying (10^{-4} Torr) at 100°C, the water content in hydrophobic ionic liquid such as EMI-TFSI will be less than 20 ppm, time needed for achieving this value is dependent on the sample volume (e.g., 1 ml ~ 30 min) [1].

2.2.4 Effect of the scan rate on the voltammetry

The scan rate is an important parameter for potential sweep methods such as cyclic voltammetry (CV) or linear sweep voltammetry (LSV). The current is proportional to the square root of the scan rate in all electrochemical systems—irreversible, reversible, and quasi-reversible systems. This indicates that the limiting potential estimated at the same current density can be shifted in the negative or positive direction by changing the scan rate. Therefore, in the case of mutual comparison among various reported voltammgrams of RTILs taken at different scan rates, the cut-off current density in each case should be changed with the relationship between square root of scan rate and a current density.

3 Double-layer capacitors

From the viewpoint of energy and power densities, double-layer capacitors show intermediate performances between conventional capacitors and rechargeable batteries.

Ionic liquids are being considered for use as liquid electrolytes for electrochemical energy storage devices because they can increase device safety by their non-volatile and non-flammable properties. The double-layer capacitor (DLC) has shown the most promise as an electrochemical energy storage device for hybrid electric vehicles and hybrid fuel cell vehicles. The double-layer capacitor is one of the "electrochemical capacitors" showing intermediate performances between conventional capacitors and rechargeable batteries from the viewpoint of energy and power densities This is because it has higher pulse power capability than conventional rechargeable batteries [4].

Electrical double-layer at the electrolyte/electrode interface is formed when an electrode (electric conductor) is contacted with an electrolyte (ionic conductor). Electrode shows some potential and attracts ions with the opposite sign. Increasing electrode potential causes further adsorption of ions (charging current) and eventually an electrode reaction (electrochemical current) occurs. The "polarizable electrode" is the one where charge transfer does not occur when the electrode potential is varied. Example of typical polarizable electrode is one made of Hg, which shows a double-layer capacitance of 10 – 20 μF/cm^2 is aqueous solutions.

Double-layer capacitance is dependent on electrode potential V_e so minimum values of differential double-layer capacitance C_d can be defined as:

$$C_\mathrm{d} = \frac{\mathrm{d}Q}{\mathrm{d}V_\mathrm{e}}, \tag{9}$$

where Q is the charge.

Capacitance C of a plane capacitor made of two parallel plates of with equal area S separated by distance d is given by equation (10), where ε_0 and ε are permittivity of vacuum and relative permittivity of the dielectric material:

$$C = \frac{\varepsilon\varepsilon_0 S}{d}. \tag{10}$$

If we consider a Helmholtz model, where the double-layer concept corresponds to the model consisting of two layers separated by very small distance (e.g., 0.3 nm), calculated value of ε is about 3~7. If we want to make a capacitor with high capacitance, we can use porous materials with high surface area as electrodes. For example, if we use activated carbon with surface area of 1000 m^2/g we can achieve capacitance of 100 F/g. It is important to note, that the capacitance measured in a unit cell is four times lower than capacitance per unit weight or volume measured on the single electrode, because cell consists of two single electrodes (half capacitance and double weight) [4]. In this case capacitance of the unit cell would be around 25 F/g.

The energy W and power P of the electrochemical can be written, when it is discharged at constant current I, as

$$W = \tfrac{1}{2} C\left(V_\mathrm{i}^2 - V_\mathrm{f}^2\right) = \tfrac{1}{2} C\left[\left(V_0 - IR_\mathrm{e}\right)^2 - V_\mathrm{f}^2\right] \tag{11}$$

$$P = \tfrac{1}{2} I\left(V_\mathrm{i} + V_\mathrm{f}\right) = \tfrac{1}{2} I\left(V_0 + V_\mathrm{f} - IR_\mathrm{e}\right), \tag{12}$$

where V_i is the initial voltage, V_f is the final voltage, V_0 is the open circuit voltage, C is the capacitance and R_e is the internal resistance. If we want to make capacitor with high power and energy, both capacitance and open circuit voltage must be large, while the internal resistance must be small.

Desired performance properties of electrolytes are:

1. *High double-layer capacitance* – it depends on choosing both electrode and electrolyte materials. Material showing high double layer capacitance for given electrode is needed.
2. *High decomposition voltage* – material with wide stable potential region is needed.
3. *High electrolytic conductivity* – internal resistance of capacitor leads to energy loss during charge-discharge process. That is also the reason, why electrolyte material should have high electrolytic conductivity.
4. *Wide operational temperature range* – electrolyte material for capacitor suitable for practical use must satisfy requirements 1 – 3 in wide range of temperatures (at least from -25 to 70 °C).
5. *Safety* - materials with operational safety and low environmental impact is needed.

3.1 Breakdown theory

The main part of the total current (J) through the barrier of oxide film is ionic one (J_i). It is the function of electric field strength (F_s) in the film. The dependence of the current on electric field can be described by the Young equation [88 - 92]:

$$J_i = M \exp\left(-\frac{N}{k_B T}\right) \exp\left(\frac{\alpha F_s - \beta F_s^2}{k_B T}\right), \tag{13}$$

where k_B is the Boltzmann constant, T is the temperature and M, N, α and β are constants related to anodized metal. This equation is valid under the assumption that the ionic current does not take an immediate part in breakdown effect and the applied voltage, $U = FL$ (L is the film thickness) is lower than the forming voltage (FV) of the oxide layer. The electrolytic contact does not only provide ions penetrating into the film, but also injects electrons into conduction band of the oxide. The Helmholtz layer is formed by localized anions. In addition, small amount of cations and anion sis present near the interface in the electrolyte. The schematic diagram is shown in Fig. 6.

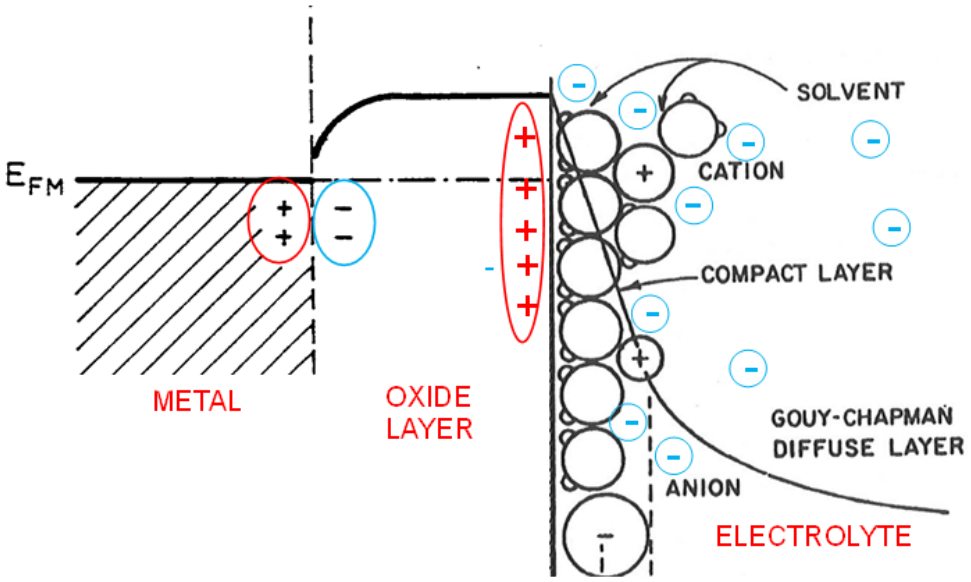

Fig. 6 Energy structure and charge distribution of [metal | oxide | electrolyte] structure without applied voltage.

The energy structure and charge distribution, depicted in Fig. 6 are the following: Energy levels in the metal are occupied up to Fermi level position E_{FM}. At the metal-oxide boundary, in the metal, a depleted positively charged layer occurs. The positive charge is compensated by electron space charge in oxide layer. At the oxide layer - electrolyte interface, from the oxide layer side, there is an accumulated positive charge (electron depletion layer). From the side of an electrolyte the Helmholtz layer, consisted mainly of solvent molecules and anions, is formed. The diffuse Gouy-Chapman layer contains anions and in some amount of cations and electrons (blue circlets).

After the application of electric field, the potential profile in oxide layer changes. The electrons are injected into the oxide layer (blue arrow) and accelerated, see Fig. 7. The energy of the electrons in oxide layer is sufficient to generate other free (secondary) electrons by impact ionization, so that an avalanche multiplication occurs. Generally, the electron energy is the specific constant for the oxide, depends negligibly on electric field (F) and correlates with the energy gap (E_g) of the oxide, being greater than it [93]. The avalanche effect causes that the density of the electron current J_e increases with the distance (x) within the anodic film.

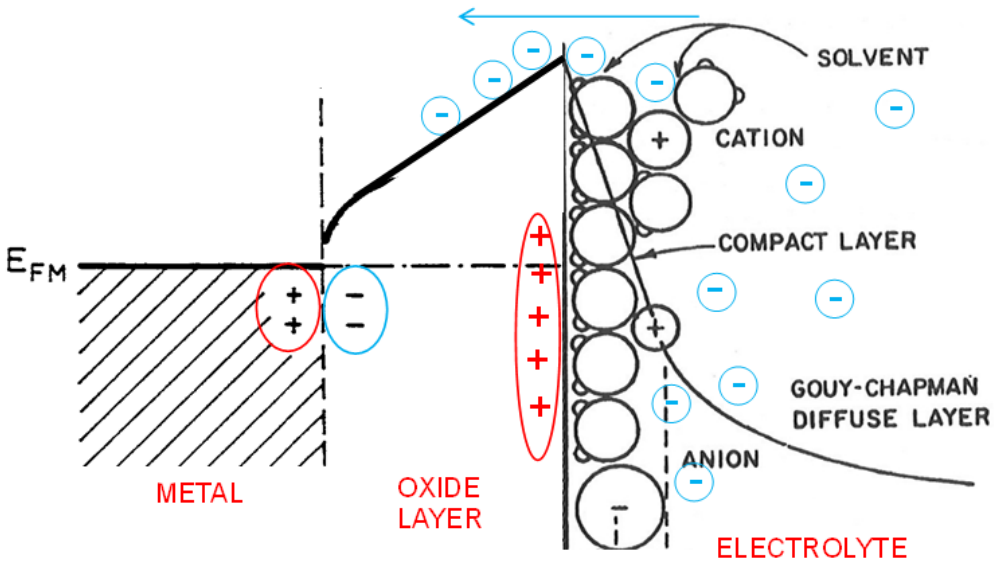

Fig. 7 Energy structure and charge distribution of [metal | oxide | electrolyte] structure under the applied voltage

According to Forlani and Minnaja [94] the dependence of the electron current $J_e(x)$ is given by the equation:

$$J_e(x) = J_e(0)\, P \exp\left[\frac{eF_s}{E}\left(\frac{1}{x} + \frac{1}{r_l}\right)^{-1}\right] \tag{14}$$

where $J_e(0)$ is the primary current density of the charge carriers injected at the electrolyte-oxide interface ($x = 0$), e is the unit charge, r_l is the recombination length, E is the electron energy and P is the probability for an electron to reach the energy which is required for surmounting the phonon scattering. For high electric field strength (higher than 1 MV/cm) and for insulator with predominating ionic bonds the value of $P = 1$. If the film (oxide layer) thickness L is smaller than recombination length, the mean value of recombination length r_l will increase with L. Under these circumstances following relation (15) can, in the first approximation, be used:

$$R_c \approx aL \tag{15}$$

where a is the constant. For the recombination constant we can also write:

$$R_c = \frac{a}{a+1} < 1 \tag{16}$$

For the maximal current density at $x = L$ we can write:

$$J_e(L) = J_e(0) \exp\left(R_c \frac{eF_s}{E} L\right), \tag{17}$$

where in general $J_e(0)$ is the function of the electric field F_s, temperature T, electrolyte composition, nature of anodized metal and electrolyte conductance G. The dependences of the $J_e(0)$ current on the parameters given above are generally unknown. They are described in literature only in the approximation of low electric field. For the field dependence of the injected current $J_e(0)$ can be written:

$$J_e(0) = \gamma \exp\left(\delta F_s^{1/2}\right), \tag{18}$$

where γ and δ are constants. Usually for electron injection it is assumed that the contact is ohmic, i.e., infinity of electrons can be injected. However it is usually not valid in reality and charge injection is contact limited. The same is valid for the electrolyte-oxide interface. It was found that injection current depends on electrolyte conductance as:

$$J_e(0) = \kappa G^{\eta} , \tag{19}$$

where κ is the constant strongly influenced by electrolyte composition, the constant η is nearly independent on it.

According to Eq. (17) J_e increases with the oxide film thickness L and can reach, at the determined thickness $L = \lambda$ (λ is the destruction thickness) a current value J_{BDV} which is sufficient for the oxide destruction (it depends on the type of oxide film). Because the breakdown occurs at the voltage *[BDV]* we can write:

$$[BDV] = F_s \lambda , \tag{20}$$

where λ is the destruction thickness. From Eqs. (17) and (20) we obtain:

$$J_e(0) \exp\left(\frac{R_c e}{E}[BDV]\right) = J_{BDV} , \tag{21}$$

where $J_e(BDV) = J_{BDV}$. After the making necessary adjustments and by combination with Eq. (19) we get:

$$[BDV] = \frac{E}{R_c e}\left[\ln J_{BDV} - \ln\kappa\right] - \frac{2.3E\eta}{R_c e} \log G . \tag{22}$$

Because the first term on the right side of Eq. (20) and the expression $E\eta/Re$ are constants we can write for the breakdown voltage:

$$[BDV] = A - B \log G \tag{23}$$

Symbols A and B, used in eq. (23) are constants. Constant A includes electron energy (E), recombination length (r_l), current density of injected electrons ($J_e(0)$) and thickness of the oxide film (L). Constant B includes electron energy (E), recombination length (r_l) and current density of injected electrons ($J_e(0)$). Other constants used during the mathematical treatment - M, N, α, β are related to the anodized metal.

Concerning the physical quantities we need:

$J_e(0)$ Primary current density of the charges injected at the electrolyte-oxide interface

L Oxide thickness

E_g Energy gap of the oxide

θ Parameter of electrolyte composition

R_c Recombination constant

E Electron energy

λ Destruction thickness

Note, that the expression (23) is always valid for particular metal and its oxide, electrolyte composition, and temperature. To increase the breakdown voltage we must improve the A constant, i.e., electrolyte composition and, especially, the current density of injected electrons. Theoretically, the dependence (23) is valid for any electrolyte concentration (and therefore

conductance). However, practically it breaks down for very high and very low conductivities of the electrolyte. For low concentration the dependence of the *[BDV]* on the logarithm of electrolyte conductance will be superlinear, for high concentration the *[BDV]* will saturate because of the electron injection limit.

4 Sensors, basic parameters and principles of detection

Sensor is a functional element. This element is the first piece of basic measurement chain, which is in direct contact with detected analyte (Fig. 8). In the simplest case analogue output signal is just amplified and transferred into digital form for other processing in CPU. Choice of measuring and signal processing method can suppress some undesirable phenomena of outputting signal, however deciding influence on signal quality have properties and parameters of a sensor [39].

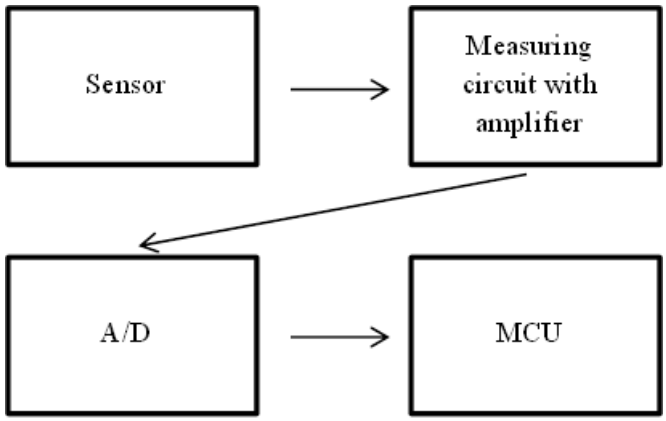

Fig. 8 Scheme of measurement setup

Typical parameters characterizing basic static and dynamic properties of sensors can be summarized as follows:

- Sensitivity and its stability
- Offset and its stability
- Hysteresis
- Linearity error
- Limit of detection
- Limit of quantification
- Dynamic range
- Dynamic parameters
- Accuracy

Sensitivity

Is defined by static conversion characteristic, which is given by dependence $y = f(x)$ of input x and output y in steady state. This dependence can be, in general, described with polynom:

$$y = a_0 + a_1 x + a_2 x^2 + \ldots + a_n x^n \,. \tag{24}$$

In the ideal case static characteristic can be written as:

$$y = y_0 + K \cdot x \tag{25}$$

where K is sensor's sensitivity, usual defined as $K = \mathrm{d}y/\mathrm{d}x$, y_0 is offset.

Offset (shift of the zero value)

Is an error caused by shift of particular linear characteristics. In association with this parameter a temperature offset ***drift*** is often mentioned at gas sensors in ppm/K.

Linearity error

Is difference of the real calibration line from ideal static conversion characteristics. The linearity error is often expressed in percentage of upper detection limit and gives a maximal deviation of any calibration point from corresponding point of the ideal characteristic. For an analogue signal linearity error is given by:

$$\delta_{\mathrm{L}} = \left(\frac{y - y_{\mathrm{L}}}{y_{\max} - y_{\min}} \right)_{\max}, \tag{26}$$

where y_{L} is defined by the ideal linear function (2).

Hysteresis

Is maximal difference between values in measured range measured firstly at increasing and then at decreasing values of analysed quantity. It is usually expressed as percentage of upper and lower limit of the measured range:

$$\delta_{\mathrm{H}} = \left(\frac{y_{\uparrow} - y_{\downarrow}}{y_{\max} - y_{\min}} \right)_{\max} \tag{27}$$

Accuracy

Is usually determined by the absolute error. Attention should be given to the fact, that absolute error is often expressed as percentage from measured range.

Limit of detection (LOD)

According to the general agreement, limit of detection is expressed as the ratio of the treble of the standard deviation value of the base line noise (measured without analyte) to the slope of the calibration line.

Limit of quantification (LOQ)

According to the general agreement, limit of quantification is expressed as the ratio of the ten times the standard deviation value of the base line noise (measured without analyte) to the slope of the calibration line.

Dynamic range

Is bounded by upper and lower limit of measurement range and gives us an interval of possible values of the measured quantity.

Dynamic parameters

Usually describe the change of output signal in dependence on the step change of measured quantity. Usual parameters describing these properties are response time t_{90} and recovery time t_{10} defined as time section between 10% and 90% of the total magnitude of measured signal. [39, 40]

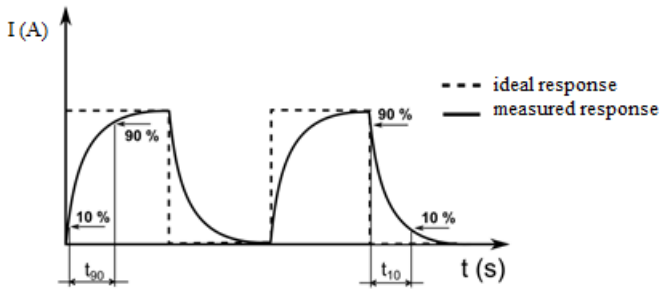

Fig. 9 Dynamic parameters – response and recovery time

Part of the experimental work of this thesis is focused on use of organic materials in detection of gaseous substances. For this reason this chapter will introduce basic methods used for detection of gases and their principles.

4.1 Infrared sensors

Contrary to above described this group of sensors uses completely different approach for gas detection. Main difference is that active (sensing) compound is not in direct contact with analyzed gas. Detected gases are very often highly reactive and/or aggressive, which places higher demands on not only sensing compound, but also on all other materials used for sensor construction. In case of highly reactive toxic gasses, functionality and durability of the sensor highly depends on quality of materials chosen for its construction.

Undisputed advantage of this sensing method is that molecules of analyzed gas interact only with the infrared (IR) radiation. The interaction takes place in an isolated sampling chamber, which can be specially designed to withstand the effects of highly toxic and reactive compounds. This setup also enables us to protect main components of the sensor with elements of proper optical properties, which can be easily cleansed or replaced if needed. These aspects belong to main reasons why are infrared sensors often used in many applications, where highly chemically reactive gasses need to be detected or monitored. Principle setup of an infrared sensor is schematically shown in Fig. 10.

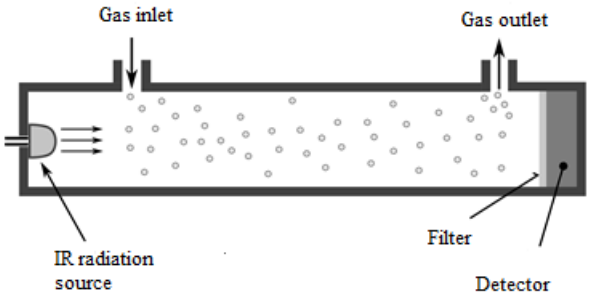

Fig. 10 Basic setup of an infrared sensor [40]

There are basically two ways to determine the concentration of an analyte. First one is based on detection of amount of absorbed radiation caused by interaction with gas molecules. If it is known which part of the IR spectra interacts with detected analyte, its concentration can be obtained simply by determination of amount of absorbed energy. When using a broad-scale source of IR radiation, IR sensor can also be used for identification of all gasses in analysed atmosphere, since each gas has unique absorption properties as can be seen in Fig. 11.

Second way of concentration determination is based on detection of heat produced during absorption of IR radiation. Absorption of the IR radiation causes the absorbing molecules to vibrate more intensively, which leads to increase of their temperature. This increment is proportional to the concentration of analyzed gas. [39]

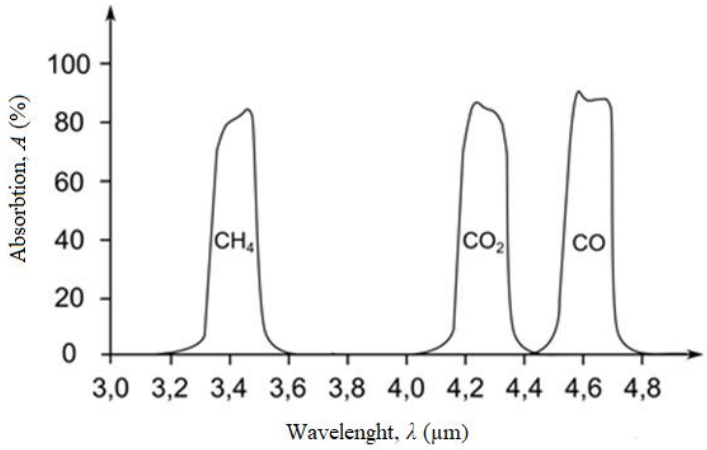

Fig. 11 Absorption spectra of several chosen gasses

4.2 Sorption sensors

To this group we can, in general, assign all sensors with active layer, which changed its properties thanks to adsorption, absorption or chemisorption of measured analyte. Ones of the most widespread representatives of this group are chemical conductive sensors (also called semi-conductive sensors). The reason for their widespread is their broad spectre of possible use in many applications. At this time one can use sorption sensors to detect over 150 different gasses, among which are gases that could be otherwise detected only using very complicated and expensive analytical methods [40]. Sorption sensors have many advantages i.e.: long lifetime, easy maintenance, broad spectre of detectable gasses at wide concentration range and also acceptable price. On the other hand these sensors are more prone to interference between gasses and they can trigger false alarms. This disadvantage can be

solved by using proper gas filters to prevent the contact of interfering gasses with sensing parts of detectors.

Principle of detection of semi-conductive sensors is based on change in conductivity of active layer as a consequence of presence of oxidation or reduction agents in atmosphere. Active layers are usually made from semi-conductive oxides stable in the air atmosphere e.g.: Fe_2O_3, ZnO, In_2O_3, SnO_2. Simplified scheme of semi-conductive sensor can be seen in Fig. 12.

Under laboratory conditions SnO_2 contains oxygen vacancies [41, 42] i.e. deficit of oxygen atoms. These vacancies act as an electron donor, therefore tin oxide is the N-type semiconductor. In the air atmosphere oxygen is chemisorbed at the surface and drain electrons from active layer forming oxygen anions O_2^- or O_2^{2-}.As a consequence of this behaviour electrical resistance of the semiconductor is increased. If a reducing agent is present in the air atmosphere (e.g. CH_4), it can react under specific conditions with chemisorbed oxygen. This results in decrease of electrical resistance of semiconductor. For the correct function the sensor is equipped by heating element, which heats active layer to working temperature (usually in order of hundreds of degrees centigrade). The heating helps to minimize the influence of the effects at the surface of active layer.

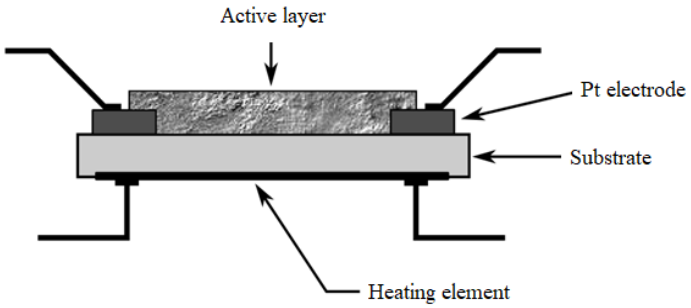

Fig. 12 Section of a semiconductor sensor

As mentioned above, semiconductive sensors operate at elevated temperatures. Due to this fact these sensors have several limitations in their applications. Due to necessity of heating they consume more power for their operation. This fact limits possibility of their use for example in small battery-powered devices. It can be presumed, that sensors with organic active layer could find wide spectre of use. As an example sensors with phtalocyanine [43] or conductive polymeric active (polypyrolle, polyaniline) [44] layers can be mentioned.

4.3 Thermocatalytic sensors

Principle of this group of sensors is based on catalytic combustion of flammable and explosive gasses (methane, propane, butane, carbon monoxide etc.) in the air atmosphere. Ignition of a flammable mixture can occur only under certain circumstances. Necessary condition is achieving the ignition point (temperature from 600°C to 900°C). To combust mixture at temperatures lower than ignition point, catalyst based on metal oxides (e.g. ThO_2) or platinum are used. Lowering the combustion temperature improves the lifetime of the sensor and decreases requirements for mechanical properties of used materials. Scheme of a catalytic sensor (also called pellistor) is shown in Fig. 13. Platinum resistance wire rolled up into coil has two functions. First – serves as a heating unit, heating active element up to required temperature and second – works as temperature sensor. In addition platinum shows

excellent mechanical and chemical properties in whole working temperature range, which improve response stability and enable significant miniaturisation of whole sensor.

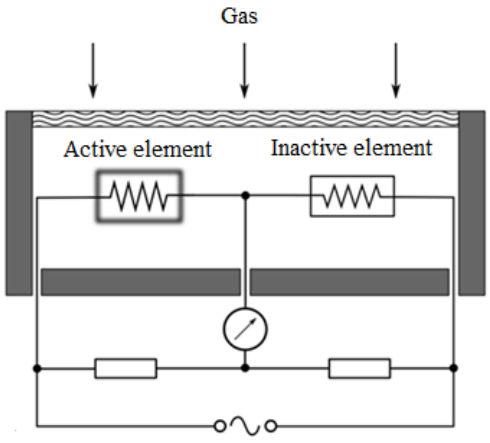

Fig. 13 Thermocatalytic sensor – pellistor [40]

Complete bridge configuration, with a pair of elements is shown in Fig. 13. Detected gas diffuses to the sensitive part of the active element, where, thanks to catalytic combustion, reaction heat is released. This heat causes the change in temperature, which causes change in resistance of platinum wire, which can be measured. Very important is choice of reference (inactive) element. This element should have same geometry and should exhibit same properties as active element, but it shouldn't respond to measured analyte. This can be achieved by surface modification minimalizing catalytic effect of the element, chemical pre-treatment, or by use of reference element at much lower temperatures, at which combustion of hydrocarbons doesn't occur. Output signal is then proportional to the number of oxidized molecules at the surface of the sensor [39 - 41].

4.4 Electrochemical sensors

Electrochemical sensors are based on redox reactions occurring on electrodes immersed in electrolyte solution. This group of sensors has a big potential of using organic materials (e.g. ionic liquids). Electrochemical sensors can be classified based on working regime, electrolyte composition or topology of electrodes as can be seen at Fig. 14.

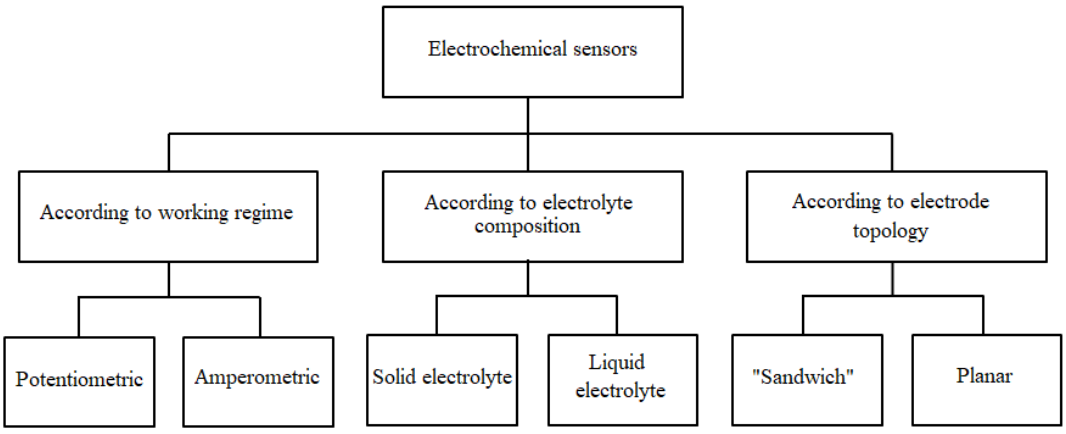

Fig. 14 Classification of electrochemical sensors

4.4.1 Potentiometric sensors

Equilibrium potentiometry is the analytical method based on non-current measurement of differential potential of electrochemical (galvanic) cell. The cell is usually made of indicator electrode immersed into measured solution and by reference electrode, which is connected to measured solution via salt bridge. The potential of the indicator electrode is dependent on analyte concentration in analysed sample. Potential of the other electrode is on this concentration independent. Choice of the indicator electrode is influenced by the type of used electroanalytical method. Reference electrodes are usually same for all methods. As an indicator electrode is usually electrode of first kind i.e. metal plate or wire immersed in solution which contains ions of used metal. However, it is possible to use all known types of electrodes whose potential is dependent on activity (concentration) of measured analyte (e.g. redox electrodes, ISE etc.). As a reference electrode, electrodes of the second kind are used only. These electrodes are made of metal covered by layer of their salt, which has to be poorly soluble in solution with anions of this salt (e.g. argentchloride electrode – Ag/AgCl or calomel electrode – Hg/Hg_2Cl_2) [39].

The relationship between potential of metal electrode and activity of measured ions in solution is given by Nernst Equation (26):

$$E = E_0 \pm \frac{\mathrm{R}T}{n\mathrm{F}} \cdot \ln \alpha_{\mathrm{i}} \,, \tag{28}$$

where E is potential of electrode, E_0 is potential of the standard hydrogen electrode (SHE), R is ideal gas constant ($R = 8{,}3144\ J \cdot K^{-1} \cdot mol^{-1}$), T is temperature (K), n is number of electrons exchanged in electrochemical reaction, F is Faraday constant ($F = 9{,}64870 \cdot 10^4\ C \cdot mol^{-1}$) and α_i is activity of ions. SHE plays an important role in electrochemistry. Its potential is conventionally considered to be zero and therefore all other tabulated values of electrodes and standard redox potentials are related to it.

4.4.2 Amperometric sensors

Amperometry is method based on measurement of current between electrodes immersed in electrolyte. There are two basic types of systems – with two or three electrodes. Two-electrode system is simpler and consists of working (cathode) and reference (anode) electrodes. Working electrode is smaller and easier to polarizable than reference electrode. The magnitude of the current at constant potential of working electrode during exposure to analyte is proportional to its concentration. Advantage of this setting is its simplicity and the fact, that current is measured on the same electrodes to which voltage is applied. Example of two electrode amperometric sensor is Clark sensor for measurement of oxygen concentration in gases or liquids [39].

More complicated three electrode system uses in adition to above mentioned electrodes third usually large area auxiliary Pt electrode (also called “counter” electrode) and uses potentiostatic connection (see Fig. 15). In this case no chemical reaction occurs at reference electrode. Potentiostat using reference electrode maintains constant voltage between working (WE) and reference (RE) electrode. Current is measured between working and auxiliary (CE) electrode. Advantage of this connection is possibility to measure higher currents without using reference electrode. Disadvantage is possibility of creation of the ohmic drop, which occurs mostly when measuring samples with very low conductivity. One way to eliminate this effect is rising of the sample conductivity by supporting electrolyte, or by placing the reference electrode as close as possible to working electrode [46, 47].

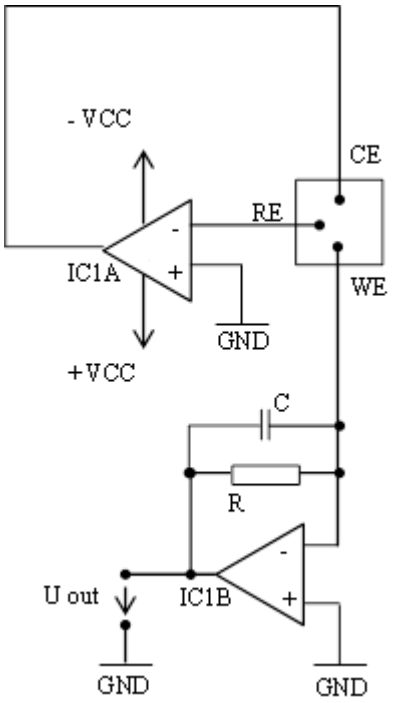

Fig. 15 Scheme of potentiostatic connection of three electrode amperometric sensor

4.4.3 Electrochemical sensors with solid and liquid electrolytes

An example of sensor with liquid electrolyte is Clark sensor mentioned in previous chapter. Liquid electrolyte is being used as medium for ion transport between electrodes and therefore has several limitations. During operation a gradual desiccation occurs, which affects function, stability and durability of sensor. On top of that thanks to toxic components, often used in these sensors, special packaging materials to prevent leakage to environment are needed.

Sensors with solid electrolytes don't have this problem. In contrast to liquid electrolytes, only transport of one type of ions is possible in solid phase electrolytes, i.e. cations or anions. There are both potentiometric and amperometric types of sensors with solid electrolytes. Well known example of potentiometric sensor with solid electrolyte is Lambda sensor, which is used for measurement of residual oxygen in exhaust gases (Fig. 16). Field of sensors with solid electrolytes seems to have good perspectives in sense of use of organic materials. Properties of solid electrolytes based on organic ionic liquids were studied in our work.

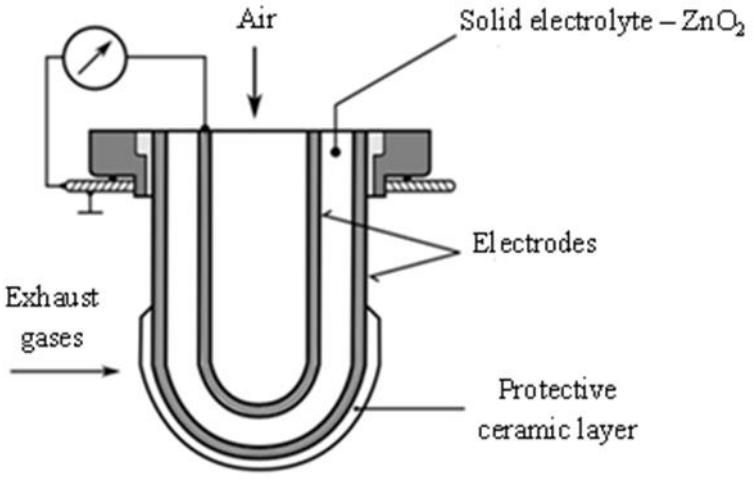

Fig. 16 Scheme of the Lambda sensor

4.4.4 Electrodes and their topology

Characteristics of sensors are influenced not only by factors as electrolyte composition, used electrode materials, but also by their topology. There are two basic topologies used with some modifications – planar and "sandwich" (Fig. 17).

Both topologies are used for sensors with solid or liquid electrolytes. For sensor detecting substances from gaseous phase, working electrode is placed on top of the electrolyte to ensure direct contact of this electrode with detected substance. Chemical reaction (oxidation or reduction) occurs at three-phase interface gas/electrode/electrolyte. According to this fact, electrode should be porous and well penetrable for molecules of detected gas, which are diffusing through working electrode to interface with electrolyte. In case, that working electrode is impenetrable for analyte, three-phase interface is only at the periphery of the electrode. Mackley, Buttner and Stetter found out in study [48] that this periphery is most electrochemically active, but its length is often short and may lead to insufficient sensitivity of sensor. To overcome this problem so called "micro-lattice" working electrodes can be used. Using this kind of electrodes on one hand multiplies its periphery, but also on the other decreases its area. Currently there is intensive research in field construction of new material structures and composition of working electrodes [49 - 51].

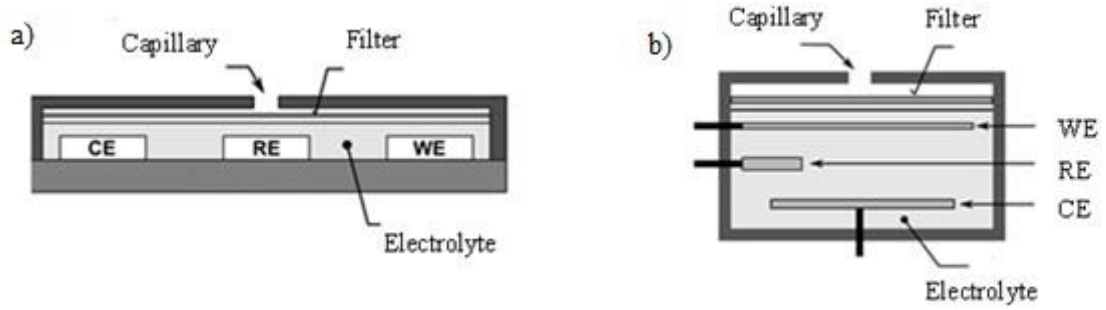

Fig. 17 Topology of electrodes:
a) planar structure
b) "sandwich" structure

Working electrode for gas detecting sensors may also be deposited right at the surface of the electrolyte to ensure direct contact of the analyte with electrode. This setup is also called quasi-plannar (Fig. 18). Chemical reaction occurs at three-phase interface of external environment/electrode/electrolyte. Considering this fact, working electrode needs to be porous and permeable enough for molecules of detected substance to enable its diffusion to the electrolyte. In case of insufficient permeability reaction only occurs at the edge of the working electrode. Despite the fact, that authors of the study [52] claim that this area is the most active by means of electrochemical reactions, its length is usually very short, which leads to insufficient sensitivity. To avoid this phenomenon working electrode is usually being deposited in form of microgrid which rapidly increases its circumference. Intense research in this area is still running [49 - 51].

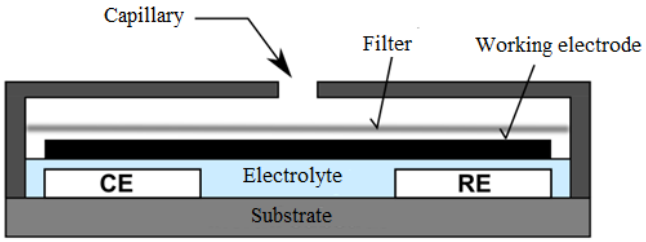

Fig. 18 Quasi-plannar structure

5 Description of basic mechanisms in amperometric gas sensors

At the beginning of description of this topic it is suitable to remind few facts stated in literature [53], which are, due to narrow specialization to specific topic, in field of gas sensors often overlooked. First thing which is good to realize is that electrochemical sensors are monitoring natural processes. The flow of these processes is directed by the second law of thermodynamics. Second, when considering the state of equilibrium as a starting point, all three laws of thermodynamics apply. It is also possible to measure the speed of monitored process. In this case general mechanisms of reaction kinetics are applied.

Mechanisms of amperometric gas sensors were thoroughly described in several studies [46, 53 - 56] and it is possible to separate them into several parts. For their accurate and unambiguous description, another specification needs to be made. Description of each mechanism will be related to gas sensors with polymeric electrolyte, which makes unique interface with electrode – analyte / electrode / electrolyte. In this setup the working electrode is directly exposed to the effect of analyzed gas, while being immersed in the electrolyte. Thanks to this setup it is needed to exclude some mechanisms for description of amperometric gas sensors stated in literature [56], simply because they won't occur. Following description of mechanisms will be related to the topology represented by Fig. 18.

Transport of the analyte to outer interface of sensor – this step is represented by transport of gaseous analyte through the capillary and inlet filter to internal components of the sensor (i.e. electrolyte and working electrode). This step can be realized by diffusion of the analyte or with help of mechanical flow. Inlet filter can represent the first element for improvement of sensor's selectivity. To do so, it is possible to use a simple mechanical principle based on the size of molecules, i.e. only molecules up to certain size may pass through the filter. Other way to improve the selectivity of inlet filter is to adjust its composition (or impregnate it by suitable compound) to chemically react with substances, which would cause intersection of the signal.

Transport of reactants/products of electrode reaction to/from working electrode/electrolyte interface – as well as gaseous analyte also other possible reactants (regardless of their state) need to get to the working electrode/electrolyte interface, where redox reactions occur i.e. either oxidation or reduction of the analyte. Dynamics of these transports are most often described by the first Fick's law i.e. velocity of the diffusion is proportional to the concentration gradient. If the velocity of analyte's diffusion (or of any other compounds involved in reaction at the working electrode) is many times slower than velocity of the reaction occurring there, then is this process considered to be a limiting factor for the amplitude of sensor's response (i.e. magnitude of measured current). In such case it is assumed, that concentration of the analyte towards the working electrode/electrolyte interface decreases. In an ideal case it decreases to zero, since the velocity of the reaction is theoretically so high, that every single molecule is being immediately reduced or oxidized when transported to the interface. Development of a stationary concentration gradient is indicated in Fig. 19 The calculation of a concentration gradient may in fact be a very difficult task, therefore it is often used term of Nernst diffusion layer (δ). Nernst diffusion layer assumes that transport of electroactive reactants in very close surroundings of the electrode is driven only by diffusion and that concentration gradient in this area is linear.

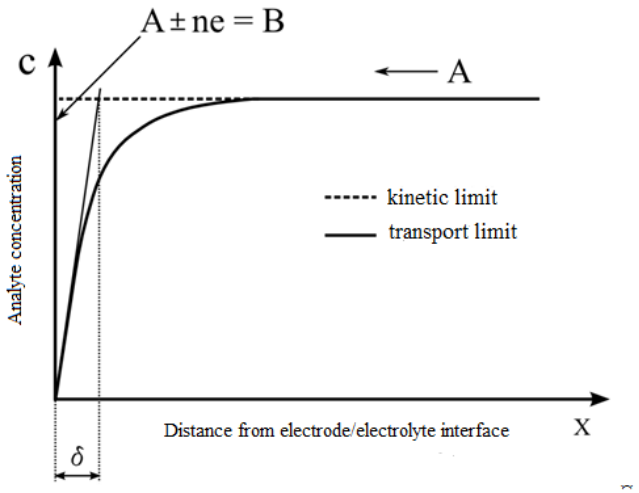

Fig. 19 Development of a stationary concentration gradient near planar electrode limited by transport of electroactive substance to electrode („transport limit"), b) rate of electrode reaction („kinetic limit")[53, 55]

As indicated above, same rules can be applied to products of electrode reaction, where concentration gradient and Nernst diffusion layer can be analogically defined. It is logical, that concentration of reaction products will be highest at the electrode surface and will decrease with increasing distance.

Considering all above-mentioned facts, following relationship between current and analyte concentration can be derived by combination of the first Fick's law and Nernst diffusion layer [53]:

$$i = \frac{n\mathrm{F}AD}{\delta} \cdot c \,, \tag{29}$$

where n and F have usual meaning, A is surface area of the working electrode, D is diffusion coefficient, δ je Nernst diffusion layer and c is concentration of the analyte.

In case when stationary state cannot be assumed, analytical solution of the problem becomes very complex, complicated, often reduced to the use of empirical formulas and sometimes even impossible. Nevertheless, even in this case one can work with the term of Nernst diffusion layer and derive relationship between current response and analyte concentration in time, which is known as Cottrell equation (28). For the derivation and further study of this equation please see literature [46, 53, 54]:

$$i(\mathrm{t}) = \frac{n\mathrm{F}AD^{\frac{1}{2}}}{(\pi t)^{\frac{1}{2}}} \cdot c. \tag{30}$$

Electrode reaction **–** is usually preceded by adsorption of the analyte by working electrode. Nevertheless, this process is usually very fast and thus not limiting overall velocity of overall redox process. Oxidation and reduction are basic processes, on which principle of electrochemical sensors are built on. In case of NO_2 detection reduction at working electrode occurs. At the auxiliary electrode, placed opposite to the working electrode, occurs most likely the oxidation of water molecules. Velocity of electrode reaction is other factor, which

can strongly influence current response of the sensor. In this case it is assumed, that transport of reactants to the electrode is far faster than reaction velocity. Concentration gradient of the analyte is constant, and velocity of the redox process is limited by reaction kinetics. Most used equation for description of charge transfer in electrochemistry is Butler-Volmer equation (31):

$$I = \mathrm{F}\,A\mathrm{k}_0 \left\{ c^{\mathrm{o}}(\mathrm{Red})\,\exp\left[\frac{(1-\alpha_{\mathrm{CT}})\mathrm{nF}}{\mathrm{R}T}\left(E - E_{\mathrm{C}}^{\mathrm{O}}\right)\right] - c^{\mathrm{o}}(\mathrm{Ox})\,\exp\left[\frac{-\alpha_{\mathrm{CT}}n\mathrm{F}}{\mathrm{R}T}\left(E\text{-}E_{\mathrm{C}}^{\mathrm{O}}\right)\right]\right\} \qquad (31)$$

where *F, A, R, T, n* have their usual meaning, k_0 is standard heterogeneous velocity constant when E=0, $c^0(Red)$ and $c^0(Ox)$ are concentrations of reduced and oxidized forms of reactants at electrode's surface, α_{CT} is charge transfer coefficient and E_C^0 is so-called normal potential. This general relationship is again derived based on several simplifying conditions, which are more in detail described in literature [16, 53] and references therein.

Desorption process – desorption of reactants and overall ability to "restore" electrochemically active surface are also important factors, which affect stability and reproducibility pf the sensor's response. In ideal case concentrations of reactants and its products will become the same as were before the measurement.

As summary of above mentioned, it is necessary to note, that any of these factors (1 to 3) and/or their combinations can significantly influence the current response of the sensor. Which one of them will be dominant strongly depends on used materials, topology of used electrodes and overall design of sensor. Parameters of all these elements should be taken into account during optimization of sensor's performance by means of sensitivity, selectivity, stability and lifetime expectancy.

6 Experimental part

6.1 Properties of ionic liquids

For our experimental studies we chose several ionic liquids according to chemical structures, which are presented in Table 2.

Table 2 List of ionic liquids used for experimental studies.

1	1-ethyl-3-methylimidazolium bis(trifluoromethylsulfonyl)imide [C_2mim][NTf_2]	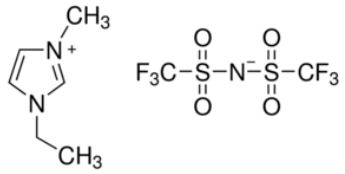
2	1-ethyl-3-methylimidazolium ethylsulfate [C_2mim][$EtSO_4$]	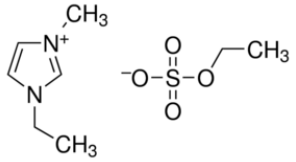
3	1-ethyl-3-methylimidazolium hydrogen sulfate [C_2mim][HSO_4]	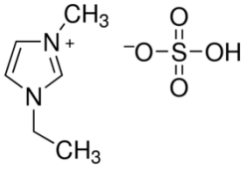
4	1-butyl-3-methylimidazolium trifluoromethanesulfonate [C_4mim][OTf]	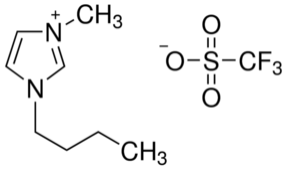
5	1-butyl-1-methylpyrrolidinium bis(trifluoromethylsulfonyl)imide [C_4mpyrr][NTf_2]	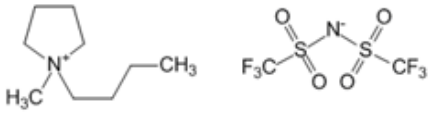
6	1-hexyl-3-methylimidazolium bis(trifluoromethylsulfonyl)imide [C_6mim][NTf_2]	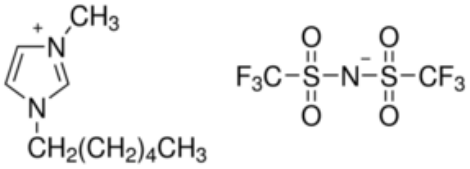
7	1-butyl-3-methylimidazolium trifluoroacetate [C_4mim][CF_3CO_2]	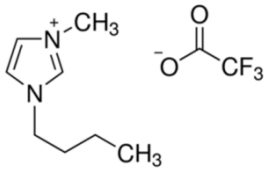
8	1-ethyl-3-methylimidazolium tetrafluoroborate [Emim][BF4]	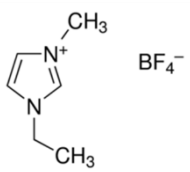

The first group of materials (ionic liquids No. 1, 2, 3 and 8) contains 1-ethyl-3-methylimidazolium cation. These substances contain quaternary nitrogen which is responsible for ionic conductivity. The positive charge is compensated by negative charge on anion. Four types of anion were selected: bis(trifluoromethylsulfonyl)imide (sample 1), ethylsulfate (sample 2), hydrogen sulfate (sample 3) and tetrafluoroborate (sample 8). There are different electrostatic forces between cations and anions which strongly influence viscosities and electrical conductivities. The other group of materials compares the influence of the length of substituent chains, i.e., ethyl vs. hexyl (samples 1 and 6) and effect of different cations, i.e. ethyl, butyl and hexyl (samples 1, 5 and 6). The sample 5 in addition compares the influence of imidazolium and pyrrolidinium rings.

6.1.1 Impedance spectroscopy

Impedance spectroscopy (IS) is an experimental analytical method based on measuring response of the system to signal with small amplitude (it studies the response of amplitudal current to the change of frequency and also dielectric properties of material as function of frequency). IS is based on interaction between applied electric field and dipole moments of molecules of the sample. The sample can be practically any type of solid or liquid material: ionic, semi-conductive, their mixture, or dielectric (insulant). This method is widely used to characterize the electrical behaviour of systems, in which complex behaviour is affected by number of interconnected processes. It enables the study characteristic of materials such as: dielectrical properties, equivalent circuit models, charge carrier dynamics and dielectric properties [57, 58].

Basic measured parameters are impedance Z and admittance Y which are following relation $Z=1/Y$. In complex plane, they can be expressed:

$$Z = U/I = |Z|\left[\cos(\varphi) - i\sin(\varphi)\right], \tag{32}$$

$$Y = I/U = |Y|[\cos(\varphi) + i\sin(\varphi)], \tag{33}$$

where φ is phase shift angle. Additionally impedance Z and admittance Y can be expressed using resistive and capacitive component:

$$Z = R_s + iX_s \text{ resp. } Y = G_p + iB_p \tag{34}$$

where R_s is resistance, X_s is reactance, G_p conductance, B_p is susceptance. Indexes s and p refer to series or parallel connection (see Fig. 20).

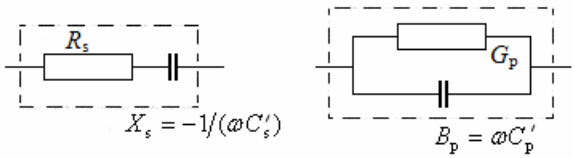

Fig. 20 series (left) and parallel connection of an RC circuit

For reactace X_s and susceptance B_p we can also write:

$$X_s = -\frac{1}{\omega C_s'} \text{ resp. } B_p = \omega C_p' \tag{35}$$

where $\omega=2\pi f$ is angular frequency, C_p' and C_s' are real parts of complex capacity $C = \frac{\varepsilon S_{AC}}{l} = C' + iC''$, where ε is complex permittivity, S_{AC} is active surface and l is distance between electrodes.

Following measurements were carried out using frequency-response analyser Solartron SI 1260 equipped with additional Solartron dielectric interface 1296A module (Solartron, Farnborough, Hampshire, UK, Fig. 21).

Fig. 21 Frequency-response analyser Solartron SI 1260 (left), Solartron dielectric interface 1296A module (right) [59]

Unless stated otherwise measurement were conducted under laboratory conditions (22 °C, 40% relative humidity). Frequency range was 10 mHz to 1MHz with logarithmical step and 10 measured points per decade, AC amplitude was 200mV, applied DC voltage was 0 V. As electrodes either pair of stainless steel plates or stainless steel plate with Ta/Ta_2O_5 capacitor electrode (D3.3/125/FV350V or V68W15311 WC) were used, distance between electrodes was 4mm and the electrode area was 25 mm^2.

6.1.2 UV-VIS, IR measurements

As it is well known and expectable, ILs are quite sensitive to impurities. Therefore, the purity of used ionic liquids was checked by infrared and UV-VIS spectroscopy in cooperation with Institute of Macromolecular Chemistry CAS using Thermo Nicolet 6700 (for IR spectra) and Perkin-Elmer Lambda 20 (for UV-VIS spectra). Typical vibrations (in cm^{-1}) are presented in Table 3. Infrared spectra of ILs under study (1 – 7) are shown in Fig. 22.

Table 3 Typical vibrations in (cm^{-1}) of ionic liquids (1 – 7) under study. The numbers in the first line correspond to the number of ionic liquid (see Table 2)

1	2	3	4	5	6
510		568	516	512	512
	576		572	570	570
600	618	648	622	614	614
				654	
740	758	760	754	740	738
790		832		788	788
	912			928	
1050	1014	1020	1028	1052	1050
1176	1168	1160	1152	1134	1132
	1214		1252	1176	1172

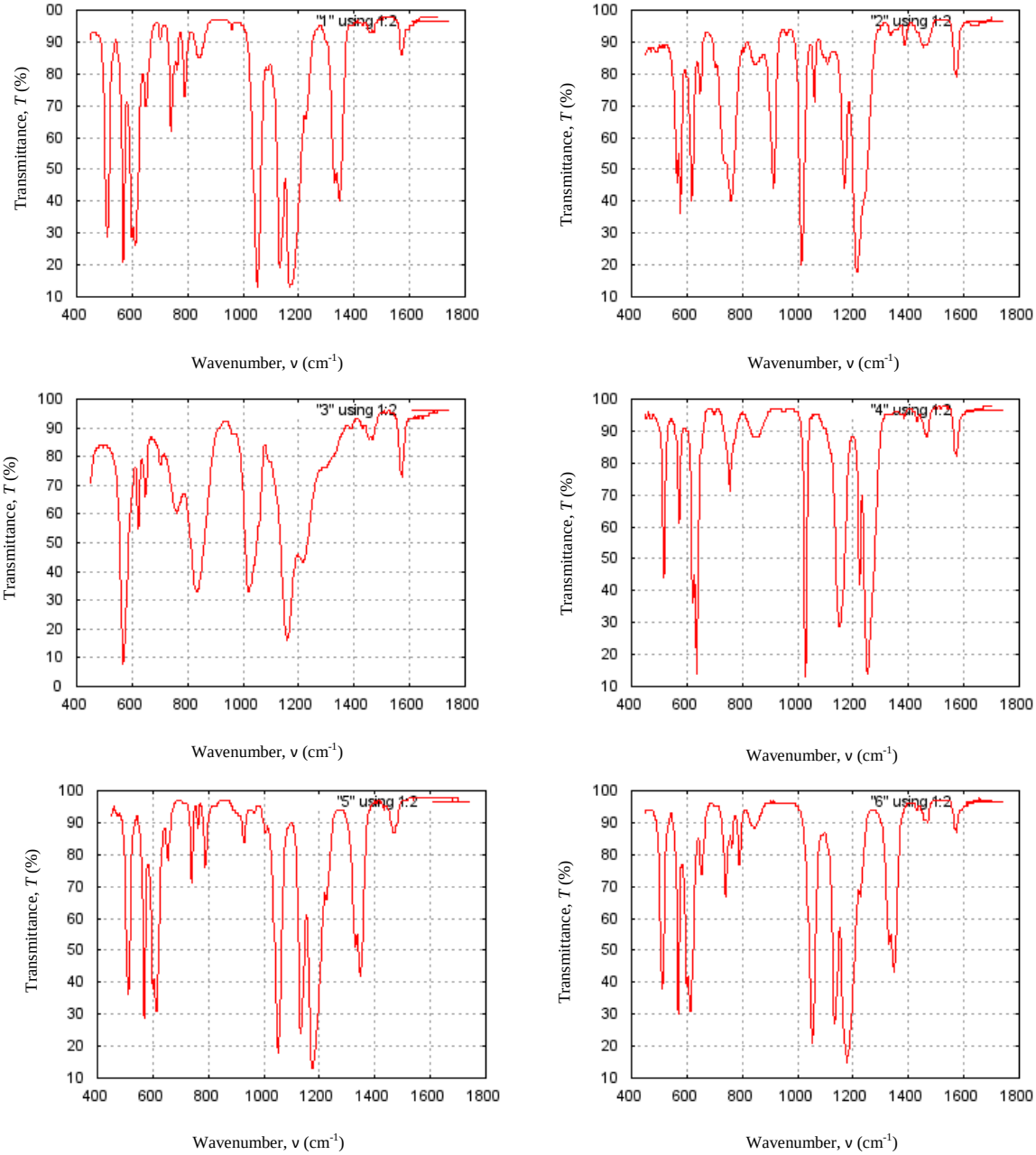

Fig. 22. Infrared spectra of ILs under study. . Sample 1 – top left, sample 2 – top right, sample 3 – the second row left, sample 4 – the second row right, sample 5 – the third row left, sample 6 – the third row right.

As another proof of the material purity UV-VIS spectra can be used. Spectra of ILs under study (1 - 6) are shown in Figs.16 (in water) and 17 (in hexane).

The characteristic absorption bands are located in UV region – the wavelengths of the maxima are around 200 nm, independently on the chemical structure of the positive and negative ions. From the view of purity the spectrum in visible region is important. Because ILs are colourless materials, no absorption is expected in this part of the spectrum. The visible part of the spectrum of ionic liquid No. 3 is given in **Fig. 23**. The absorption bands in this part of the spectrum suggest some chemical impurities in this material. Visually, the material is not colourless but it embodies yellow coloration.

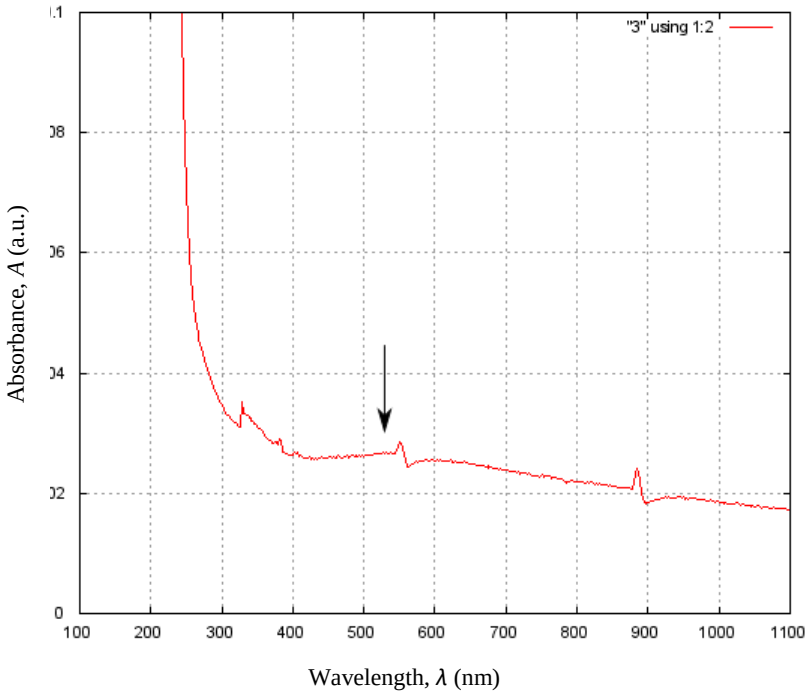

Fig. 23 UV-VIS spectrum of ionic liquid [C_2mim][HSO_4]. The arrow shows the possition of the maximum of the absorption band. Small spikes are of spectrophotometer errors.

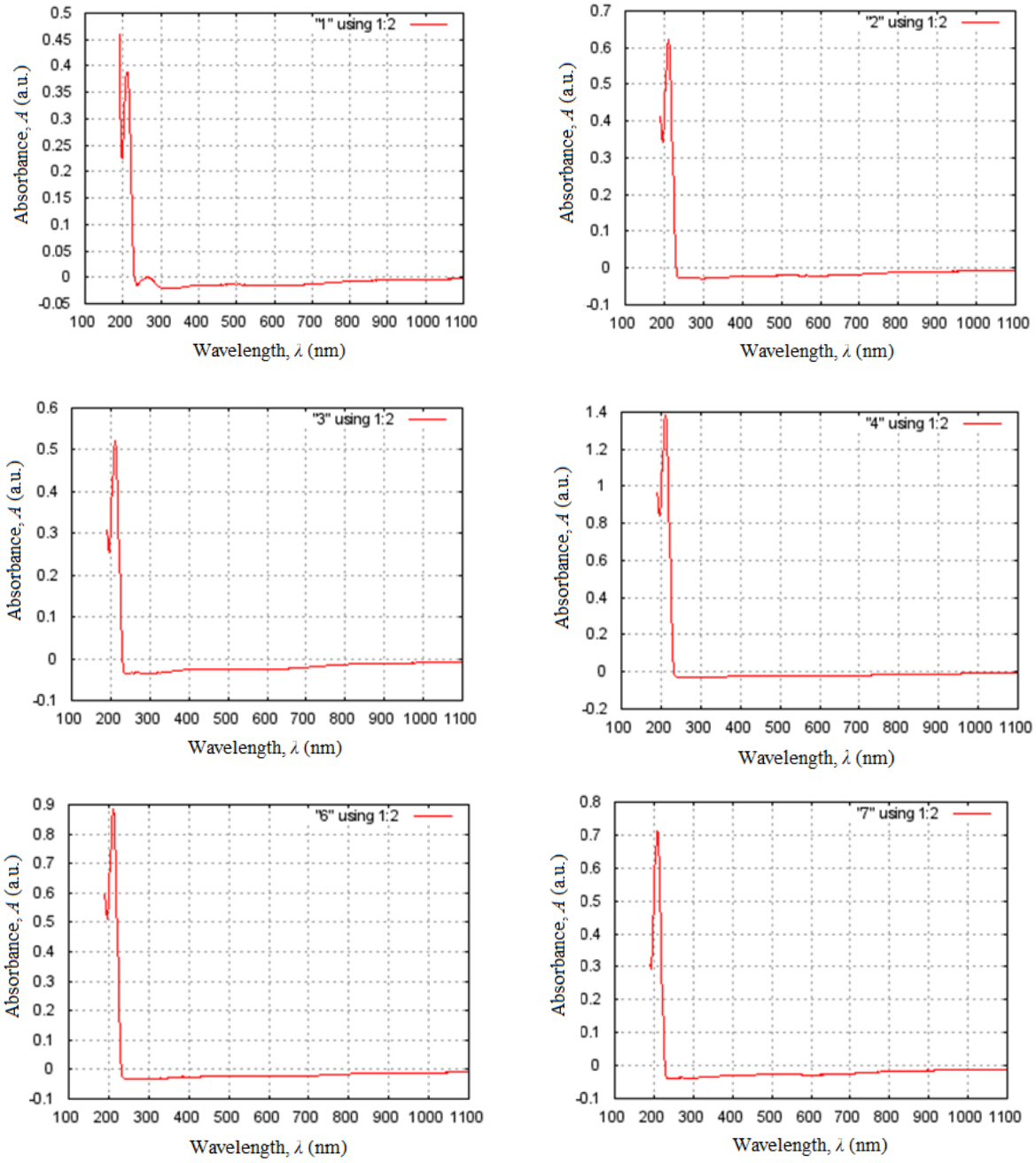

Fig. 24 UV-VIS spectra of ILs (in water) under study. Sample 1 – top left, sample 2 – top right, sample 3 – the second row left, sample 4 – the second row right, sample 6 – the third row left, sample 7 – the third row right.

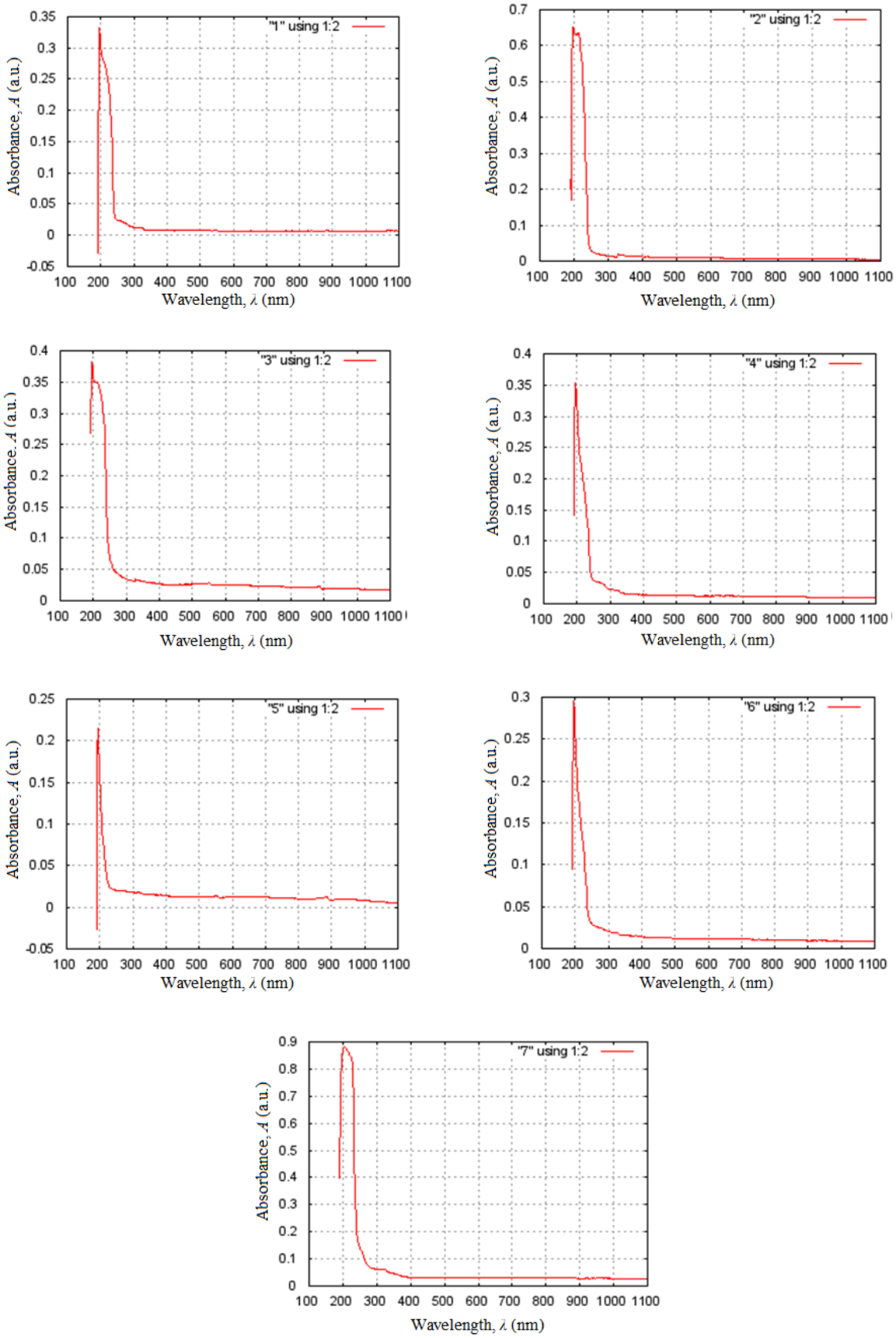

Fig. 25 UV-VIS spectra of ILs under study (in hexane). Sample 1 – top left; 2 – top right; 3 – the second row left; 4 – the second row right; 5 – the third row left; 6 – the third row right; 7 – down.

6.1.3 TGA measurements

In order to properly design an experiment which could be executed under elevated temperature, it is necessary to determine for each used ionic liquid "safe" range of temperatures, where no decomposition occurs. To find it out, thermogravimetric analysis was performed using simultaneous TGA/DSC analyser SDT Q600 (TA Instruments). 12 mg samples were heated in nitrogen atmosphere, heating ramp was 5 °C/min.

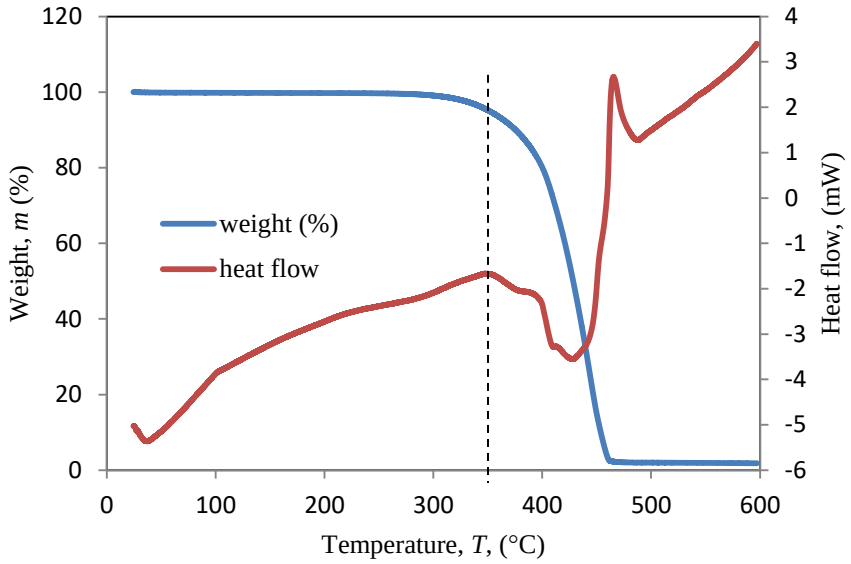

Fig. 26 TGA/DSC curve of ionic liquid [C_2mim][NTf_2].

Fig. 26 shows a TGA/DSC curve of ionic liquid [C_2mim][NTf_2] as dependence of weight loss in % and heat flow on temperature. The temperature stability was determined as a temperature at which endothermic peak in heat flow line starts (black dashed line). Note that sample was fully stable up to 345 °C (any significant weight loss occurs). Curves of other measured ILs can be seen in APPENDIX A. Results for all measured liquids are summarized in Table 4.

Table 4 Determined temperature of thermal stability for „safe" use of studied ionic liquids.

IL	[C_2mim][NTf_2]	[C_2mim][$EtSO_4$]	[C_2mim][HSO_4]	[C_4mim][OTf]	[C_4mpyrr][NTf_2]	[C_6mim][NTf_2]	[Emim][BF_4]*
Temperature (°C)	345	278	290	313	351	325	≥350

* Data acquired from manufacturer.

Considering ionic liquids with [C_2mim] cation, temperature stability grows with different anion following way: [$EtSO_4$] < [HSO_4] < [NTf_2] < [BF_4].

Considering the length of alkyl chain on imidazolium ring, it can be stated that longer the chain, the lower thermal stability: [C_6mim][NTf_2] < [C_2mim][NTf_2].

When comparing ILs with different cation, highest stability showed IL with pyrrolidinium ring: [C_6mim][NTf_2] < [C_2mim][NTf_2] < [C_4mpyrr][NTf_2].

6.2 Ionic liquids for use in capacitors

Ionic liquids are interesting materials for capacitor fabrication because of their broad working windows (up to 5 V). Some of them are stable at high temperatures. Both these properties make them suitable candidate for use as an electrolyte in “high temperature” capacitors.

6.2.1 Impedance measurements

To get some information about the possibility of the application of ionic liquids in capacitor technology, some of them were studied by dielectric spectroscopy in detail.

The list of ionic liquids under study and their chemical structures is given in Table 2. Their dielectric characteristics are given in APPENDIX C. In Fig. 27 and Fig. 28 frequency dependencies of impedance and phase angle respectively are shown. The ionic liquids were used as received without any additives. Concerning electrodes the system was asymmetric. One electrode was prepared from platinum plate, for the other one, the V68 W15311WC capacitor electrode was used (system Pt plate | Ionic liquid | V68 W15311WC). No DC bias was applied. Note, that the application of bias voltage can open a new area for the study of electrode properties, namely, electrode polarization. No data of this type were found in literature.

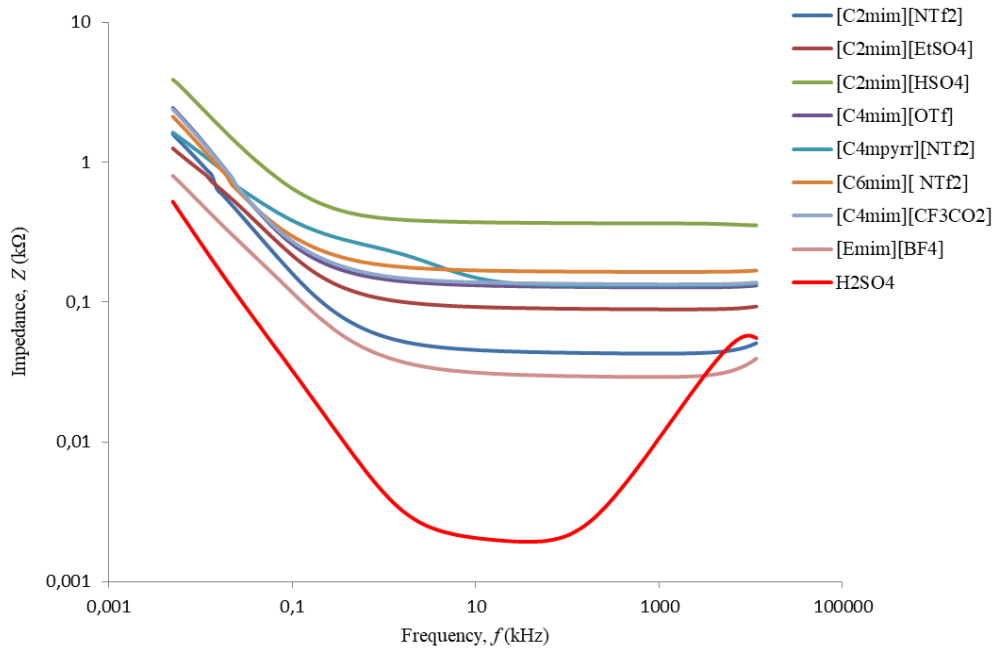

Fig. 27 Dependence of impeadance on frequency of chosen ionic liquids, H_2SO_4 is added for comparison.

For all measured ionic liquids, impedance decreases with frequency. At higher frequencies saturation is observed. The value which corresponds to zero phase angle gives us the information about DC resistance (in (Ω) or conductance as an inverted value of resistance) of the electrolyte. Values of impedance and conductance at $\varphi = 0°$ of measured electrolytes are summarized in Table 5. Positive values of phase angle $\varphi(°)$is noted for all measured samples at high frequencies. This phenomenon suggests an influence of induction – the feature of this effect in our case is attributed to induction of the measuring device („wires“).

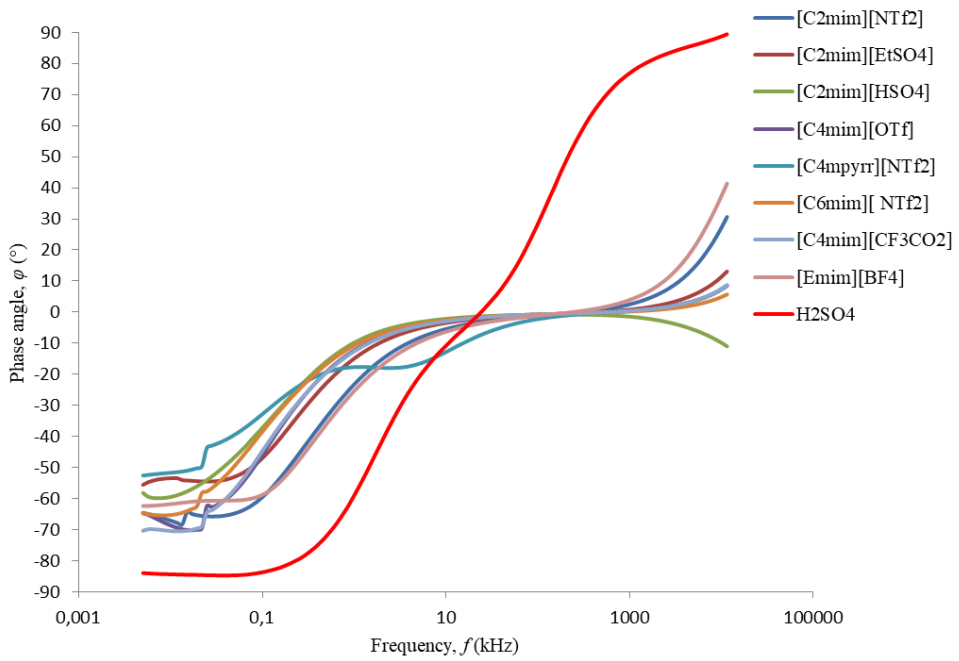

Fig. 28 Dependence of phase degree on frequency of chosen ionic liquids, H_2SO_4 is added for comparison.

It is evident, that conductivities of ionic liquids are significantly lower than conductivity of H_2SO_4. Therefore, capacitances are expected to be also lower.

Table 5 Summary of measured properties of ionic liquids under study, system Pt plate | Ionic liquid | V68 W15311WC.

Ionic liquid	Frequency of φ = 0° (kHz)	Impedance (Ω)	Conductance (mS)
$[C_2mim][NTf_2]$	286	43	23.3
$[C_2mim][EtSO_4]$	414	89	11.2
$[C_2mim][HSO_4]$	224	366	2.7
$[C_4mim][OTf]$	530	128	7.8
$[C_4mpyrr][NTf_2]$	678	131	7.6
$[C_6mim][NTf_2]$	678	165	6.1
$[C_4mim][CF_3CO_2]$	530	134	7.5
[Emim][BF4]	224	30	33.3
H_2SO_4	24	2	500.0

The characteristic parameters are summarized in Table 6. The Table contains several usually determined parameters as measured at 123 Hz, i.e. B_p – parallel susceptance, C_p – parallel capacitance, G_p – parallel conductance, and C_s – serial capacitance of the system V68 W15311WC | Ionic liquid | platinum plate.

Considering ionic liquids with $[C_2mim]$ cation, conductance grows with different anion following way: $[HSO_4] < [EtSO_4] < [NTf_2] < [BF_4]$.

Considering ionic liquids with $[C_4mim]$ cation, conductance grows with different anion following way: $[CF_3CO_2] < [OTf]$.

Considering the length of alkyl chain on imidazolium ring, it can be stated that longer the chain, the lower is conductance: $[C_6mim][NTf_2] < [C_2mim][NTf_2]$.

When comparing ILs with different cation, conductance was rising in following order: $[C_6mim][NTf_2] < [C_4mpyrr][NTf_2] < [C_2mim][NTf_2]$. It seems that in this case the length of the alkyl chain of cation plays slightly more important role (conductance decreases with the length of alkyl chain) than in case of thermal stability.

Table 6 Measured parameters at 123 Hz for system Pt plate | Ionic liquid | V68 W15311WC.

Ionic liquid	G_p [mS]	B_p [mS]	C_p [µF]	C_s [µF]
$[C_2mim][NTf_2]$	3.91	6.01	7.79	11.10
$[C_2mim][EtSO_4]$	3.70	3.60	4.67	9.61
$[C_2mim][HSO_4]$	1.38	0.94	1.22	3.84
$[C_4mim][OTf]$	3.16	2.83	3.67	8.24
$[C_4mpyrr][NTf_2]$	2.39	1.42	1.84	7.07
$[C_6mim][NTf_2]$	2.97	2.09	2.72	8.18
$[C_4mim][CF_3CO_2]$	3.04	2.63	3.41	7.98
[Emim][BF4]	5.25	8.15	10.60	15.00
H_2SO_4	4.43	36.60	47.5	48.20

The highest capacitance shows, as expected, H_2SO_4. Concerning ionic liquids the most suitable material for capacitor applications seems to be 1-ethyl-3-methylimidazolium tetrafluoroborate ([Emim][BF_4]). Mentioned capacitances were measured on the system with Pt counter electrode and V68 W15311WC counter electrode. It is important, given to the fact that also other electrode systems were used in this study, that it is possible to compare only capacitances of ionic liquids where electrode potentials are comparable. The capacitance of the capacitor with H_2SO_4 electrolyte is mentioned only for comparison.

Considering ionic liquids with [C_2mim] cation, capacitance grows with different anion following way: $[HSO_4] < [EtSO_4] < [NTf_2] < [BF_4]$.

Considering ionic liquids with [C_4mim] cation, capacitance grows with different anion following way: $[CF_3CO_2] <$ [OTf].

Considering the length of alkyl chain on imidazolium ring, it can be stated that longer the chain, the lower is capacitance: $[C_6mim][NTf_2] < [C_2mim][NTf_2]$.

When comparing ILs with different cation, capacitance was rising in following order: $[C_4mpyrr][NTf_2] < [C_6mim][NTf_2] < [C_2mim][NTf_2]$.

6.2.2 Temperature dependence of C-V properties

For following experiment ionic liquids $[C_2mim][NTf_2]$ $[C_4mim][OTf]$ and $[C_6mim][NTf_2]$ were chosen. As electrodes stainless steel plate and Ta/Ta_2O_5 electrode (D3.3/125/FV350V) were used. C-V characteristics were measured using electrometer Keithley 6517B (Keithley Instruments, Cleveland, Ohio, USA). Voltage was increased linearly by 0,5 V every 4s, cut-off current was 1 mA (current reached at breakdown voltage). Samples were measured at room temperature, 50 °C, 90 °C, 120 °C and 150 °C (see Fig. 29).

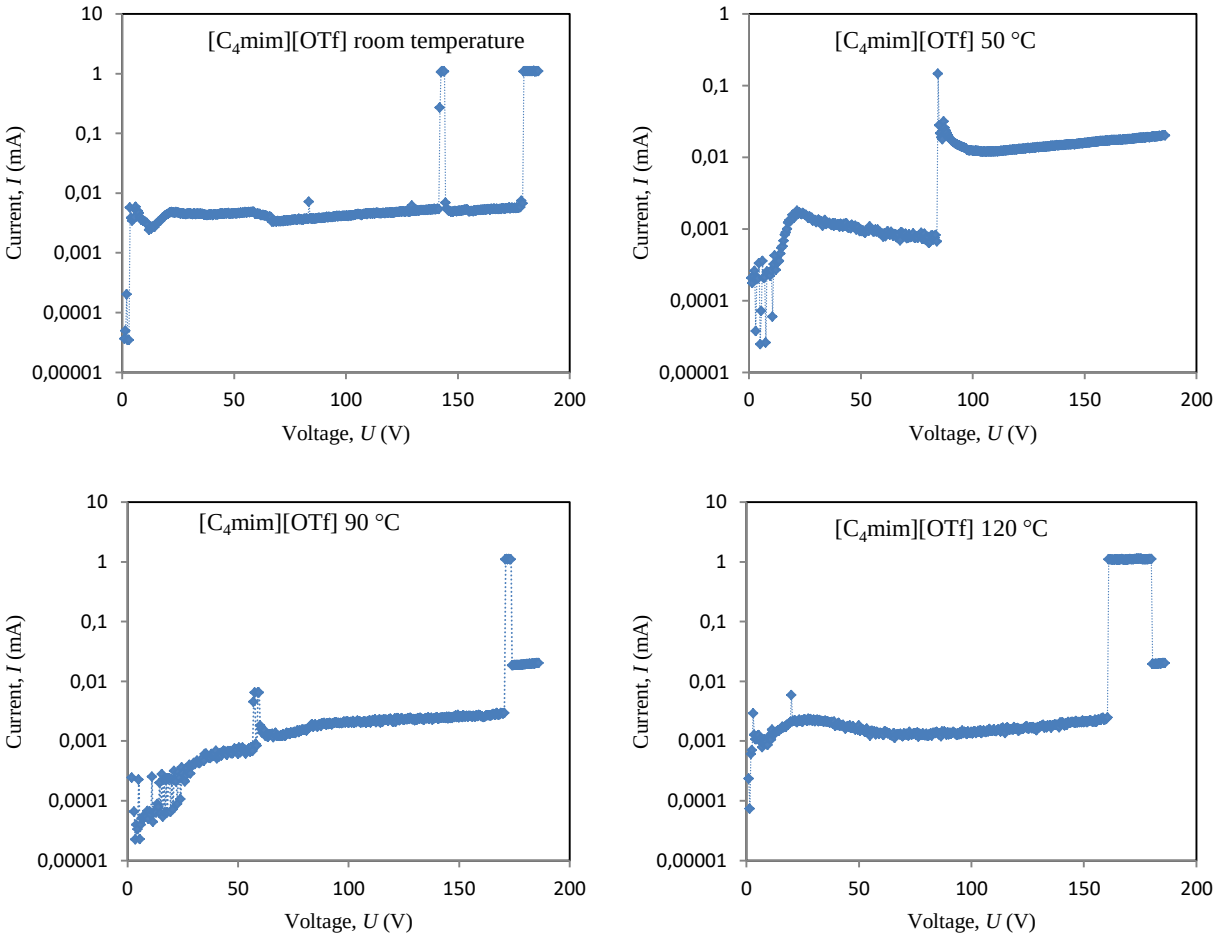

Fig. 29 C-V characteristics of [C_4mim][OTf] at different temperatures in semi-logarithmic scale.

In **Fig. 29** C-V characteristics for ionic liquid [C_4mim][OTf] at different temperatures are shown. Applied voltage was stepwise increased and direct current was measured. The breakdown voltage (BDV) was determined as the voltage at which a steep current increase was observed. Data for other studied ILs are in APPENDIX B. In Fig. 30 temperature dependences of BDV for studied Ils are shown. The dependence for all liquids shows linear decrease with increasing temperature. The values for 200 °C were extrapolated for all liquids, since they are all stable at this temperature (see **Table 4**).

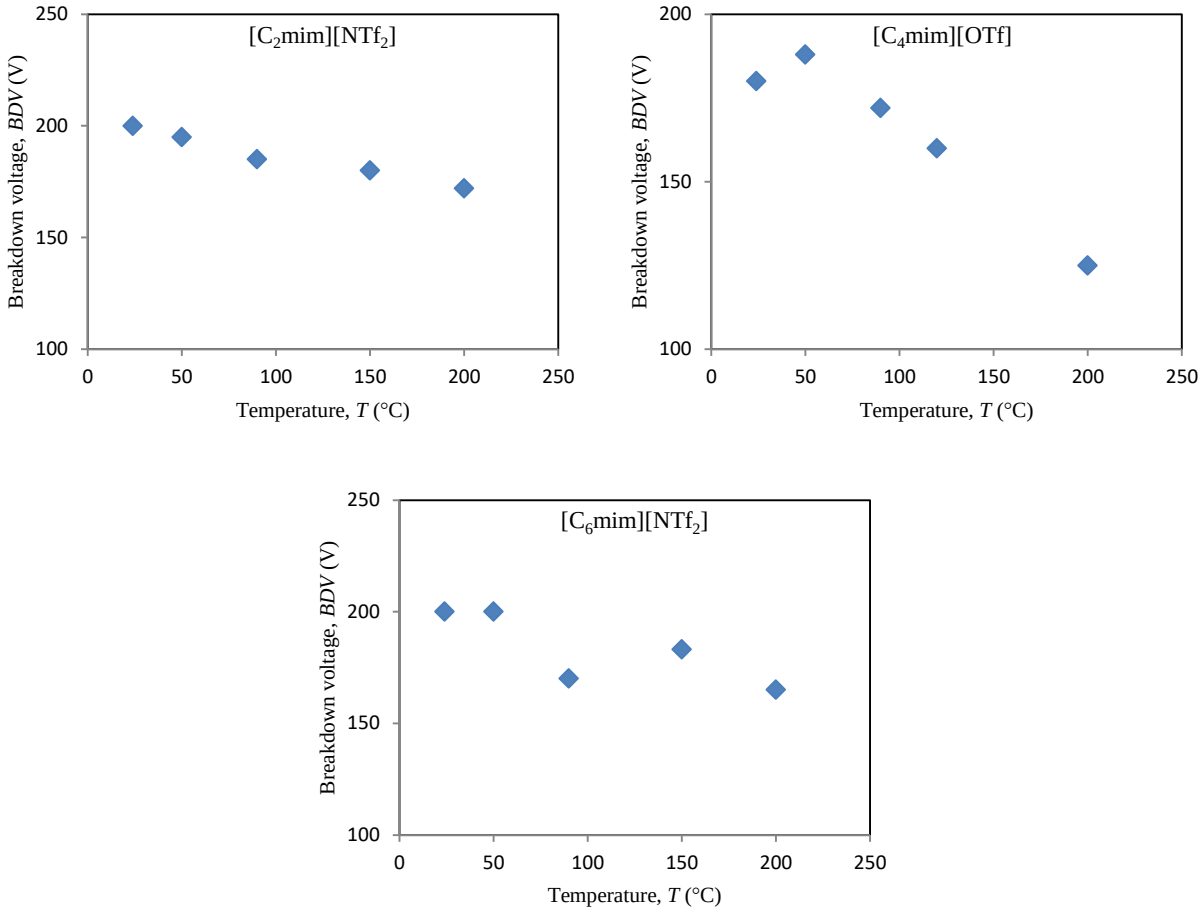

Fig. 30 Temperature dependence of the breakdown voltage on temperature for selected ionic liquids

From Fig. 30 is clear that BDV decreases linearly with temperature in range 50 – 150°C for all compared liquids. On the other hand, both conductance and capacitance increase in all cases (see Fig. 31). Extrapolated data for 200 °C are summarized in Table 7. All liquids were fully stable at 200 °C.

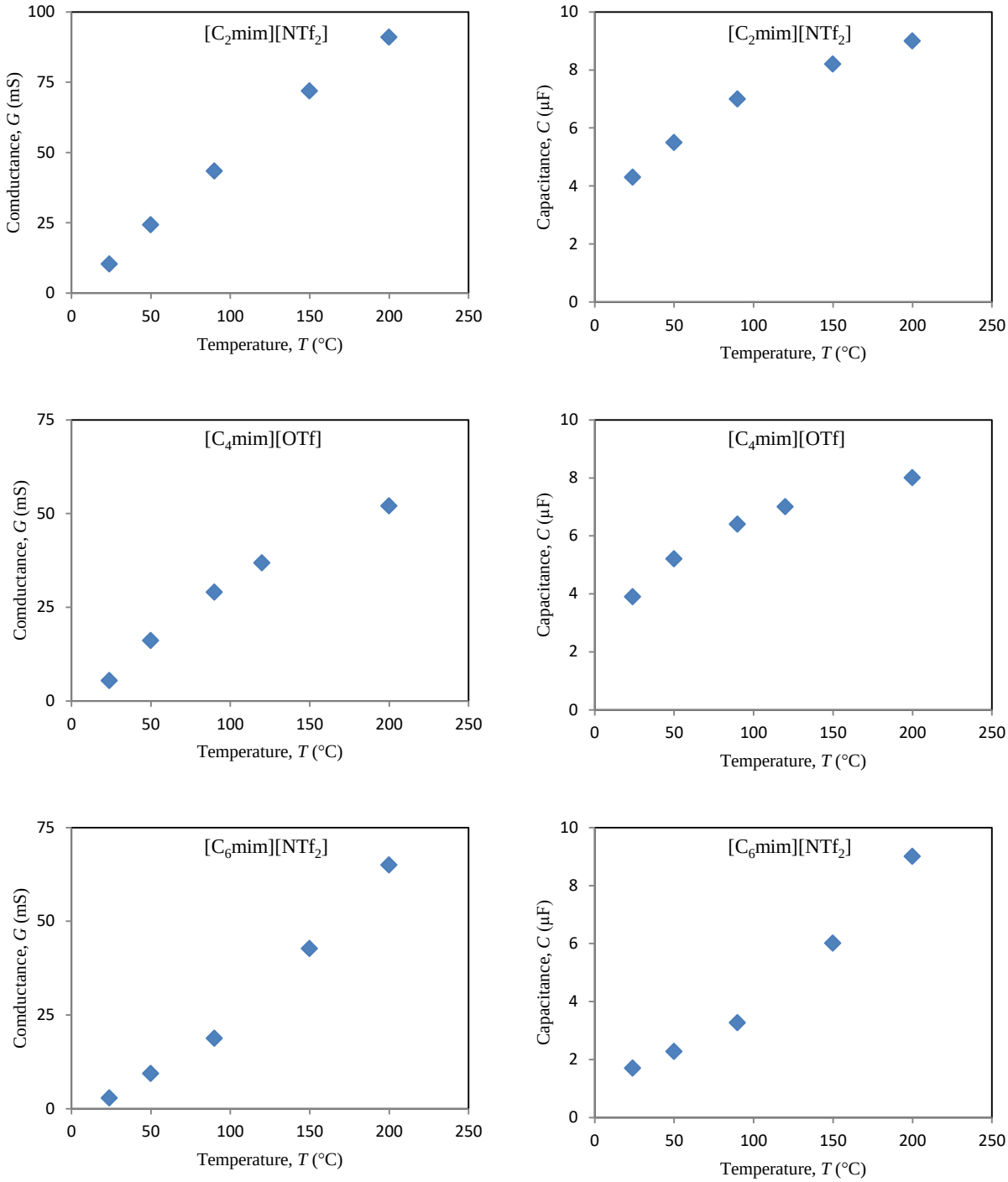

Fig. 31 Temperature dependence of conductance (left column) and capacitance (right column) of studied ionic liquids

Fig. 31 shows temperature dependence of conductance and capacitance of measured capacitors with different ionic liquids. Both values, as can be expected, increase with increasing temperature.

Table 7 Extrapolated data for 200 °C

	BDV (V)	Conductance (mS)	Capacitance (μF)
$[C_2mim][NTf_2]$	172	91	9
$[C_4mim][OTf]$	125	52	8
$[C_6mim][NTf_2]$	165	65	9

6.2.3 Dependence of BDV on conductance of the electrolyte

The experimental fact that the breakdown voltage decreases with conductivity increase can be simulated in the first approximation by the theory of diffusion controlled by electric field which was developed by Onsager [60]. The representative expression of this theory is known in literature as Smoluchowski equation [61]. It describes the relation of the probability of ion dissociation on applied electric field. The theory is not presented here. In Fig. 33 is shown the theoretical plot of the probability as the function of electric field for various distances of ion pairs: the curves from the top – 3.5, 3.2, 2.7 and 1.8 nm. It is clear that the breakdown voltage increases with the decreasing distance of ions in ion-pairs. From this fact we can make a conclusion that high breakdown voltage can be expected in electrolytes with small ions. From this point of view the size and morphology of ions play an important role.

A series of experiment were conducted in order to improve properties of tested capacitor. As electrolytes several groups of materials were used. First properties of capacitors with neat ionic liquids were measured and consequently compared with commercially used electrolytes. Some of the electrolytes were modified by addition of substances which would increase the BDV while preserving its conductivity.

Used materials can be divided into following groups:

Ionic liquids

Electrolytes containing –OH groups

Electrolytes containing additives with –OH groups

All materials and their measured properties are summarized in Table 8 (note that numbers mentioned in this table are “laboratory working marks”).

To construct the comparison graph, impedance spectra and C-V characteristics (step 0.5 V /4s) were measured at system stainless-steel plate/electrolyte/Ta/Ta_2O_5 electrode (D3.3/125/FV350V).

Table 8 Measured properties of different electrolytes

Sample	Electrolyte	Conductance (mS)	BDV (V)	Capacitance (μF)
81	EGN (Glycol-ammonium adipate)	28.20	275	4.51
82	EGN + Glycerine (8:2 vol.)	20.90	295	4.00
83	EGN + 1M H3PO4 (8:2 vol.)	27.30	279	3.46
84	EGN + Cellulose (8:2 vol.)	28.30	274	3.99
85	1-Ethyl-3-methylimidazolium bis(trifluoromethylsulfonyl)imide	10.70	192	4.20
86	1-Ethyl-3-methylimidazolium ethylsulfate	4.81	185	4.13
87	1-Ethyl-3-methylimidazolium hydrogen sulfate	1.13	197	4.21
88	1-Butyl-3-methylimidazolium trifluoromethanesulfonate	3.60	193	4.26
89	1-Butyl-1-methylpyrrolidinium bis(trifluoromethylsulfonyl)imide	2.81	213	4.60
90	1-Methylimidazolium phosphate + phosphoric acid	1.86	254	3.70
91	1-Butyl-3-methylimidazolium tetrafluoroborate	5.68	146	4.30
92	Poly(vinylimidazolium butyl bromide)	4.98	191	4.24
93	Poly(vinylimidazolium methyl iodide)	12.00	179	4.21
95	R3 (0.01M solution of $H_3PW_{12}O_{40}$ in PC (fosfowolframic acid in propylene carbonate)	0.45	354	4.53
98	Methylimidazolium bis(trifluoromethyl sulfonyl)imide	7.39	222	4.21
99	4M H_2SO_4 (in water)	248.00	178	4.34
102	R3 + R8 (0.1M solution of $H_3PMo_{12}O_{40}$ in water) (9:1 vol.) *	1.20	315	4.49
111	R7 (0.1M solution of $H_3PW_{12}O_{40}$ in PC (fosfowolframic acid in propylene carbonate)	53.80	236	4.61
112	R7 + Propylene carbonate (7 : 1 vol.)	32.40	257	4.10
113	R7 + Propylene carbonate (3 : 1 vol.)	23.10	266	4.35
114	R3 + Butoxyethanol (3 : 1 vol.)	0.47	313	3.75

Table 8 - continuation

Sample	Electrolyte	Conductance (mS)	BDV (V)	Capacitance (µF)
115	R3 + Dipropyleneglycol (3 : 1 vol.)	0.30	330	4.14
116	R3 + Diethyleneglycol (3 : 1 vol.)	0.31	349	3.81
117	R3 + propyleneglycol (3 : 1 vol.)	0.36	330	4.47
118	R3 + Poly(ethylene glycol) ($CHCl_3$) (3 : 1 vol.)	0.22	404	3.80
119	R3 + Citric acid (EtOH) – (3 : 1 vol.)	0.94	383	4.14
120	R3 + Buckminster fullerene (toluene), (3 : 1 vol.)	0.60	257	4.15
121	R3 + benzophenone (EtOH), (3 : 1 vol.)	0.86	320	4.16
122	R3 + Tetrachloro-p-benzoquinone, (3 : 1 vol.)	0.67	361	4.74
123	4M H_2SO_4 + Water (3 : 1 vol.)	250.00	183	3.48
124	4M H_2SO_4 + Water (1 : 1 vol.)	320.00	178	3.96
126	0.1M Citric acid in EtOH	0.0003	448	4.47
127	0.1M Citric acid in water	3.62	408	3.82
128	R3 + Citric acid (EtOH, 0.1 M)	0.73	393	4.00
129	Citric acid in EtOH + water, (0.1 M)	1.00	392	4.10
130	4M Citric acid in water	5.42	336	3.64
131	2M Citric acid in water	9.20	365	3.70
132	1M Citric acid in water	2.00	358	3.78
133	4M Citric acid in water + 4M H_2SO_4, (2 : 1 vol.)	160.00	219	3.38
134	4M Citric acid in water + 4M H_2SO_4, (1 : 2 vol.)	242.00	190	3.82
135	R3 + 0.1M Citric acid (EtOH), (2 : 1 vol.)	3.00	395	4.06
136	R3 + 0.1M Citric acid (EtOH), (1 : 2 vol.)	0.13	440	3.74
137	EGN + 0.1M Citric acid (EtOH), (2 : 1 vol.)	22.40	322	3.72
138	EGN + 0.1M Citric acid (EtOH), (1 : 2 vol.)	4.00	368	3.83

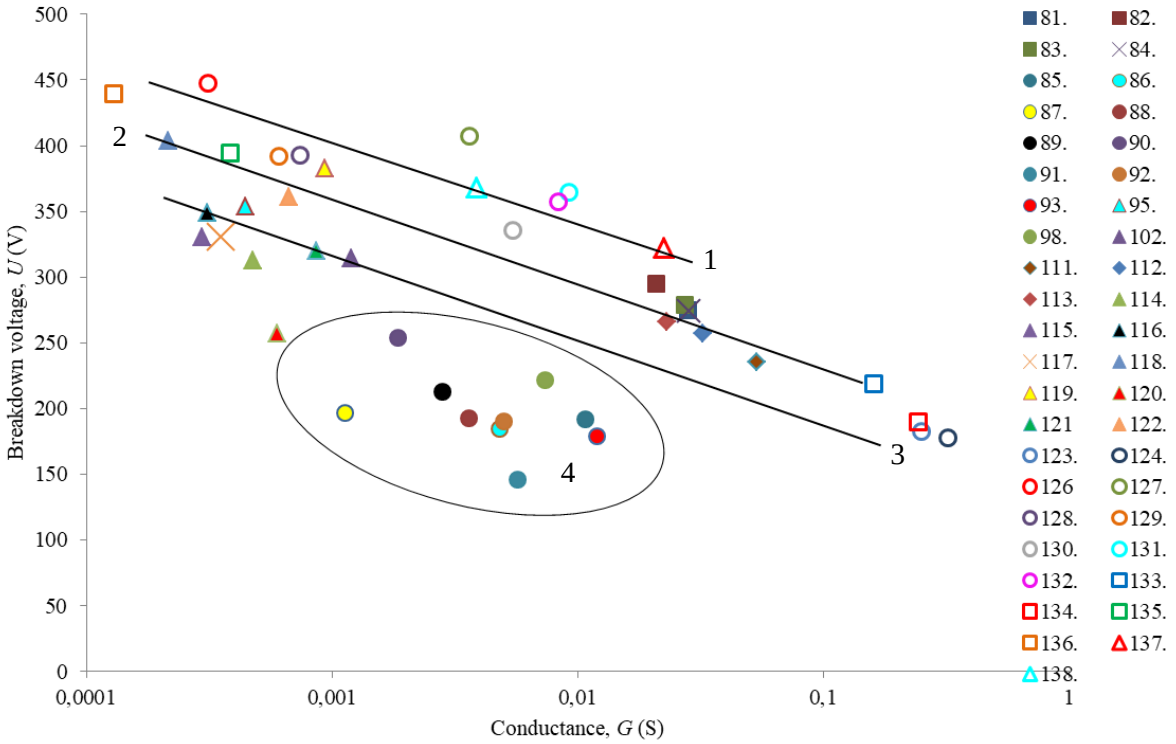

Fig. 32 Dependence of BDV on conductance of studied electrolytes (semi-logarithmic plot); group 1 – electrolytes containing citric acid as an additive, group 2 electrolytes containing molecules with OH groups, group 3 electrolytes containing molecules with OH groups as additives, group 4 – ionic liquids.

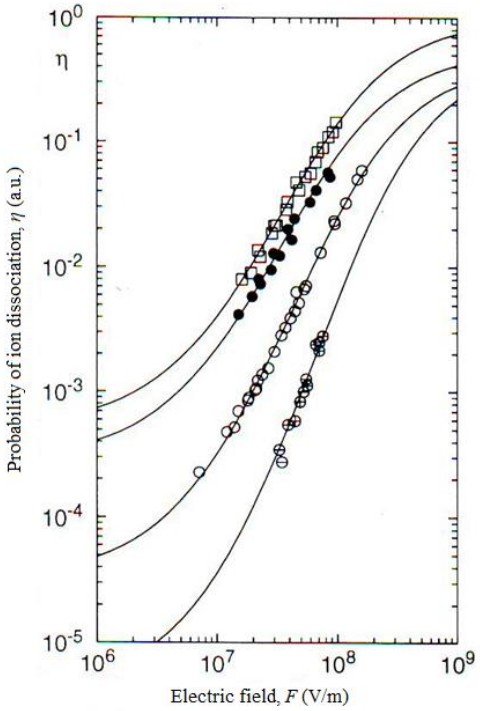

Fig. 33 Dependence of the probability of ion dissociation on electric field for various distances of ion pairs. The curves from the top – 3.5, 3.2, 2.7, and 1.8 nm

Since EGN electrolyte has already been commercially used, let me summarize the influence of additives here. The main interest was focused on finding an additive, which would increase BDV and conductivity. Ideally both of those values, or one of them while the other one would remain the same. Glycerine increases the breakdown voltage from 275 V to 295 V but conductance decreased from 28 to 21 mS. Other additives, like cellulose and H_3PO_4 did not influence either breakdown voltage or conductivity (samples 81 – 84). Citric acid (CA) increases the breakdown voltage to 368 V (322 V – depending on CA concentration) but conductance decreases from 28 to 4 mS (22 mS), respectively. In the first case the volume ratio EGN to citric acid was 2 : 1, in the second case 1 : 2 vol. Comparing the values of breakdown voltages and conductances, a positive influence of citric acid on capacitor parameters can be seen.

To sum up the measured data following conclusions can be done:

1. The highest breakdown voltage [BDV] = 448 V was reached with the system: Electrode D3.3uF / 125V/FV350V / Electrolyte / Stainless steel plate. Electrolyte: Citric acid, 0.1 M ethanol solution. However, the conductivity is low, 0.3 mS/cm.

2. For following electrolytes citric acid (CA) represents a new additive which increases the breakdown voltage [BDV] and maintains the electrical conductivity (σ) nearly at the same level as measured before addition:

H_2SO_4 (4 M, H_2O)	[BDV] = 178 V, σ = 372 mS/cm
H_2SO_4 (4 M, H_2O) + CA (4 M, EtOH), 1 : 2	[BDV] = 190 V, σ = 363 mS/cm
EGN	[BDV] = 275 V, σ = 42 mS/cm
EGN + CA (4 M, EtOH), 2 : 1	[BDV] = 322 V, σ = 33 mS/cm

3. Due to the hydrophility of Ta_2O_5 it is useful to add to the electrolyte a small amount of polymer with hydrophilic groups (e.g., OH groups – [BDV] increases). Low molecular mass materials are not efficient in this way.

4. Concerning ionic liquids - the higher electrolyte conductivity, the lower breakdown voltage. In the first approximation the following formula is valid: [BDV] = A + B log (1/σ), A and B are constants. Electron injection from the electrolyte to Ta_2O_5 layer must be taken into consideration to explain the experimental data. The higher injection efficiency, the lower [BDV].

6.3 Ionic liquid-based amperometric NO_2 sensor

An interesting application is the use of RTILs for the electrochemical detection of various substances in gaseous or liquid phase [62 - 66]. In the recent past, electrochemical sensors based on different ionic liquids have been used for the detection of nitrogen dioxide [67], ammonia [67 - 69], oxygen [70, 71], ozone [67] and ethylene [98]. Unfortunately, the use of ionic liquid in electronic devices requires a specific design and the fabrication of a micro-chamber for the storage of the ionic liquid electrolyte in order to prevent its leakage from the sensor package. This approach was used, e.g., by Stetter et al. [67, 69, 72], for the construction of ionic liquid-based amperometric sensors. Another approach to the preparation of gas sensors with ionic liquid is the use of solid polymer electrolyte (SPE) in which the ionic liquid is immobilized in the polymer matrix [73 - 76]. The experimental results described in this chapter were obtained on this type of sensor for NO_2 detection. Among other advantages, this approach allows the fabrication of a low cost, fully printed, and flexible gas sensor on a PET substrate [76].

The generally accepted overall reaction of NO_2 reduction at the working electrode is [77 - 79]:

$$NO_2 + 2H^+ + 2e^- \rightarrow NO + H_2O \quad (36)$$

However, according to Ref. [43], two-step reduction with the formation of nitrite during the first step is more probable:

$$NO_2 + e^- \rightarrow NO_2^- \quad (37)$$

$$NO_2^- + 2H^+ + e^- \rightarrow NO + H_2O \quad (38)$$

The reaction mechanism may be quite complicated and depends on many factors, such as structure of the electrolyte and properties of the electrode materials. Most probably, water is oxidized at the counter electrode according to reaction:

$$H_2O \rightarrow 2H^+ + 2e^- + 1/2O_2 \quad (39)$$

and the complete reaction in the sensor can be written as:

$$NO_2 \rightarrow NO + 1/2O_2 \quad (40)$$

6.3.1 Influence of the polymer electrolyte conductivity on sensor sensitivity

Based on results obtained in previous part (6.2.1) 1-ethyl-3-methyl imidazolium bis(trifluoromethylsulfonyl) imide [C_2mim][NTf_2], 1- butyl-3-methyl imidazolium trifluoro-methanesulfonate [C_4mim][OTf], and 1-ethyl-3-methylimidazolium tetrafluoroborate [Emim][BF4] were chosen for preparation of solid polymer electrolyte for amperometric NO_2 sensors and their characterisation. The sensor platform was based on a well-established, three electrode topology that was successfully tested and thoroughly described in works [75, 76]. A ceramic substrate with platinum counter (CE) and pseudoreference (RE) electrodes (see Fig. 34) was chosen as a reference electrode layout for the comparative study.

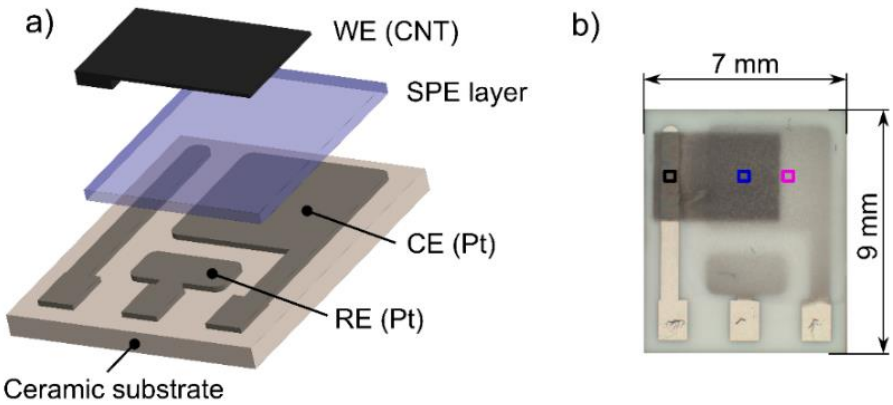

Fig. 34 a) sensor layout; b) photograph of prepared NO_2 sensor (colored squares represent areas captured by SEM microscope in further studies – in section 6.3.2.) [80]

The solid polymer electrolytes (SPEs) in the study were prepared in accordance with the procedure described in [75]. They consisted of a 1:1:3 weight ratio of an ionic liquid, poly-(vinylidene fluoride) (PVDF), and 1-methyl-2-pyrrolidone (NMP), where PVDF was used as polymer matrix and NMP as the solvent of the PVDF. Each SPE formulation with a particular ionic liquid was kept at 70 °C for 3 min to decrease its viscosity. Subsequently, 15 mg of the SPE formulation was drop-casted onto the ceramic substrate (Figure 1), which was then placed on a hot plate (120 °C for 3.5 min). Finally, before the last step of the fabrication process, *i.e.*, the deposition of the carbon working electrode by AJP technology, all samples were kept under laboratory condition for 24 h.

Prepared sensors were tested by means of their electrochemical response to change of NO_2 concentration (sensitivity), which was consecutively put into relation with properties of used ionic liquids and solid polymer electrolytes respectively.

The testing apparatus for the measurement of electrochemical response during NO_2 exposure consisted of two gas tanks (one filled with a mixture of gaseous nitrogen dioxide and synthetic air at a concentration of 100 ppm, and the other one filled with pure synthetic air), three mass flow controllers, and a test chamber. The signal response was measured by the source-measure unit (KEITHLEY 2636). The required concentrations of the analyte (NO_2) were obtained by mixing the nitrogen dioxide mixture with humidified synthetic air. The analyte flow rate was 500 ml/min. The measurements were performed under laboratory conditions (25 °C, 40 % RH).

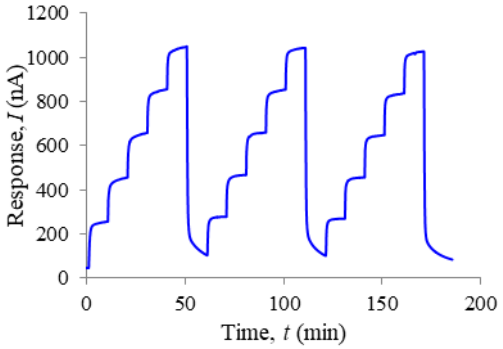

Fig. 35 Measured data of sensor with $[C_2mim][NTf_2]$ based electrolyte - dependence of reduction current ("response") on time, the steps are for concentration change of 1 ppm NO_2

Fig. 35 a shows three consecutive kinetic sets of signal responses for the change in NO2 concentration from 0 to 5 ppm in 1 ppm steps (the working potential was - 500 mV vs. the platinum pseudoreference electrode). It can be seen, that responses are stable and well reproducible even over longer periods of time (tens of minutes) which is significantly better then in chemiresistive organic sensors [81]. From data depicted in Fig. 35 calibration curve of a sensor (see Fig. 36) can be made. First it is necessary to take the value of response of steady state for each measured concentration and then subtract the value of response for zero concentration of analysed gas. Acquired data (dependence of response to concentration of the analyte) were intersected by a line, out of which's slope we get value of sensors sensitivity.

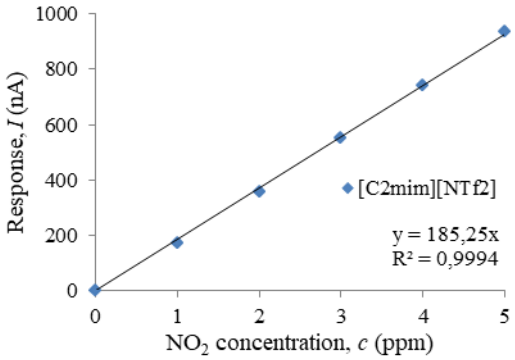

Fig. 36 Calibration curves for the sensor with the ionic liquids [C_2mim][NTf_2], [C_4mim][OTf] and[Emim][BF_4]

Response of all prepared sensors showed good linear behaviour. All parameters of prepared sensors are summarized in Table 9.

Table 9 Properties of prepared sensors and respective ionic liquids.

Ionic liquid	[C_2mim][NTf_2]	[C_4mim][OTf]	[Emim][BF_4]
Sensitivity (nA/ppm)	185	302	286
Reliability (R^2)	0.9994	0.9897	0.9879
IL's AC resistance* (Ω)	71	212	37
Sensors AC resistance* (Ω)	926	361	689
Sensors AC conductance* (mS)	1.1	2.8	1.5
* Determined by Solartron SI 1260			

It follows from Table 9 that sensor sensitivity and electrolyte conductance correlate: the higher the conductance of the electrolyte, the greater the sensor sensitivity. This is not true for the relationship between sensor sensitivity and the conductance of the ionic liquid. Results suggest that the morphology and structure of SPE layers with the ionic liquid additive play an important role in electrolyte conductivity. It is well known, that PVDF, depending on the conditions, can form up to four described crystalline structures [82]. Therefore, next chapter is focused on study of this phenomenon.

6.3.2 Influence of the polymer electrolyte morphology on sensor sensitivity

Preparation of SPE

For this study, five ionic liquids were chosen based on their porperties suitable for good formation of SPE with PVDF:
1-ethyl-3-methylimidazolium bis(trifluoromethylsulfonyl)imide [C_2mim][NTf_2];
1-butyl-3-methylimidazolium trifluoromethanesulfonate [C_4mim][OTf];
1-ethyl-3-methylimidazolium tetrafluoroborate [Emim][BF_4];
1-hexyl-3-methylimidazolium tris(pentafluoroethyl)trifluorophosphate [Hmim][FAP];
1-butyl-1-methylpyrrolidinium bis(trifluoromethylsulfonyl)imide [C_4mpyrr][NTf_2].

Preparation of the SPE layer was the same as in previous chapter i.e. each SPE formulation with a particular ionic liquid was kept at 70 °C for 3 min to decrease its viscosity. 15 mg of the SPE formulation was drop-casted onto the ceramic substrate, which was subsequently placed on a hot plate (120 °C for 3.5 min) and then kept under laboratory condition for 24 h. As a working electrode in this case carbon nanotubes (CNT) layer was deposited by aerosol jet printing technique (AJP).

Gregorio and Borges [82] described the influence of temperature on the crystallization rate. They also described its effect on the formation of the different crystalline phases of PVDF dissolved in NMP and found a relationship between the porosity of the prepared layers and the crystallization temperature. It was observed that β – phase is dominant after crystallization at 25 °C. This phase is composed of spherules with diameter from 7 to 8 μm. On the other hand, crystallization at higher temperature (140 °C) results in formation of α – phase made of spherules with diameter of 10 to 12 μm. The temperature at which both phases are in equilibrium was determined to be 120°C. Based on these observations authors predicted, that higher crystallization temperatures cause the formation of less porous layers due to crystallization of α – phase of PVDF. This prediction was confirmed by series of SEM pictures and infra-red spectroscopy of individual layers. Based on this acknowledgement morphology of prepared SPE was studied more in detail. SPE with [C_2mim][NTf_2] was chosen due to its best properties by means of adhesiveness, film forming properties and properties of the sensor (see Table 9). Preparation of the SPE for morphology study was slightly modified. Four samples were prepared under different crystallization conditions (see Table 10). After deposition samples were again kept under laboratory conditions for 24 h. The morphology and structure of prepared layers were studied scanning electron microscopy (Phenom-World Eindhoven, The Netherlands). Analysed areas are depicted by coloured squares in Fig. 34 b. Picture analysis was carried out using the HarFa computer program [83]. CNT working electrode was deposited subsequently.

Table 10 [C_2mim][NTf_2] SPE preparation conditions for morphology study

Sample	Temperature (° C)	Time (min)
No.1	80	1.5
No.2	120	1.5
No.3	120	3.5
No.4	160	10.0

Working Electrode deposition and characterisation

For the deposition of the carbon nanotube working electrode (WE), new additive technology, Aerosol Jet Printing (AJP), was used. This non-contact, direct-write printing process enables deposition of wide variety of materials to basically any suitable substrate. With the use of

computer-aided design/computer-aided manufacturing (CAD/CAM) software, AJP allows rapid prototyping in a large area of printed electronics [84]. Moreover, this fabrication process significantly reduces ink consumption, which is important for cost reduction when suspensions of noble metals (e.g., Pt and Au) are considered for use as materials for the working electrode. Water-based carbon nanotube (CNT) ink (CNTRENE C100LM, Brewer Science, Rolla, MO, USA) was used for the printing of the working electrode. CNT sensing layers are generally used due to their unique material properties, high surface-to-volume ratio and hollow structure which are ideal for adsorption of gas molecules. In total 4 layers of CNTs were printed one over another, area of the electrode was 10 mm^2, its thickness about 10 – 20 nm (layer was transparent). Pictures of prepared layers were taken using electron microscope a JSM 7600F (JEOL, Peabody, MA, USA) in cooperation with Faculty of electrical engineering at University of West Bohemia and are shown in Fig. 37. Fig. 37a shows the active boundary of SPE/WE electrode, detailed on one spherical object of the SPE covered by thin layer of CNT which could have been taken thanks to very low thickness and high transparency of the layer achieved by using the AJP technique. Fig. 37b shows the detail of CNT layer on a flat surface. It should be noted, that quality, structure and morphology of the working electrode plays an important role regarding the parameters of the sensor and signal response quality.

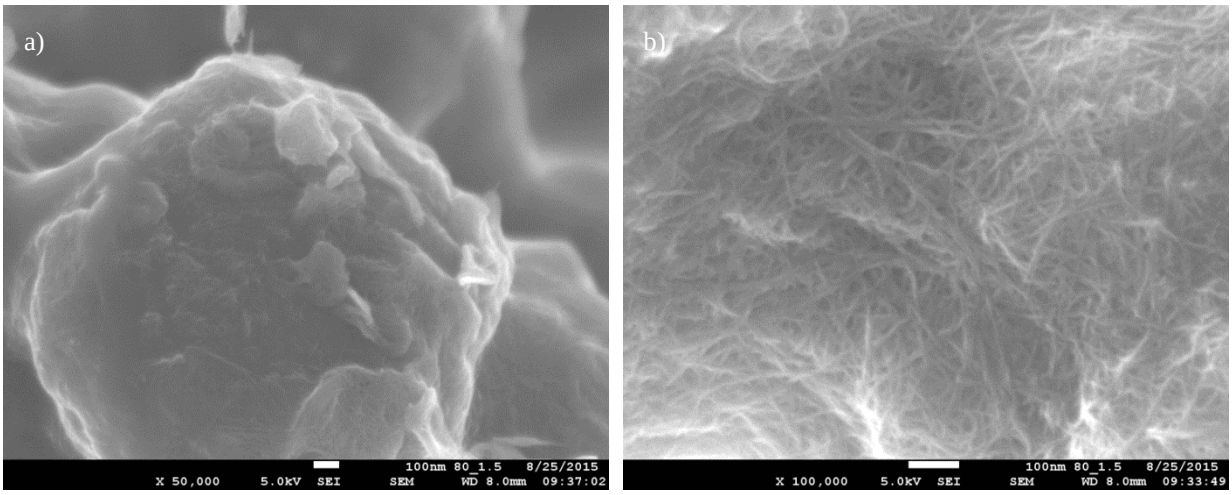

Fig. 37 SEM image of CNT layer
a) active SPE/WE interface - spherical object of SPE covered by CNT layer (magnification 80 000x)
b) detail of CNT layer on a flat surface (magnification 100 000x)

Measurement of sensor characteristics

Parameters of prepared sensors were measured at Faculty of electrical engineering at University of West Bohemia. The gas test system for the measurement of sensor characteristics consisted of two gas tanks (the first filled with a reference mixture of gaseous nitrogen dioxide [100 ppm NO_2] and synthetic air; the second filled with pure synthetic air), five PC-controlled mass flow controllers, and a test chamber which enabled the measurement of six sensors within one experiment. The characteristics of all sensors were measured under identical conditions (unless otherwise stated: 22 °C, 40% RH, analyte flow rate = 500 mL/min). A six-channel evaluation board with configurable analogue front end (AFE) potentiostats (LMP91000, Texas Instruments, Dallas, TX, USA) was used as the electronics read-out. The output analogue voltage level from each potentiostat was sampled every other second by two four-channel 24-bit analogue to digital converters ADC (LTC2493, Linear Technology, New York, NY, USA) and data were subsequently transferred to the PC via a USB bus. The optimal bias voltage, −500 mV·*vs.* the platinum pseudoreference electrode, was obtained from a steady state polarization curve [76]. Even though the potential stability of the

platinum pseudo/quasi-reference electrode is unknown, it has been demonstrated that such sensor can exhibit good response stability during a long term test [75].

Following experiments were focused on the systematic study of five chosen ionic liquids. All sensors were prepared as described in previous sections. SPE layers were formed under same thermal conditions (120°C for 3.5 mins) in order to minimize the effect of thermal history of the sample on its properties. Measured parameters of prepared sensors are summarized in Table 11.

Table 11 Parameters of prepared sensors with different ionic liquids immobilized in SPE

Ionic liquid	Sensitivity (nA/ppb)	Response/recovery time* (s)	Hysteresis ΔI (%)	Limit of detection
$[C_2mim][NTf_2]$	149	(53±3)/(68±3)	7	0.9
$[C_4mim][OTf]$	48	(70±4)/(74±4)	5	2.0
$[Emim][BF_4]$	59	(64±3)/(90±3)	5	1.6
[Hmim][FAP]**	--	(43±3)/(38±3)	42	--
$[C_4mpyrr][NTf_2]$	91	(46±3)/(44±3)	13	0.3

* Average values with 99% confidence interval were calculated from five consecutive exposures.

** Sensitivity and LOD of the sensor were not determined because of the non-linear calibration curve resulting from the instability of the sensor response.

Sensor characterisation consisted of two basic tests. First, sensors were tested under repeated exposure to constant concentration of NO_2 (see Fig. 38a), followed by measurement of response to stepwise increase and decrease of NO_2 concentration (see Fig. 38b).

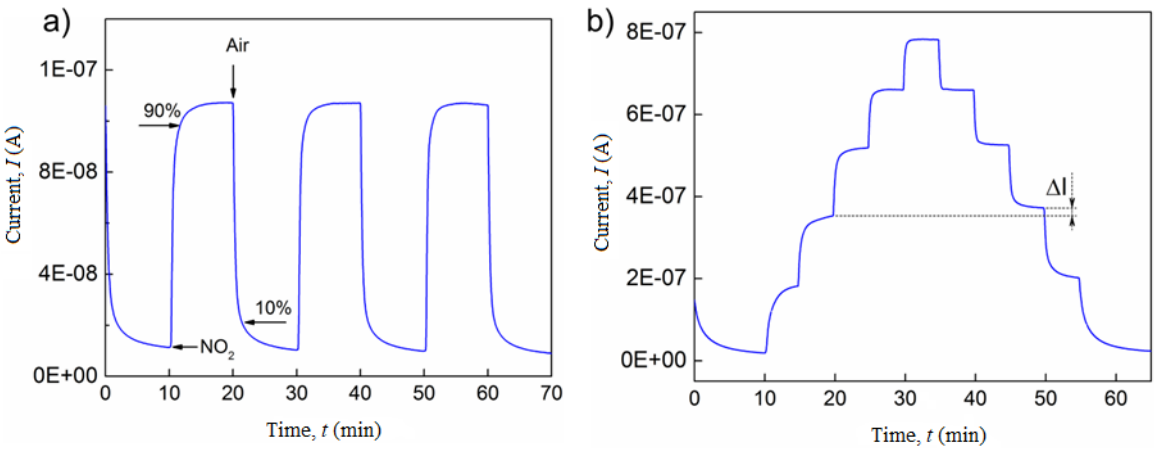

Fig. 38 Response of prepared sensors to:
a) repeated exposure to constant NO_2 concentration of 1ppm – used IL $[C_4mpyrr][NTf_2]$
b) stepwise increase/decrease of NO_2 concentration – used IL $[C_2mim][NTf_2]$

The response/recovery times and hysteresis of the sensors response were determined following the usual procedure: the response time is defined as the time in which response signal reaches 90% of its steady state value after exposure to the analysed gas. Recovery time describes the time period after which response signal drops to 10 % of its original value (steady state) after exposition to pure air (without analysed gas, see Fig. 38a). The hysteresis of each sensors response is defined as the difference between the output currents for the same NO_2 concentration during its stepwise increase followed by stepwise decrease (Fig. 38b). The maximum difference was related to the upper limit of the measured current and expressed as a percentage (Table 11).

The other parameters - the sensitivity and the theoretical limit of detection (LOD), were calculated from the calibration curves of the particular sensors (see Fig. 39). The sensitivity was determined as the slope of the calibration curve, and the LOD was taken to be equal to:

$$3rms_{noise}/slope \tag{41}$$

where rms_{noise} is the root-mean-square noise of the baseline. It should be noted that the actual LOD values may differ from those calculated according to the above mentioned expression because the activation of the working electrode surface (or the interface SPE/WE) may require a minimal amount of analyte. The sensitivity of sensors was studied within a low concentration range from 0 to 1 ppm (Fig. 39), where the NO_2 concentration was increased in the following steps: 200, 400, 600, 800 and 1000 ppb. The calibration curves of the sensors in Fig. 39 were obtained and compared using a normalization approach, according to equation 42:

$$I = I_{ss} - I_0 \tag{42}$$

where I_{ss} represents the steady state current response of the sensor under analyte exposure of given concentration and I_0 is the "background current" i.e. response current when the sensor is exposed to pure air. Table 11 provides an overview of the key sensor parameters for all tested ionic liquids.

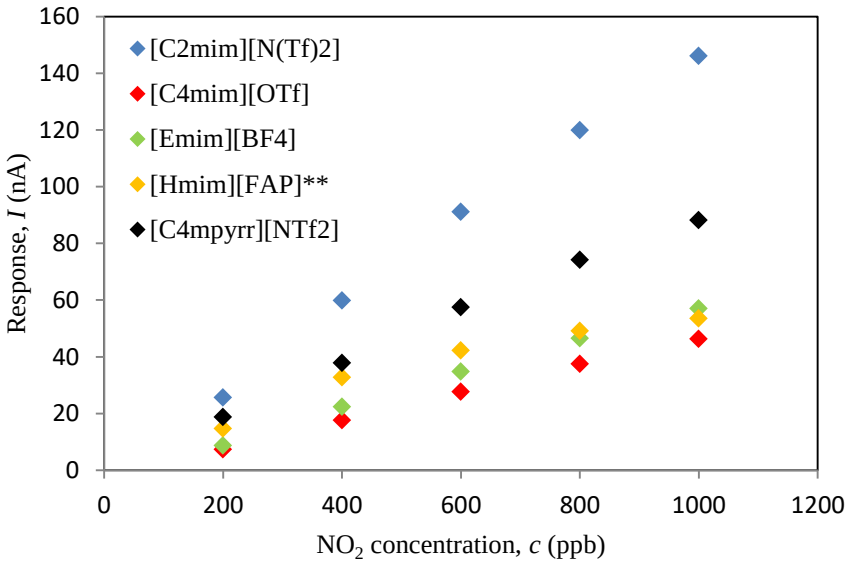

Fig. 39 Dependence of sensor current on NO_2 concentration for different ILs immobilized in SPE layer.

The highest sensitivity was found for the sensor based on [C_2mim][NTf_2] ionic liquid, the lowest LOD was obtained for the sensor based on [C_4mpyr][NTf_2] (due to the lowest rms_{noise} of the background current). Response/recovery times were in the order of tens of seconds for all sensors. The levels of hysteresis were acceptable for all tested sensors except the sensor based on [Hmim][FAP] ionic liquid - its value was influenced by the instability of the sensor response, which can be, among others, observed in Fig. 39. It is clear, that response to rising NO_2 concentration does not show linear behaviour in this case. This effect was probably caused by poor film forming properties of prepared SPE.

The sensor based on [C_2mim][NTf_2] ionic liquid was selected for further detailed study because it exhibited the highest sensitivity, a fast response/recovery time, an acceptable hysteresis level and because of the good film-forming properties of the SPE formulation in terms of the absence of defects in the SPE layer after thermal treatment and good adhesion to the ceramic substrate (electrodes)

Morphology of SPE Layer

Further detailed study of sensor based on [C_2mim][NTf_2] ionic liquid consisted of preparation of 4 sensors under different thermal condition (crystallization of SPE, see Table 12). Following study was carried out to obtain additional information about relation between sensitivity of the sensor and morphology of SPE.

Table 12 [C_2mim][NTf_2] based sensor – conditions of preparation and properties

Sample	SPE preparation conditions	Sensitivity (pA/ppb)
1	80°C 1.5 min	381
2	120°C 1.5 min	301
3	120°C 3.5 min	206
4	160°C 10 min	106

Sensitivity of each prepared sensor was measured using the same apparatus and setup as in previous set of experiments. In Fig. 40 calibration curves of prepared sensors are shown. It can be seen, that sensitivity of the sensor strongly depends on conditions, under which the sensor has been prepared.

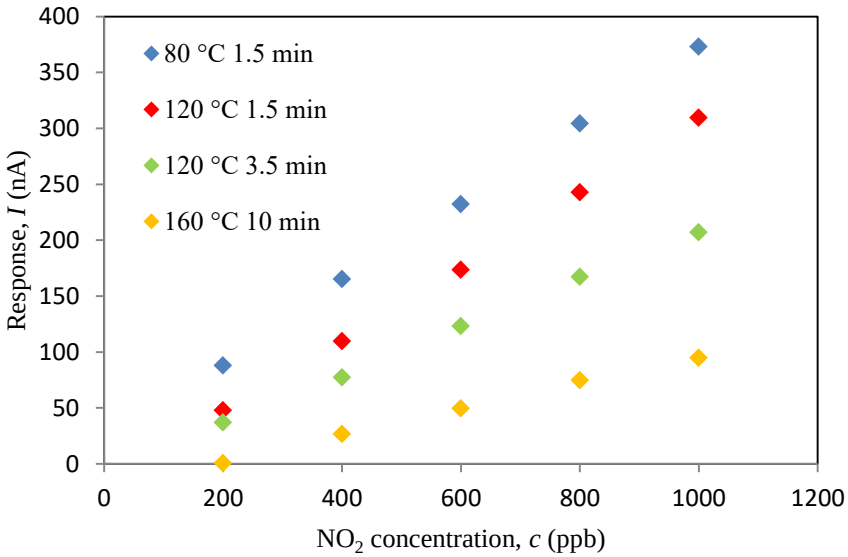

Fig. 40 Dependence of sensor response on NO_2 concentration for different thermal treatment conditions during the formation of the SPE layer with [C_2mim][NTf_2] ionic liquid: sample No. 1, 80 °C for 1.5 min; sample No. 2, 120 °C for 1.5 min; sample No. 3, 120 °C for 3.5 min and sample No. 4, 160 °C for 10 min.

Pictures of prepared sensors are depicted in Fig. 41. It can be seen that treatment under different thermal conditions has effect on structure of prepared layers and their appearance. It can be observed, that with increasing temperature and time, SPE layer changes from opaque to transparent. This fact is in good agreement with the theory of different crystal phase growth.

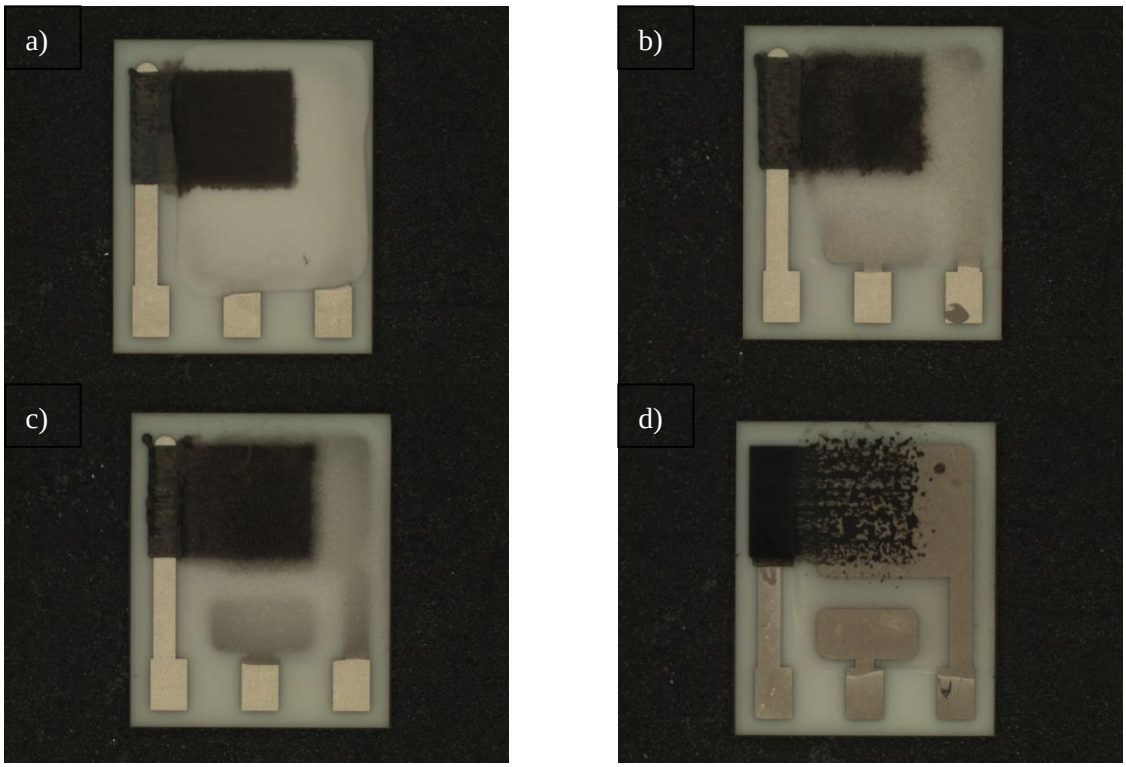

Fig. 41 Pictures of prepared sensors based on [C_2mim][NTf_2] under different thermal treatment conditions:
a) 80 °C, 1.5 min; b) 120°C, 1.5 min
c) 120°C, 3.5 min; d) 160 °C, 10min.

Fig. 42 shows SEM pictures of prepared SPE layers. This picture is a confirmation of changes in inner structure of SPE layers caused by different thermal treatment. The surface of the most sensitive layer (Fig. 42a, treatment 80 °C, 1.5 min) is made of smaller spherical objects, the active surface is large, and the surface structure is very ragged. In contrast, the surface of the least sensitive layer (Fig. 42d, treatment 160 °C, 10 min), as can be seen, is predominantly made of large crowded and deformed spherical objects. It follows that the active surface is much smaller and the complexity of the edge structure is significantly reduced.

In order to find the relation between the size and deformation of the objects and sensor sensitivity the method of fractal image analysis was used. It is possible to determine the active surface area and its complexity of edge structure (topological entropy), respectively by use of the fractal measure and fractal dimension [85, 86]. The HarFA 5.1 computer program [83] was used to calculate the fractal parameters. By applying the method of box counting, which is based on wavelet analysis (the Haar transformation) [87], it is possible to determine areas of the surface in different depth from the SPE surface (contour lines areas) and their complexity.The Haar transformation is an integral transformation with a base of "square-shaped" functions. Wavelet analysis is similar to Fourier analysis in the sense that it allows a target function over an interval to be represented in terms of an orthonormal function basis.

"The principle of the wavelet method is based on the screening of black and white images. The screening can be generally performed by low level filtering. In the case of the Haar transformation, it can be calculated simply by averaging the nearest four pixels (or squares of screened image)." [80]

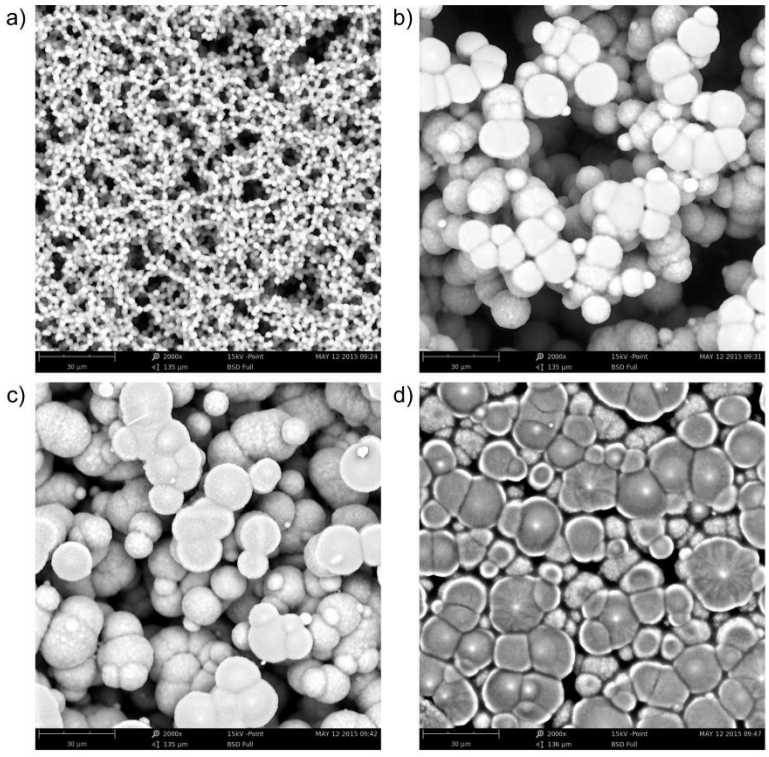

Fig. 42 Morphology of the SPE layers based on [EMIM][NTf_2] ionic liquid under different thermal treatment conditions (Phenom ProX electron microscope, magnification 2000×):
a) 80 °C for 1.5 min; b) 120 °C for 1.5 min;
c) 120 °C for 3.5 min; d) 160 °C for 10 min.

Surface areas in planes of different depths and their complexity influence the activity of the SPE surface. The calculation of the parameters by the box counting method is based on the known expression:

$$N_{px} = K r_{sq}^{D_F} \tag{43}$$

where N_{px} is the number of pixels, K is the fractal measure, r_{sq} is the size of squares (in pixels) and D_F is the fractal dimension. This relationship describes the dependence of number of squares with defined properties (*i.e.*, whether they are all black, all white, or contain both black and white pixels *etc.*) in the threshold image on their dimension. From the logarithmic dependencies of equation 43 for various sizes of squares (1 × 1, 2 × 2, 4 × 4, 8 × 8, …, pixels), it is possible to use a linear regression in order to determine both fractal parameters—fractal measure K and fractal dimension D_F — for all cases with three independently defined properties (BBW—black area including interface, WBW — white area including interface, and BW—area of interface). From the fractal measures K_{BBW}, K_{WBW}, and K_{BW}, the relative areas A_B (number of pixels in the black area), A_W (number of pixels in the white area), and A_{BW} (number of pixels in contour line) can be calculated according to the expressions:

$$A_B = \frac{K_{BBW} - K_{BW}}{K_{BBW} + K_{WBW} - K_{BW}} \tag{44}$$

$$A_W = \frac{K_{WBW} - K_{BW}}{K_{BBW} + K_{WBW} - K_{BW}} \tag{45}$$

$$A_{BW} = \frac{K_{BW}}{K_{BBW} + K_{WBW} - K_{BW}} \tag{46}$$

These areas are usually normalized to 1, *i.e.*, $A_B + A_W + A_{BW} = 1$. The maximal fractal measure has the value of $K_{max} = K_B + K_W + K_{BW}$ = (1024 × 1024) pixels. Using a similar procedure it is possible to determine the relation between Hausdorff fractal dimensions and the complexity of the surface structure expressed by means of topological entropies:

$$S_{BBW} = D_{BBW} \ln r_{sq} \tag{47}$$

$$S_{WBW} = D_{WBW} \ln r_{sq} \tag{48}$$

$$S_{BW} = D_{BW} \ln r_{sq} \tag{49}$$

or by their deviations from a plane surface ($D_F = 2$). Here, D_{BBW}, D_{WBW}, and D_{BW} are the fractal dimensions of the black area including interface, the white area including interface, and the area of interface, respectively.

As a way of measuring surface area two-dimensional image analysis was applied to a 3-dimensional material following way. Black areas were taken as a zero level. The space bounded by “black” area and sensor surface (the whitest places in microscopic image) were cut into 250 slices.

Positions of cut parts are given in Fig. 43 and Fig. 44 as threshold levels. The black part of the microscopic image - the deepest level is positioned to zero. From each slice the total area (A_{BW}) of parts of spherical objects visible from the direction of the sensor surface, sum of the circumferences of spherical objects (relief division) were determined. Therefore, fractal dimension on the position of the threshold level (*i.e.*, in 3-dimensional space) is known as well. The total “active surface area” of the sensor and its entropy were determined by counting up the areas.

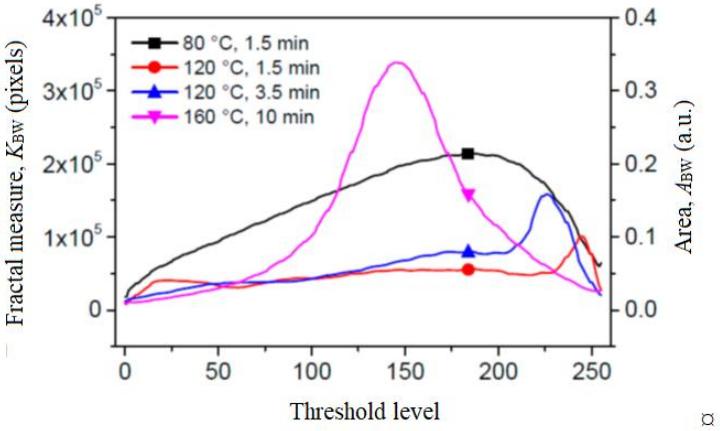

Fig. 43 Dependence of the fractal measure of the surface between contour lines (threshold levels) on the magnitude of the threshold of grey scale images for sensors with differently thermally treated SPE layers

Fig. 43 shows the dependence of the fractal measure of the surface between contour lines (between threshold levels) on the threshold level of the "grey scale" image. The threshold level is the position of the contour line; it is defined as "0" in the bulk of the SPE layer—the maximal depth accessible by microscope (black colour); "255" was set for the surface of SPE layer. Concerning the sensitivity profile of SPE, the most sensitive "layer" is located at the threshold level "180". At this depth the active sensor area is the greatest.

The dependence of fractal measure on threshold level is influenced by two parameters. The first parameter is the active area of the sectional plane which influences the sensitivity of the sensor at the respective distance from the electrolyte surface. The second parameter is the area which characterizes the deformation of the objects – this contribution decreases the sensor sensitivity. It should be noted that the fractal measure is positive in both cases. Each curve in Fig. 43 contains both contributions with different benefits.

No deformation of objects was observed for the sample treated at 80 °C for 1.5 min (structure (a) in Fig. 42, black curve in Fig. 43). The fractal measure for this sensor is high and therefore it is highly sensitive. On the other hand, analysis of the sample as treated at 160 °C for 10 min (structure (d) in Fig. 42, magenta curve in Fig. 43) showed that the deformation contribution is dominant in this case. The maximum of the deformation activity is at the threshold level "145", *i.e.*, deeper than the maximum of the sensitivity for the sample which was thermally treated at 80 °C for 1.5 min. This fact results in low sensitivity of the prepared sensor. The deformation depth is extended up to about 40% of the "visible" depth.

Both active (sensitivity) and deformation contributions are visible for the sensors in which the thermal treatment of SPE was carried out at 120 °C for 1.5 min (structure (b) in Fig. 42 , red curve in Fig. 43) and at 120 °C for 3.5 min (structure (c) Fig. 42, blue curve in Fig. 43) . The threshold levels with higher deformation activities are located near the sensor surface; the maxima of the "deformation" peaks are positioned at the threshold level "245" (red curve) and "225" (blue curve). The threshold active levels with the highest "sensitivity" have a position at about "180". Therefore, it can be concluded that the highest sensitivity of the sensor is not at the SPE/working electrode boundary but in a certain distance from the SPE surface. From this distance to the SPE surface, the "deformation areas" occur, *i.e.*, regions where spherical objects of SPE are deformed, aggregated or crowded. Taking into account

both sensitivity and deformation contributions, the calculated progression of the sensitivity agrees well with experimental results.

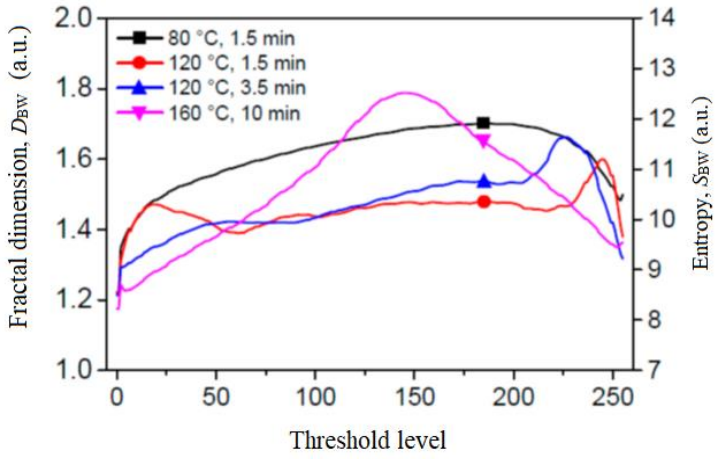

Fig. 44 Dependence of the fractal dimension on the threshold images boundary (resp. surface inhomogeneity expressed as topological entropy) on the threshold level of greyscale images.

Fig. 44 shows the dependence of the fractal dimension of the boundary on the threshold images corresponding to the edge relief of the surface expressed as topological entropy on the threshold level. The conclusions from this figure are in good agreement with those following from Fig. 43.

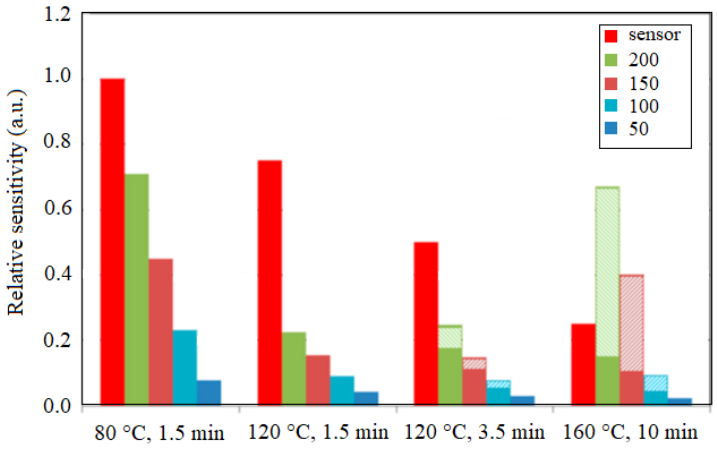

Fig. 45 Experimental relative sensitivities of repared sensors (red columns). Calculated relative active (sensitivity) areas (full columns) and deformation contribution areas (hatched columns). Differently coloured columns indicate the contributions below the defined threshold level.

Fig. 45 compares the experimental and theoretical results. Red columns indicate the relativized experimental sensitivities (highest sensitivity is equal to 1 and the rest is expressed as percentage of it) of prepared structures from Fig. 42. All the full columns (except red) indicate contributions to sensitivity of the sensor under defined threshold levels. Hatched columns indicate the contribution of deformation, which leads to the decrease of the sensor sensitivity. The calculated relative active areas (full columns) below the defined threshold levels ("50"—dark blue columns, "100"—light blue columns, "150"—brown columns, and "200"—green columns) agree well with the experimental progression of the sensor sensitivity. The same is true for areas, which cause the decrease of sensitivity.

It can be seen, that the sensitivity is strongly influenced by the thermal treatment during and after deposition of sensing layer. Changes in structure are visible by an eye (see Fig. 40) and

this observation was confirmed by SEM analysis (Fig. 42). Increased temperature and/or prolonged time of treatment can both lead to the deformation of SPE objects (crowding, clustering *etc*.). Deformation in this case results in decrease of sensitivity. The deformation started at 120 °C for time of 3.5 minutes and became more significant for longer times and higher temperatures.

7 Conclusions

Presented thesis is focused, in general, on study of electrical and dielectrical properties of ionic liquids and possibilities of their use in field of capacitors and electrochemical sensors.

Theoretical part of thesis describes basic properties of ionic liquids (e.g. conductivity, viscosity and their temperature dependencies, electrochemical window), and description of parameters important for use in capacitors and sensors.

Experimental part can be divided into two main parts. In the first part all ionic liquids and other materials suitable for use as electrolytes for capacitor (for comparison) were characterised by means of C-V measurements and impedance spectroscopy. Relationship between conductance, capacitance and breakdown voltage was observed and evaluated. Additionally, chosen electrolytes were modified in order to improve their properties concerning BDV.

Results showed decreasing values of BDV with increasing conductivity. Ionic liquids, in comparison with practically used electrolytes, showed the same type of behaviour, but values of BDV were in general lower. Out of different additives, best results were achieved by addition of citric acid solution. In case of H_2SO_4 electrolyte, BDV was increased by 6 %, in case of EGN electrolyte, BDV was increased by 14 %, while conductance of both remained comparable.

In second part, a systematic study of an electrochemical NO_2 sensor with an ionic liquid-based solid polymer electrolyte and an aerosol jet printed carbon nanotube working electrode was performed.

First experiments were focused to determine influence of addition of ionic liquid into solid polymer electrolyte (SPE) on sensors sensitivity. Based on results another set of sensors was prepared to evaluate the effect of thermal treatment of prepared SPE layers on its morphology and sensitivity.

In this case contrary to original assumption – the most conductive ionic liquid would form SPE layer with best sensitivity – best sensitivity showed sensor based on 1-butyl-3-methylimidazolium trifluoromethanesulfonate ([C_4mim][OTf]). From performed IS analysis it was found out, that most important role plays conductivity of whole SPE layer, which was, in case of [C_4mim][OTf], the highest.

Following experiments focused on study of relationship between morphology of SPE layer and sensitivity showed, that the sensor with 1-ethyl-3-methylimidazolium bis(trifluoromethylsulfonyl)imide ([C_2mim][NTf_2]) exhibited the best sensitivity among all studied samples. The lowest sensitivity was exhibited by the sensor with the ionic liquid 1-butyl-3-methylimidazolium trifluoromethanesulfonate ([C_4mim][CF_3SO_3]). It was found, that thermal treatment during and after deposition of SPE strongly influences its morphology and sensitivity. The longer heating time and higher temperature increase deformation and crowding of PVDF sphere-shaped objects resulting in decrease of sensors sensitivity. From picture analysis of prepared SPE layers is apparent, that sensors sensitivity depends on fractal dimensions of PVDF objects in SPE. The most sensitive sensor was prepared by thermal treatment at 80°C for 1.5 mins. This layer exhibited the highest area of PVDF spherical objects (sensitive area) and no deformation area. Thermal treatment at 160°C for 10 minutes resulted in highly deformed structure. Sensitivity was 3.5 times lower than in the first case.

Regardless the thermal treatment, it was observed, that the highest contribution to sensitivity of the SPE layer was from “deeper” layers in the bulk.

8 Used symbols

η viscosity
Λ molar conductivity
z valence of charge carriers
e_0 elementary charge
N_A Avogadro number
k_B Boltzmann constant
F Faraday constant
D diffusion coefficient
r effective radius
V volume
σ specific conductivity
N number of charge carriers
ρ density
P_M molar polarisation
α polarizability
T temperature
β degree of dissociation
U_{IE} interaction energy
E_{CL} cathodic limiting potential
E_{AL} anodic limiting potential
C_d double-layer capacitance
Q charge
C capacitance
S area of parallel capacitor plates
d distance between plates
ε permittivity of dielectric material
ε_0 permittivity of vacuum
W energy of capacitor
P power of capacitor
V_i initial voltage
V_f final voltage
R_e internal resistance of capacitor
I current
E electrode potential
E_0 standard hydrogen electrode potential
n number of exchanged electrons
α_i activity of ions
J_i ionic current
J total current
F_S strength of electric field
U applied voltage
L thickness of the film
FV forming voltage
E_g energy gap of oxide
J_e primary current density of injected charge carriers

r_l recombination length
R_c recombination constant
G conductance
BDV breakdown voltage
λ destruction thickness
K sensitivity of the sensor
δ_H hysteresis of the sensor
t_{10} recovery time
t_{90} response time
WE working electrode
CE auxiliary electrode
RE reference electrode
A surface area of the working electrode
δ Nernst diffusion layer
c concentration of the analyte
k_0 standard heterogeneous velocity constant
α_{CT} charge-transfer coefficient
E_C^0 normal potential
Z impedance
Y admittance
φ phase shift angle
R_s resistance
X_s reactance
G_p conductance
B_p susceptance
ω angular frequency
C' real part of complex capacity
C'' imaginary part of complex capacity
S_{AC} active surface
l distance between electrodes
rms_{noise} root mean square noise of the baseline
I_{ss} current response of the sensor under exposure to analyte
I_0 background current
N_{px} number of pixels
K fractal measure
r_{sq} size of squares
D_F fractal dimension
A_B number of pixels in black area
A_W number of pixels in white area
A_{BW} number of pixels in contour line
D_{BBW} fractal dimensions of the black area including interface,
D_{WBW} white area including interface
D_{BW} area of interface
S topological entropy

9 List of tables

Table 1 Summary of factors determining the conductivity of electrolyte solution. 13
Table 2 List of ionic liquids used for experimental studies. 36
Table 3 Typical vibrations in (cm^{-1}) of ionic liquids (1 – 7) under study. The numbers in the first line correspond to the number of ionic liquid (see Table 2) 38
Table 4 Determined temperature of thermal stability for „safe“ use of studied ionic liquids. 43
Table 5 Summary of measured properties of ionic liquids under study, system Pt plate | Ionic liquid | V68 W15311WC. 45
Table 6 Measured parameters at 123 Hz for system Pt plate | Ionic liquid | V68 W15311WC. 46
Table 7 Extrapolated data for 200 °C 50
Table 8 Measured properties of different electrolytes 51
Table 9 Properties of prepared sensors and respective ionic liquids. 57
Table 10 [C_2mim][$N(Tf)_2$] SPE preparation conditions for morphology study 58
Table 11 Parameters of prepared sensors with different ionic liquids immobilized in SPE 60
Table 12 [C_2mim][$N(Tf)_2$] based sensor – conditions of preparation and properties 62

10 List of figures

Fig. 1 Cations and anions used in ionic liquids 7
Fig. 2 Scheme of cell for measurement of conductivity by impedance spectroscopy 9
Fig. 3 Linear sweep voltammogram as typically observed. Note that two separate voltammograms are indicated here. Taken from [4] 14
Fig. 4 Electrochemical windows of [Emim][BF_4] estimated with various reference electrodes. Taken from [4] 15
Fig. 5 Linear sweep voltammogram of TMPA-TFSI with different amount of water. Working electrodes: (a) Pt and (b) GC. Scan rate is 50mV/s. Taken from [4]. 16
Fig. 6 Energy structure and charge distribution of [metal | oxide | electrolyte] structure without applied voltage. 19
Fig. 7 Energy structure and charge distribution of [metal | oxide | electrolyte] structure under the applied voltage 20
Fig. 8 Scheme of measurement setup 23
Fig. 9 Dynamic parameters – response and recovery time 25
Fig. 10 Basic setup of an infrared sensor [40] 26
Fig. 11 Absorption spectra of several chosen gasses 26
Fig. 12 Section of a semiconductor sensor 27
Fig. 13 Thermocatalytic sensor – pellistor [40] 28
Fig. 14 Classification of electrochemical sensors 28
Fig. 15 Scheme of potentiostatic connection of three electrode amperometric sensor 30
Fig. 16 Scheme of the Lambda sensor 30
Fig. 17 Topology of electrodes: a) planar structure b) “sandwich” structure 31
Fig. 18 Quasi-plannar structure 32
Fig. 19 Development of a stationary concentration gradient near planar electrode limited by transport of electroactive substance to electrode („transport limit“), b) rate of electrode reaction („kinetic limit“)[53, 55] 34
Fig. 20 series (left) and parallel connection of an RC circuit 37
Fig. 21 Frequency-response analyser Solartron SI 1260 (left), Solartron dielectric interface 1296A module (right) [59] 38
Fig. 22. Infrared spectra of ILs under study. . Sample 1 – top left, sample 2 – top right, sample 3 – the second row left, sample 4 – the second row right, sample 5 – the third row left, sample 6 – the third row right. 39
Fig. 23 UV-VIS spectrum of ionic liquid [C_2mim][HSO_4]. The arrow shows the possition of the maximum of the absorption band. Small spikes are of spectrophotometer errors. 40
Fig. 24 UV-VIS spectra of ILs (in water) under study. Sample 1 – top left, sample 2 – top right, sample 3 – the second row left, sample 4 – the second row right, sample 6 – the third row left, sample 7 – the third row right. 41
Fig. 25 UV-VIS spectra of ILs under study (in hexane). Sample 1 – top left; 2 – top right; 3 – the second row left; 4 – the second row right; 5 – the third row left; 6 – the third row right; 7 – down. ... 42
Fig. 26 TGA/DSC curve of ionic liquid [C_2mim][NTf_2] 43
Fig. 27 Dependence of impeadance on frequency of chosen ionic liquids, H_2SO_4 is added for comparison. 44
Fig. 28 Dependence of phase degree on frequency of chosen ionic liquids, H_2SO_4 is added for comparison. 45
Fig. 29 C-V characteristics of [C_4mim][OTf] at different temperatures in semi-logarithmic scale. 47

Fig. 30 Temperature dependence of the breakdown voltage on temperature for selected ionic liquids 48
Fig. 31 Temperature dependence of conductance (left column) and capacitance (right column) of studied ionic liquids..... 49
Fig. 32 Dependence of BDV on conductance of studied electrolytes (semi-logarithmic plot); group 1 – electrolytes containing citric acid as an additive, group 2 electrolytes containing molecules with OH groups, group 3 electrolytes containing molecules with OH groups as additives, group 4 – ionic liquids. 53
Fig. 33 Dependence of the probability of ion dissociation on electric field for various distances of ion pairs. The curves from the top – 3.5, 3.2, 2.7, and 1.8 nm 53
Fig. 34 a) sensor layout; b) photograph of prepared NO_2 sensor (colored squares represent areas captured by SEM microscope in further studies – in section 6.3.2.) [80] 56
Fig. 35 Measured data of sensor with $[C_2mim][NTf_2]$ based electrolyte - dependence of reduction current ("response") on time, the steps are for concentration change of 1 ppm NO_2..... 56
Fig. 36 Calibration curves for the sensor with the ionic liquids $[C_2mim][NTf_2]$, $[C_4mim][OTf]$ and$[Emim][BF_4]$..... 57
Fig. 37 SEM image of CNT layer a) active SPE/WE interface - spherical object of SPE covered by CNT layer (magnification 80 000x) b) detail of CNT layer on a flat surface (magnification 100 000x) 59
Fig. 38 Response of prepared sensors to: a) repeated exposure to constant NO_2 concentration of 1ppm – used IL $[C_4mpyrr][NTf_2]$ b) stepwise increase/decrease of NO_2 concentration – used IL $[C_2mim][NTf_2]$ 61
Fig. 39 Dependence of sensor current on NO_2 concentration for different ILs immobilized in SPE layer. 62
Fig. 40 Dependence of sensor response on NO_2 concentration for different thermal treatment conditions during the formation of the SPE layer with $[C_2mim][NTf_2]$ ionic liquid: sample No. 1, 80 °C for 1.5 min; sample No. 2, 120 °C for 1.5 min; sample No. 3, 120 °C for 3.5 min and sample No. 4, 160 °C for 10 min. 63
Fig. 41 Pictures of prepared sensors based on $[C_2mim][NTf_2]$ under different thermal treatment conditions: a) 80 °C, 1.5 min; b) 120°C, 1.5 min c) 120°C, 3.5 min; d) 160 °C, 10min..... 63
Fig. 42 Morphology of the SPE layers based on $[EMIM][NTf_2]$ ionic liquid under different thermal treatment conditions (Phenom ProX electron microscope, magnification 2000×): a) 80 °C for 1.5 min; b) 120 °C for 1.5 min; c) 120 °C for 3.5 min; d) 160 °C for 10 min. 64
Fig. 43 Dependence of the fractal measure of the surface between contour lines (threshold levels) on the magnitude of the threshold of grey scale images for sensors with differently thermally treated SPE layers 66
Fig. 44 Dependence of the fractal dimension on the threshold images boundary (resp. surface inhomogeneity expressed as topological entropy) on the threshold level of greyscale images. 67
Fig. 45 Experimental relative sensitivities of repared sensors (red columns). Calculated relative active (sensitivity) areas (full columns) and deformation contribution areas (hatched columns). Differently coloured columns indicate the contributions below the defined threshold level. 67

11 References

[1] HANUSEK, J.; Iontové kapaliny – nový směr v “zelené” chemii. *Chemické listy*. 99, 2005, 263 - 294.

[2] FARIDBOD, F.; GANJALI, M.R.; NOROUZI, P.; RIAHI, S.; RASHEDI, H. Application of room temperature ionic liquids in electrochemical sensors and biosensors. *Ionic liquids: Applications and perspectvies.* InTech 2011, https://doi.org/10.5772/14702.

[3] GALINSKI, M.;LEWANDOWSKI, A.; STEPNIAK, I. Ionic liquids as electrolytes, *Electrochimica Acta.* 51, 2006, 5567 - 5580.

[4] OHNO, H. Electrochemical Aspects of Ionic liquids. Willey Interscience, New York, 2005.

[5] FERNICOLA, A.; SCROSATI, B.; OHNO, H. Potentialities of ionic liquids as new electrolyte media in advanced electrochemical devices. *Ionics* 12, 2006, 95 - 102.

[6] OHNO, H. Functional design of ionic liquids . *Bulletin of the Chemical Society of Japan*, 79, 2006, 1665 - 1680.

[7] OHNO, H.; YOSHIZAWA, M.; OGIHARA, W. Development of new class of ion conductive polymers based on ionic liquids. *Electrochimica. Acta,* 50, 2004, 255.

[8] YOSHIZAWA, M.; NARITA, A.; OHNO, H. Design of ionic liquids for electrochemical applications. *Australian Journal of Chemistry*, 57, 2004, 139.

[9] ARMAND, M.; ENDRES, F.; MacFARLANE, D.R.; OHNO, H. Ionic-liquid materials for the electrochemical challenges of the future. *Nature Materials*, 8, 2009, 621 - 629.

[10] NISHI, N.; MURAKAMI, H.; YASUI, Y.; KAKIUCHI, T. Use of highly hydrophobic ionic liquids for ion-selective electrodes of the liquid membrane type. *Analytical Sciences,* 24, 2008, 1315 - 1320.

[11] ZHANG, S.; SUN, N.; HE, X.; LU, X.; ZHANG, X. Physical properties of ionic liquids: database and evaluation. *Journal of Physical and Chemical Reference Data*, 35, 2006, 1475 - 1518 .

[12] MASTRAGOSTINO, M.; SOAVI, F. *Encyklopedia of Electrochemical Power Sources*, Elsevier, Amsterdam, 2009.

[13] BÉGUIN, F.; FRACKOWIAK, E. *Supercapacitors*. Wiley-VCH, Weinheim, 2013.

[14] DOBOS, D. *Electrochemical Data.* Akademiai Kiado, Budapest, 1975.

[15] McEWEN, A.B.; NGO, K.; LE COMPTE, K.; GOLDMAN, X.L. Electrochemical properties of imidazolium salt electrolytes for electrochemical capacitor applications, *Journal of the Electrochemical Society*, 146, 1999, 1687 – 1695.

[16] BARROSE-ANTLE, L.E.; BOND, A.M.; COMPON, R.G.; O’MAHONY, A.M.; ROGERS, E.I.; SILVESTER, D.S. Voltammetry in room temperature ionic liquids:

comparisons and contrasts with conventional electrochemical solvents. *Chemistry – An Asian Journal*. 5, 2010, 202 - 230.

[17] OKOTURO, O.O.; VANDER-NOOT, T.J. Temperature dependence of viscosity for room temperature ionic liquids. *Journal of Electroanalytical Chemistry*. 568, 2004, 167 - 181.

[18] VOGEL, H. Das Temperaturabhaengigkeitsgesetz der Viskositaet von Fluessigkeiten," *Physikalische Zeitschrift*, 22, 1921, 645.

[19] ANGEL, C.A. The glass transition. *Current Opinion in Solid State & Materials Science*. 1, 1996, 578 - 585.

[20] ANGEL, C.A. Thermodynamic aspects of the glass transition in liquids and plastic crystals. *Pure and Applied Chemistry*. 63, 1991, 1387 - 1392.

[21] ANGEL, C.A. Formation of glasses from liquids and biopolymers. *Science*. 267, 1995, 1924 - 1935.

[22] KIRKWOOD, J.G.; OSTER, G. The influence of hindered molecular rotation on the dielectric constants of water, alcohols and other polar liquids. *The Journal of Chemical Physics.* 11, 1943, 175.

[23] SMYTH, C.P. Dielectric Behavior and Structure. McGrow-Hill, New York, 1938.

[24] FRÖLICH, H. Theory of Dielectrics. Oxford University Press, Oxford, 1949.

[25] BÖTTCHER, C.J.F. The Theory of Electric Polarization. Elsevier, Amsterodam, 1952.

[26] BOCKRIS, J.O'M.; DEVANATHAN, M.A.V., MÜLLER, K. On the structure of charged interfaces. *Proceedings of the Royal Society of London.* A 274, 1963, 55.

[27] MARSHAL, S.; CONWAY, B.E. Analysis of molecular polarization and interaction in adsorbed monolayers at electrodes part 1. Interaction between adsorbed dipoles. *Journal of Electroanalytical Chemistry.* 337, 1992, 1 – 18.

[28] MARSHAL, S.; CONWAY, B.E. Analysis of molecular polarization and interaction in adsorbed monolayers at electrodes: Part 2. Surface salvation energy of adsorbed charges. *Journal of Electroanalytical Chemistry*. 337, 1992, 19 - 43.

[29] CONWAY, B.E. Ionic Hydration in Chemistry and Biophysics. Elsevier, Amsterodam, 1981.

[30] POPOV, A.I. Alkali metal n.m.r. and vibrational spectroscopic studies on solvates in non-aqueous solvents. *Pure and Applied Chemistry*. 41, 1975, 275 -289.

[31] CONWAY, B.E. Electrochemical Supercapacitors. Kluwer Academic/Plenum Publishers, New York, 1999.

[32] UE, M.; TAKEDA, M.; MORI, S. Electrochemical properties of quaternary ammonium salts for electrochemical capacitors. *Journal of the Electrochemical Society*. 144, 1997, 2684 - 2688.

[33] McEWEN, A.B.; NGO, H.L.; LeCOMPTE, K.; GOLDMAN, J.L. Electrochemical Properties of imidazolium salt electrolytes for electrochemical capacitor applications. *Journal of the Electrochemical Society.*146, 199, 1687 – 1695.

[34] XU, K.; DING, M.S.; JOW, T.R. Quaternary onium salts as nonaqueous electrolytes for electrochemical capacitors. *Journal of the Electrochemical Society.* 148, 2001, A267 – A274.

[35] KATAYAMA, Y.; DAN, S.; MIURA, T.; KISHI, T. Electrochemical behavior of silver in 1-ethyl-3-methylimidazolium tetrafluoroborate molten salt. *Journal of the Electrochemical Society,* 148, 2001, C102 – C105.

[36] FULLER, J.; CARLIN, R.T.; OSTERYOUNG, R.A. The Room Temperature Ionic Liquid 1-Ethyl-3-methylimidazolium Tetrafluoroborate: Electrochemical Couples and Physical Properties. *Journal of the Electrochemical Society*. 144, 1997, 3881 – 3886.

[37] NISHIDA, T.; TASHIRO, Y.; YAMAMOTO, M. Physical and electrochemical properties of 1-alkyl-3-methylimidazolium tetrafluoroborate for electrolyte. *Journal of Fluorine Chemistry.* 120, 2003, 135 – 141.

[38] CONVINGTON, A.K. Definition of pH scales, standard reference values, measurement of pH and related terminology (Recommendations 1984). *Pure and Applied Chemistry.* 57, 1985, 531 – 542.

[39] RIPKA, P.; DAĎO, S.; KREIDL, M.; NOVÁK, J. Senzory a převodníky. Praha: ČVUT, 2005.

[40] BUCHTA, J. Metody detekce toxických a hořlavých plynů. Praha: ČSTZ, 2006, 2-16. ISSN:1212 8929.

[41] VRŇATA, M.; VYSLOUŽIL, F. Detekce plynů a par pomocí připravených vodivostních senzorů. [online]. [cit. 10.11.2011]. Dostupné z: https://vscht.cz/ufmt/cs/pomucky/el_pomucky.html

[42] Figaro group. General information for TGS sensors [online]. 2005 [cit. 10.6.2011]. Dostupné z: http://www.figarosensor.com/.

[43] KUBERSKY, P.; HAMACEK, A.; DZUGAN, T.; KROUPA, M.; CENGERY, J.; REBOUN, J. Phthalocyanine layers for humidity detection. *33rd International Spring Seminar on Electronics Technology*. 2010, 14 17. DOI: 10.1109/ISSE.2010.5547247.

[44] DZUGAN, T.; HAMACEK, A.; REBOUN, J.; KUBERSKY, P.; PRETL, S.; VIK, R. Organic materials for humidity detection. *34th International Spring Seminar on Electronics Technology*. 2011, 22 26. DOI: 10.1109/ISSE.2011.6053543.

[45] OPEKAR, F. Elektroanalytické metody / Potenciometrie [online]. [cit. 10.4.2011]. Dostupné z: http://web.natur.cuni.cz/~opekar/.

[46] BARD, A. J.; FAULKNER, L. R. Electrochemical methods – Fundamentals and applications. 2nd edition, J. Wiley, New York, 2001.

[47] KRONĎÁK M. Když se řekne... Clarkovo čidlo. *Automatizace*. roč. 50. č. 7-8. [online] VŠCHT Praha: 2007 available at http://www.automatizace.cz.

[48] MACLAY, G.J.; BUTTNER, W.J.; STETER, J.E. Microfabricated amperometric gas sensors. *IEEE Transactions on Electron Devices*, 35, 1988, 793 - 799.

[49] HRNČÍŘOVÁ, P.; OPEKAR, F.; ŠTULÍK, K. An amperometric solid-state NO_2 sensor with a solid polymer electrolyte and a reticulated vitreous carbon indicator electrode. *Sensors & Actuators B.* 69, 2000, 199 – 204.

[50] HOHERČÁKOVÁ, Z.; OPEKAR, F. Au/PVC composite—a new material for solid-state gas sensors: Detection of nitrogen dioxide in the air, *Sensors & Actuators B.* 97, 2004, 379.

[51] SERRA, A.; BUCCOLIERI, A.; FILIPPO, E.; MANNO, D. Nanographite assembled films for sensitive NO2 detection. *Sensors & Actuators B.* 161, 2012, 359 – 365.

[52] MACLAY, G.J.; BUTTNER, W.J.; STETER, J.E. Microfabricated amperometric gas sensors. *IEEE Transactions on Electron Devices*, 35, 1988, 793 - 799.

[53] BAREK, J.; OPEKAR, F.; ŠTULÍK, K. Elektroanalytická chemie. Praha: Nakladatelství Karolinum. 2005. ISBN: 80-246-1146-5.

[54] KISSINGER, P.T.; HEINEMANN, W.R. . Laboratory Techniques in Electroanalytical Chemistry, 2nd ed. New York. 1996. ISBN: 0827418647.

[55] STETTER, J.R.; LI, J. Amperometric gas sensor – a review. *Chemical Reviews.* 108, 2008, 352 – 366.

[56] CAO, Z.; BUTTNER, W.J.; STETTER, J.R. The properties and applications of amperomeric gas sensors. *Electroanalysis*, 4, 1992, 253-266.

[57] AYOUCHI, R.; LEINEN, D.; MARTIN, F.; GABAS, M.; DALCHIELE, E.; RAMOSBARRADO, J. R. Preparation and characterization of transparent ZnO thin films obtained by spray pyrolysis. *Thin Solid Films.* 426, 2003, 68–77.

[58] VÁRY, M.; PERNÝ, M.; ŠÁLY, V.; PACKA, J. AC characterization of bulk organic solar cell in the dark and under illumination. *Applied Surface Science.* 312, 2014, 176–181.

[59] 1260A Impedance/gain-phase Analyzer. 2017, [cit. 12. 10. 2017]. Dostupné z: <http://www.ameteksi.com/-/media/ameteksi/download_links/documentations/1260a/1260aa4.pdf>

[60] ONSAGER, L. Initial Recombination of Ions. *Physical Review*. 54, 1938, 554.

[61] SMOLUCHOWSKY, M. "Drei Vorträge über Diffusion, Brownsche Molekularbewegung und Koagulation von Kolloidteilchen". *Physikalische Zeitschrift*. 17 1916, 557–571, 585–599.

[62] BUZZEO, M.C.; HARDACRE, C.; COMPTON, R.G. Use of room temperature ionic liquids in gas sensor design. *Analytical Chemistry*. 76, 2004, 4583–4588.

[63]. ROGERS, E.I.; O'MAHONY, A.M.; ALDOUS, L.; COMPTON, R.G. Amperometric gas detection using room temperature ionic liquid solvents. *ECS Transactions*. 33, 2010, 473–502.

[64]. FARIDBOD, F.; GANJALI, M.R.; NOROUZI, P.; RIAHI, S.; RASHEDI, H. Application of room temperature ionic liquids in electrochemical sensors and biosensors. *Ionic liquids: Applications and perspectvies.* Kokorin, A., Ed.; InTech: Rijeka, Croatia, 2011; pp. 643–658.

[65]. SILVESTER, D.S. Recent advances in the use of ionic liquids for electrochemical sensing. *Analyst*. 136, 2011, 4871–4882.

[66]. XIONG, L.; COMPTON, R.G. Amperometric gas detection : A review. *International Journal of Electrochemical Science*, 9, 2014, 7152–7181.

[67]. CARTER, M.T.; STETTER, J.R.; FINDLAY, M.W.; PATEL, V. Amperometric gas sensors with ionic liquid electrolytes. *ECS Transactions*. 58, 2014, 7–18.

[68]. JI, X.; BANKS, C.E.; SILVESTER, D.S.; ALDOUS, L.; HARDACRE, C.; COMPTON, R.G. Electrochemical ammonia gas sensing in nonaqueous systems: A comparison of propylene carbonate with room temperature ionic liquids. *Electroanalysis*. 19, 2007, 2194–2201.

[69]. CARTER, M.T.; STETTER, J.R.; FINDLAY, M.W.; PATEL, V. Printed amperometric gas sensors. *ECS Transactions*. 50, 2013, 211–220.

[70]. HUANG, X.J.; ALDOUS, L.; O'MAHONY, A.M.; CAMPO, F.J.; COMPTON, R.G. Toward membrane-free amperometric gas sensors: A microelectrode array approach. *Analytical Chemistry*. 82, 2010, 5238–5245.

[71]. TONIOLO, R.; DOSSI, N.; PIZZARIELLO, A.; DOHERTY, A.P.; SUSMEL, S.; BONTEMPELLI, G. An oxygen amperometric gas sensor based on its electrocatalytic reduction in room temperature ionic liquids. *Journal of Electroanalytical Chemistry*. 670, 2012, 23–29.

[72]. STETTER, J.R.; STETTER, E.F.; EBELING, D.D.; FINDLAY, M.; PATEL, V. Printed Gas Sensor. U.S. Patent No. 8,798,484, 2013.

[73]. NÁDHERNÁ, M.; OPEKAR, F.; REITER, J. Ionic liquid–polymer electrolyte for amperometric solid-state NO2 sensor. *Electrochimica Acta*. 56, 2011, 5650–5655.

[74]. NÁDHERNÁ, M.; OPEKAR, F.; REITER, J.; ŠTULÍK, K. A planar, solid-state amperometric sensor for nitrogen dioxide, employing an ionic liquid electrolyte contained in a polymeric matrix. *Sensors and Actuators B: Chemical*. 161, 2012, 811–817.

[75]. KUBERSKÝ, P.; HAMÁČEK, A.; NEŠPŮREK, S.; SOUKUP, R.; VIK, R. Effect of the geometry of a working electrode on the behavior of a planar amperometric NO_2 sensor based on solid polymer electrolyte. *Sensors and Actuators B: Chemical*. 187, 2013, 546–552.

[76]. KUBERSKÝ, P.; SYROVÝ, T.; HAMÁČEK, A.; NEŠPŮREK, S.; SYROVÁ, L. Towards a fully printed electrochemical NO2 sensor on a flexible substrate using ionic liquid based polymer electrolyte. *Sensors and Actuators B: Chemical*. 209, 2015, 1084–1090.

[77] OPEKAR, F. An amperometric solid-state sensor for nitrogen dioxide based on a solid polymer electrolyte. *Electroanalysis*. 4, 1992, 133 - 138.

[78] CHANG, S.C.; STETTER, J.R**.** Electrochemical NO_2 gas sensors: Model and mechanism for the electroreduction of NO_2. *Electroanalysis*. 2, 1990, 359 - 365.

[79] DO, J.S.; SIEH, R.Y. Electrochemical nitrogen dioxide gas sensor based on solid polymeric electrolyte. *Sensors and Actuators B: Chemical.* 37, 1996, 19 - 26.

[80] KUBERSKÝ, P.; ALTŠMÍD, J.; HAMÁČEK, A.; NEŠPŮREK, S.; ZMEŠKAL, O. An Electrochemical NO_2 Sensor Based on Ionic Liquid: Influence of the Morphology of the Polymer Electrolyte on Sensor Sensitivity. *Sensors*. 15, 2015, 28421-28434.

[81] POCHEKAILOV, S., NOŽÁR, J., NEŠPŮREK, S., RAKUŠAN, J., KARÁSKOVÁ, M. Interaction of nitrogen dioxide with sulfonamide-substituted phthalocyanines: Towards NO_2 gas sensor. *Sensors and Actuators B.* 169, 2012, 1 – 9.

[82]. GREGORIO, R.; BORGES, D.S. Effect of crystallization rate on the formation of the polymorphs of solution cast poly(vinylidene fluoride). *Polymer*. 49, 2008, 4009–4016.

[83]. ZMEŠKAL, O.; BZATEK, T.; NEZADAL, M. HarFA—Harmonic and Fractal Image Analyser Software. Available online: http://www.fch.vutbr.cz/lectures/imagesci/includes/harfa_download.inc.php (access on 6 November 2015).

[84]. HOEY, J.M.; LUTFURAKHMANOV, A.; SCHULZ, D.L.; AKHATOV, I.S. A Review on aerosol-baseddirect-write and its applications for microelectronics. *Journal of Nanoscience and Nanotechnology*. 9, 2012, 1–22.

[85]. ZMESKAL, O.; NESPUREK, S.; VESELY, M.; DZIK, P. Statistics of Fractal Systems. In Advances in Intelligent Systems and Computing; Springer International Publishing: Heidelberg, Germany, 2014; pp. 55–63.

[86]. ZMESKAL, O.; DZIK, P.; VESELY, M. Entropy of fractal systems. *Computers & Mathematics with Applications*. 66, 2013, 135–146.

[87]. JEŘÁBKOVÁ, P.; ZMEŠKAL, O.; HADERKA, J. Fractal Analysis of the Images using Wavelet Transformation. In Complexus Mundi—Emergent Patterns in Nature; World Scientific: Singapore, 2006; pp. 300–312.

[88] IKONOPISOV, S. Theory of electrical breakdown during formation of barrier anodic films. *Electrochimica Acta*, 22, 1977, 1077.

[89] ZHU, Q.; SONG, Y.; ZHU, X.; WANG, X. Ionic liquid-based electrolytes for capacitor applications. *Journal of Electroanalytical Chemistry.* 601, 2007, 229 - 236.

[90] KIM, I.T.; EGASHIRA, M.; YOSHIMOTO, N.; MORITA, M. Effects of electrolytic composition on the electric double-layer capacitance at smooth-surface carbon electrodes in organic media. *Electrochimica Acta*, 55, 2010, 6632 - 6638.

[91] SHIONO, K.; NITTA, Y. US Patent 5,870.275, 1999.

[92] ZUO, X.; XU, C.; XIN, H.. Simulation of voltammogram on rough electrode. *Electrochimica Acta*, 42, 1997, 2555 – 2558.

[93] SONG, Y.; ZHU, X.; WANG, X.; CHE, J.; DU, Y. Anodic oxidation behaviour of Al–Ti alloys in acidic media. *Journal of Applied Electrochemistry*. 31, 2001, 1273 - 1279.

[94] FORLANI, F.; MINNAJA, N., Thickness Influence in Breakdown Phenomena of Thin Dielectric Films, *Physica Status Solidi B.* 4, 1964, 311-324.

12 List of publications and other activities

Articles in impact journals

ALTŠMÍD, J.; SYROVÝ, T.; SYROVÁ, L.; KUBERSKÝ, P.; HAMÁČEK, A.; ZMEŠKAL, O.; NEŠPŮREK, S. Ionic liquid based polymer electrolytes for NO_2 electrochemical sensors. *Materials science (Medžiagotyra),* 21, 2015, 415 – 418. ISSN: 1392–1320.

KUBERSKÝ, P.; ALTŠMÍD, J.; HAMÁČEK, A.; NEŠPŮREK, S.; ZMEŠKAL, O. An Electrochemical NO_2 Sensor Based on Ionic Liquid: Influence of the Morphology of the Polymer Electrolyte on Sensor Sensitivity. *Sensors*. 15, 2015, 28421-28434.

Other publications and conference contributions

ZMEŠKAL, O.; POSPÍŠIL, J.; ALTŠMÍD, J.; NEŠPŮREK, S. Barrier Properties of Printed Composite Zinc-Phthalocyanine/Fullerene Sandwiched between Indium Tin Oxide and Alluminium Electrodes. *International Journal of Information and Electronics Engineering*, **2013**, roč. 377, č. 1, s. 156-160. ISSN: 2010-3719.

ALTSMID, J.; KUBERSKY, P.; NAVRATIL, J.; HAMACEK, A.; NESPUREK, S.; ZMESKAL, O. New ionic liquid based electrolytes for application in electrochemical sensors. *Chemistry and Life 2015 - Book of Abstracts*. Brno: 2015.

APPENDIX A: TGA/DSC curves of ionic liquids under study

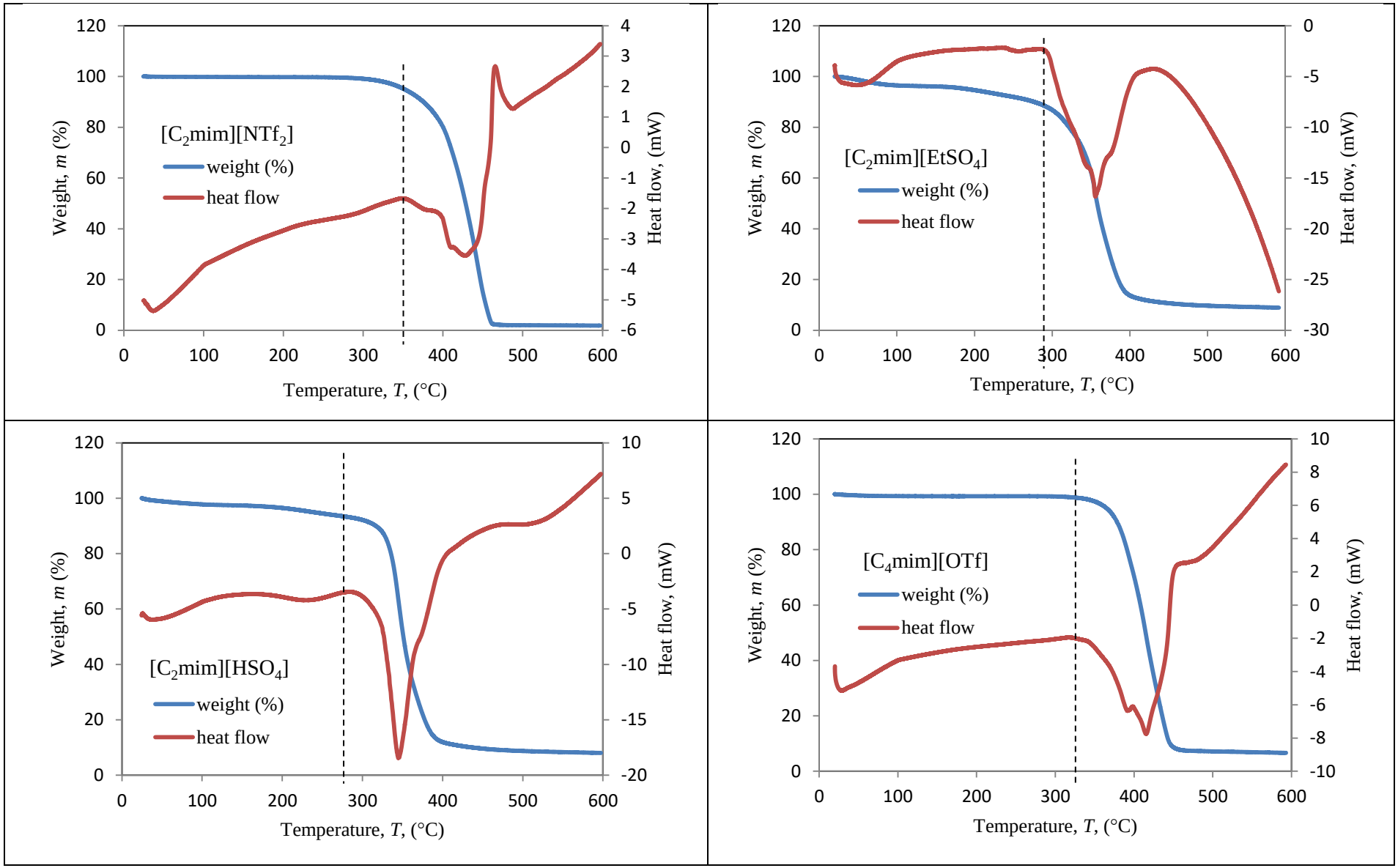

APPENDIX A: TGA/DSC curves of ionic liquids under study

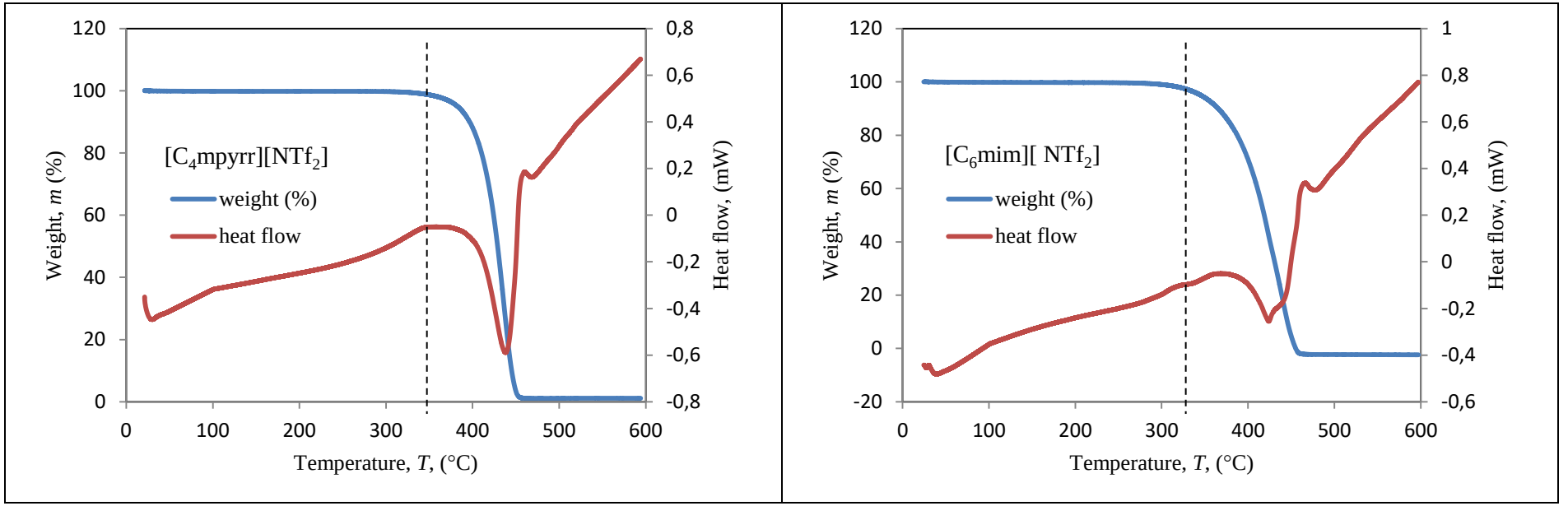

IL	$[C_2mim][NTf_2]$	$[C_2mim][EtSO_4]$	$[C_2mim][HSO_4]$	$[C_4mim][OTf]$	$[C_4mpyrr][NTf_2]$	$[C_6mim][NTf_2]$	$[Emim][BF_4]$*
Temperature (°C)	345	278	290	313	351	325	≥350

* Data acquired from manufacturer.

APPENDIX B: C-V characteristics of chosen ILs at different temperatures

1) 1-ethyl-3-methylimidazolium bis(trifluoromethylsulfonyl)imide [C_2mim][NTf_2]

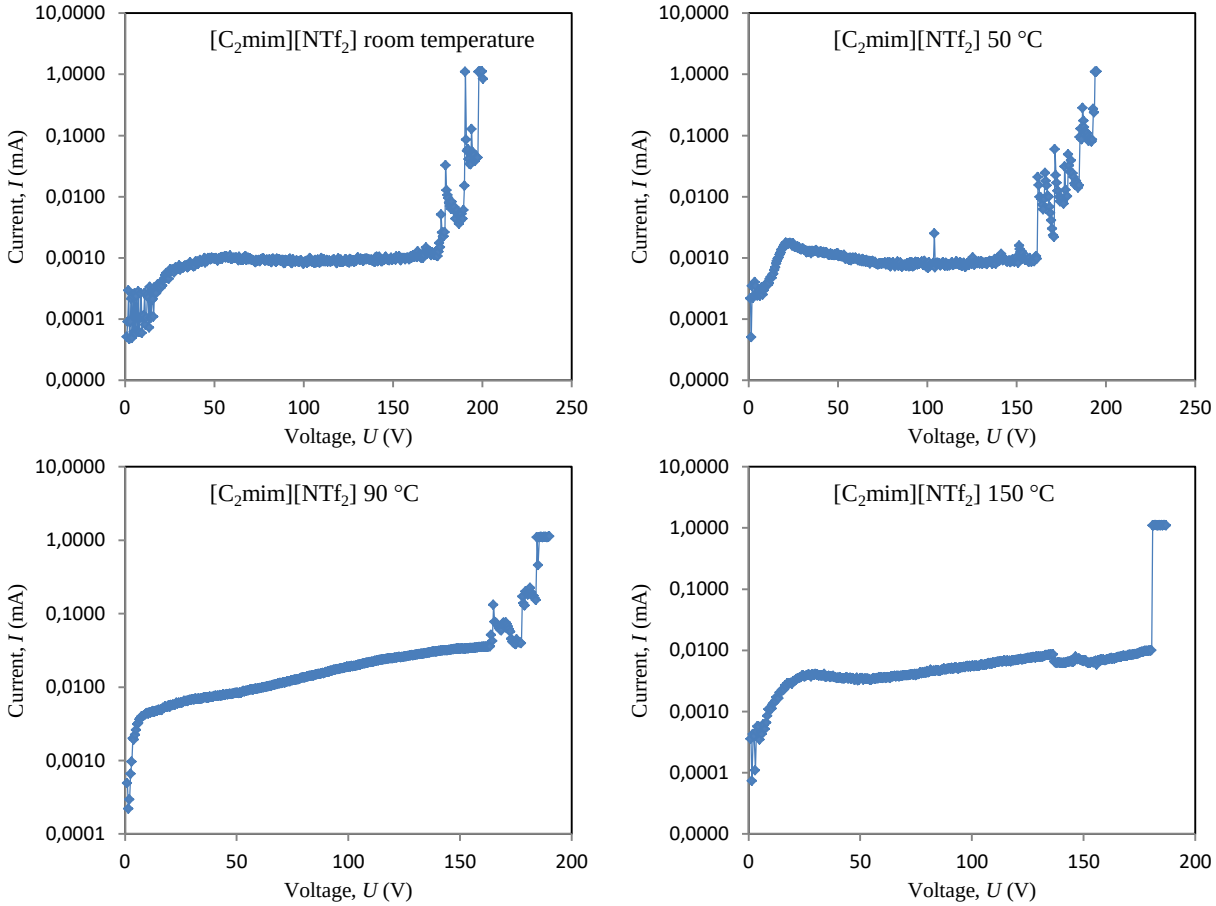

Temperature (°C)	BDV (V)	Conductance (mS)	Capacitance (µF)
24	200	10,3	4,3
50	195	24,3	5,5
90	185	43,4	7
150	180	71,9	8,2

APPENDIX B: C-V characteristics of chosen ILs at different temperatures

2) 1-butyl-3-methylimidazolium trifluoromethanesulfonate [C_4mim][OTf]

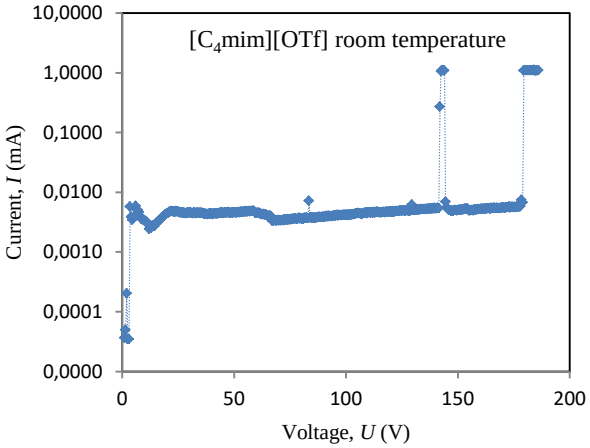

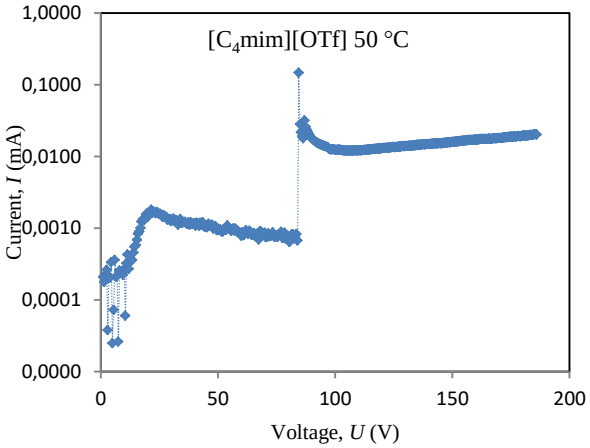

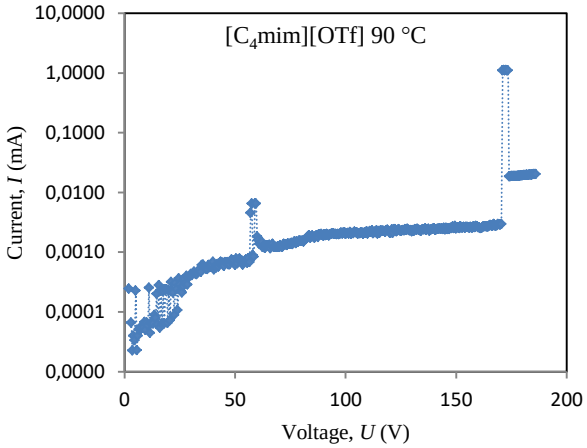

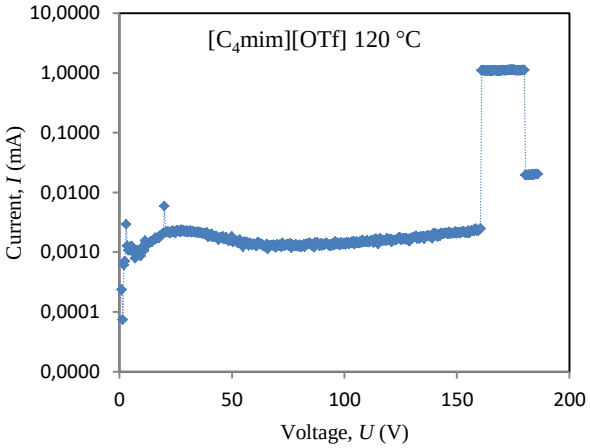

Temperature (°C)	BDV (V)	Conductance (mS)	Capacitance (µF)
24	180	5,4	3,9
50	188	16,1	5,2
90	172	29	6,4
120	160	36,8	7

APPENDIX B: C-V characteristics of chosen ILs at different temperatures

3) 1-hexyl-3-methylimidazolium bis(trifluoromethylsulfonyl)imide [C_6mim][NTf_2]

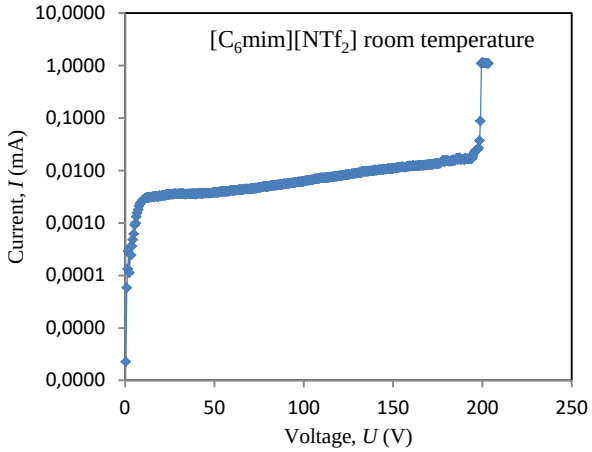

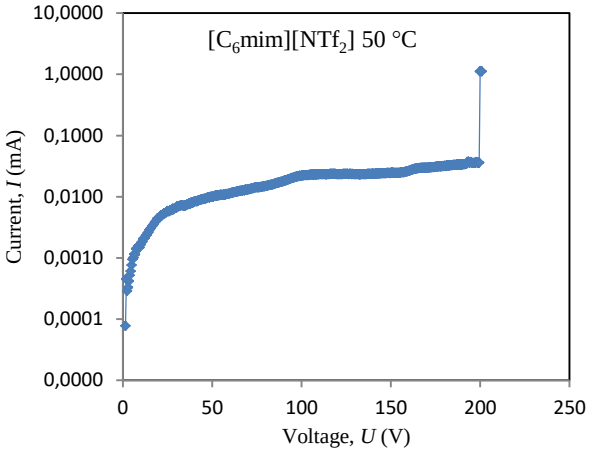

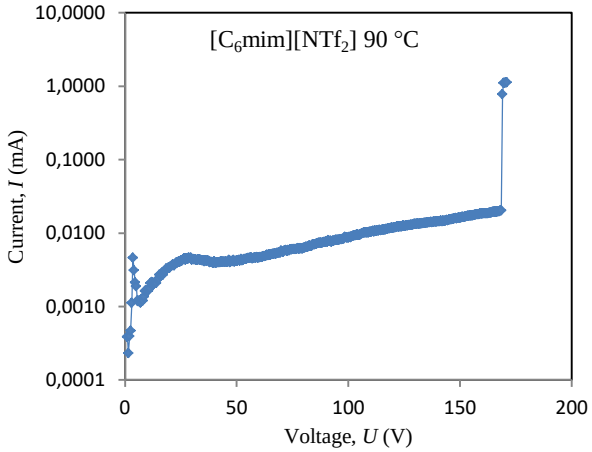

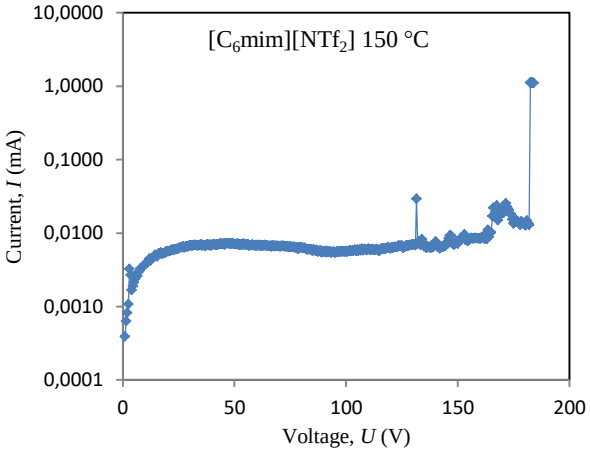

Temperature (°C)	BDV (V)	Conductance (mS)	Capacitance (µF)
24	200	2,8	1,7
50	200	9,3	2,27
90	170	18,7	3,27
150	183	42,7	6,01

APPENDIX C: Impedance spectra of studied ILs

Ionic liquid: 1-ethyl-3-methylimidazolium bis(trifluoromethylsulfonyl)imide [C_2mim][NTf_2]

Electrode system: D3.3/125/FV350V – stainless steel plate

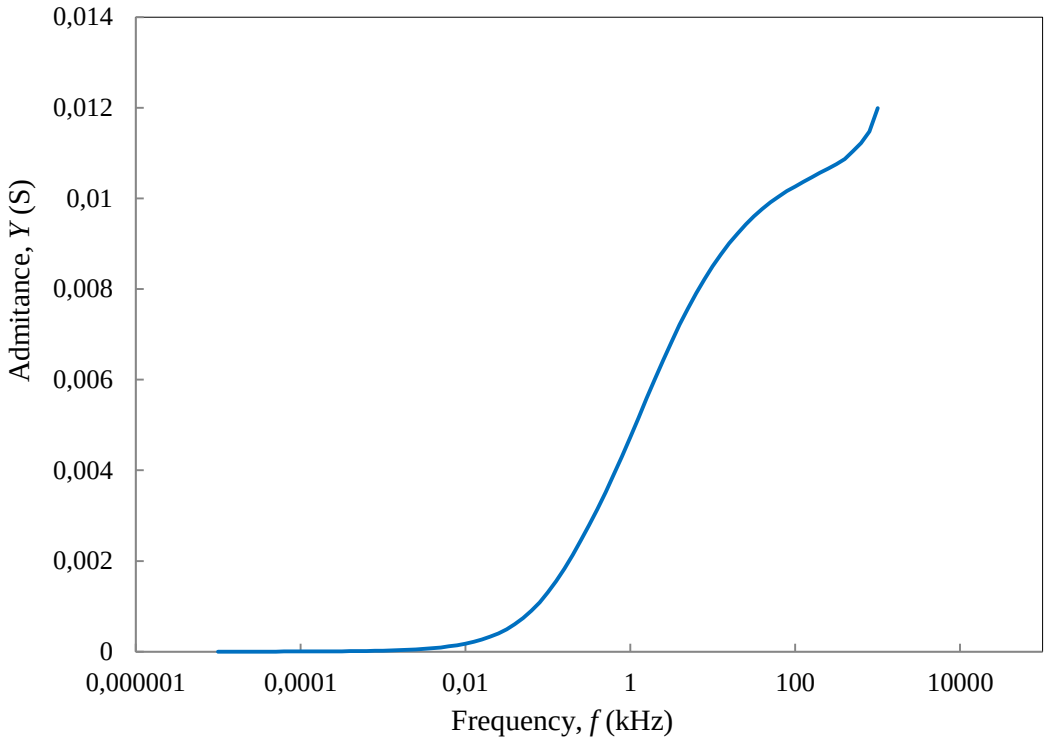

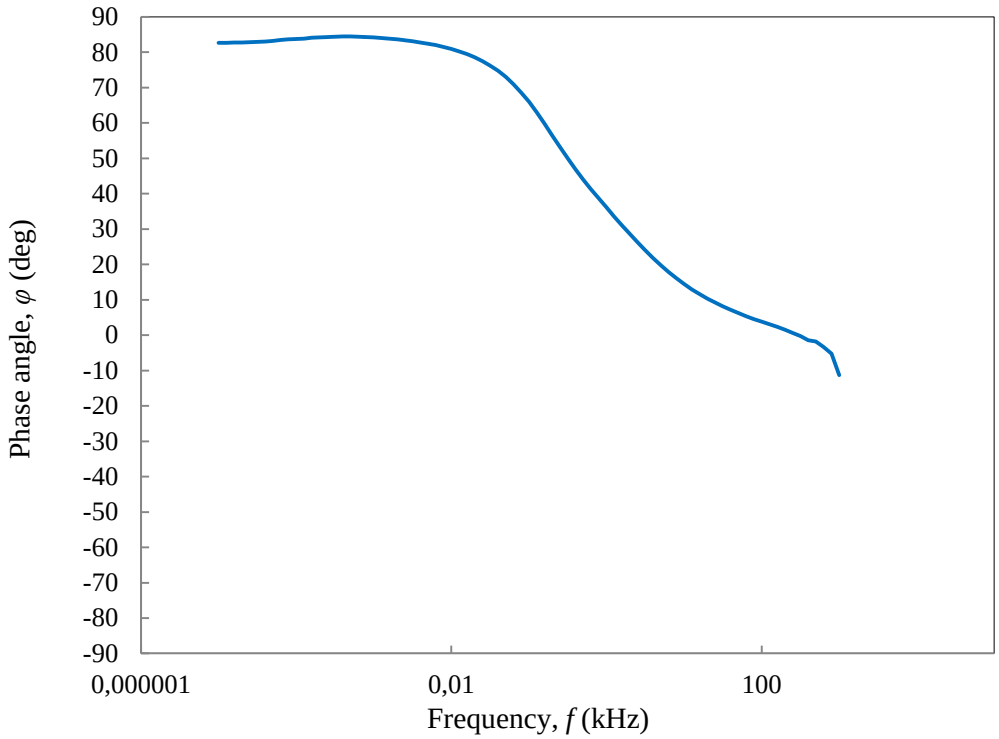

APPENDIX C: Impedance spectra of studied ILs

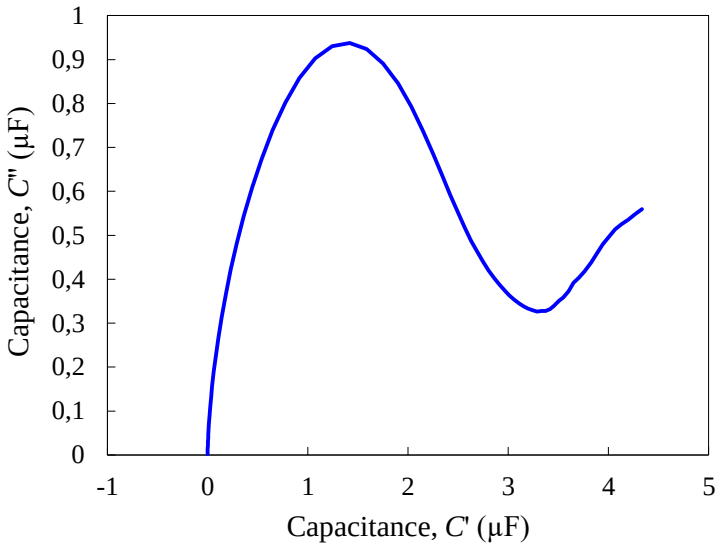

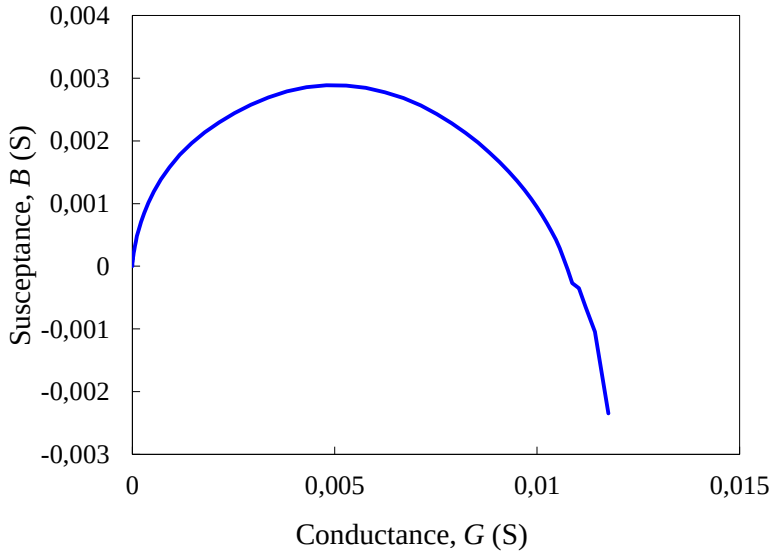

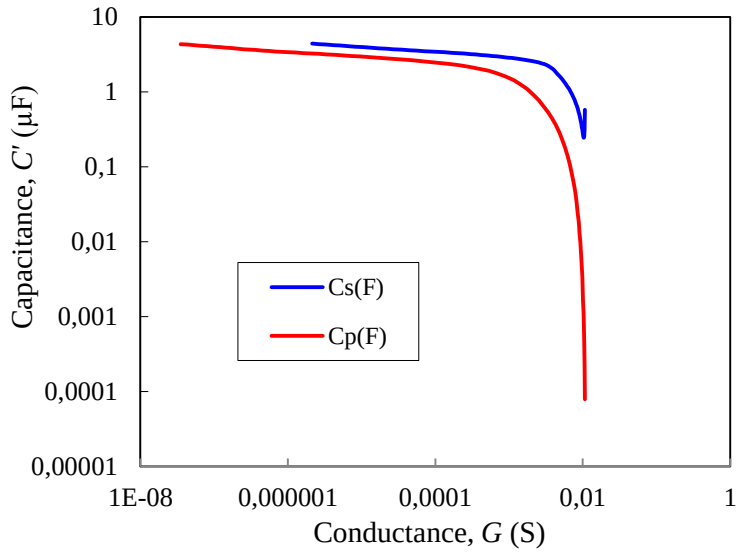

APPENDIX C: Impedance spectra of studied ILs

Ionic liquid: 1-ethyl-3-methylimidazolium ethylsulfate [C_2mim][$EtSO_4$]

Electrode system: D3.3/125/FV350V – stainless steel plate

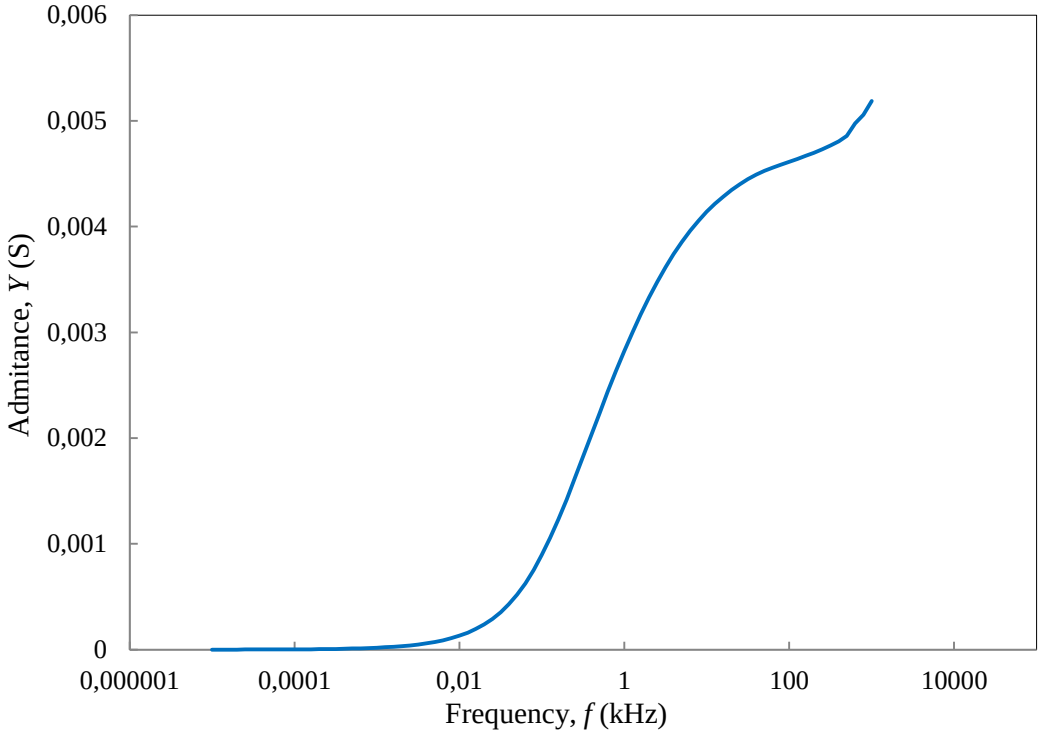

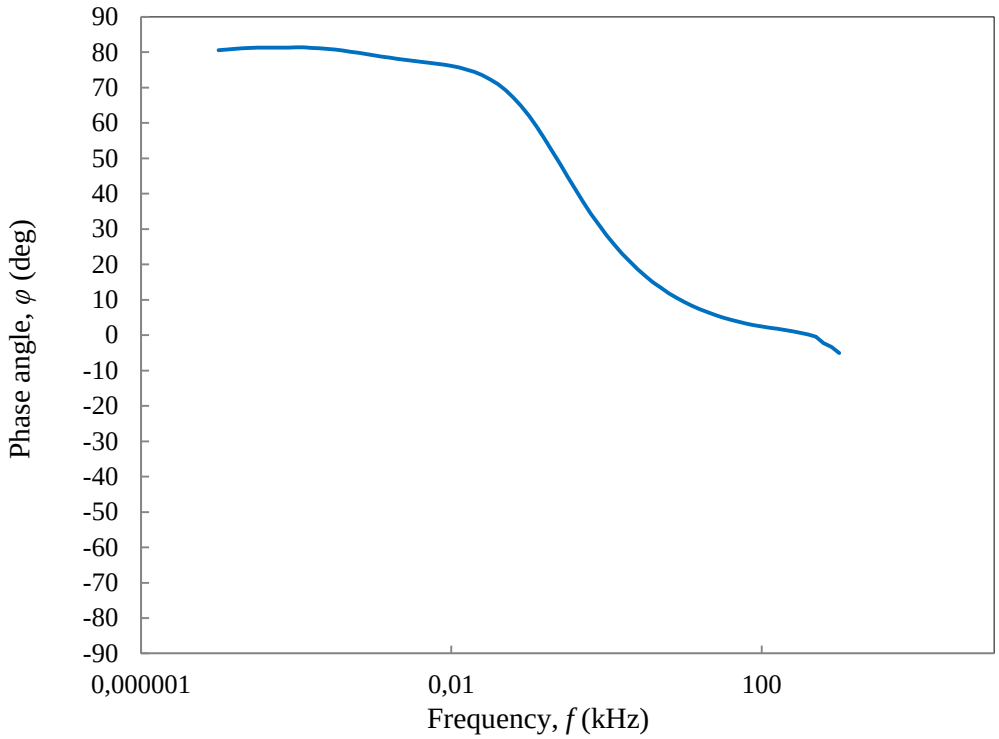

APPENDIX C: Impedance spectra of studied ILs

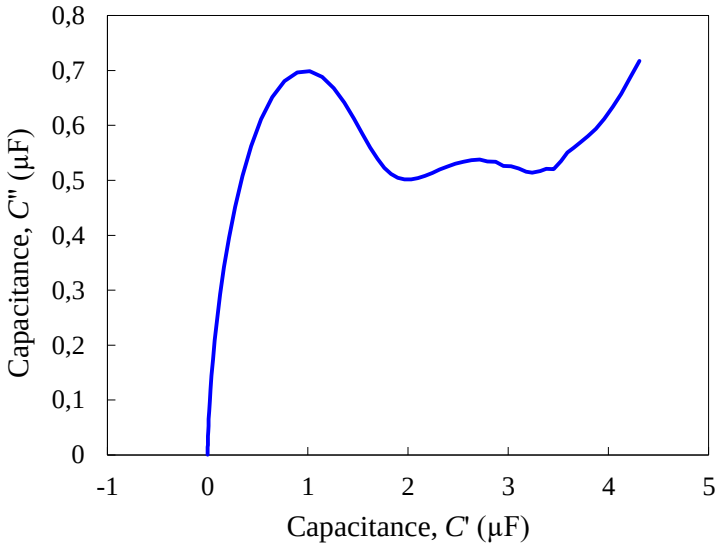

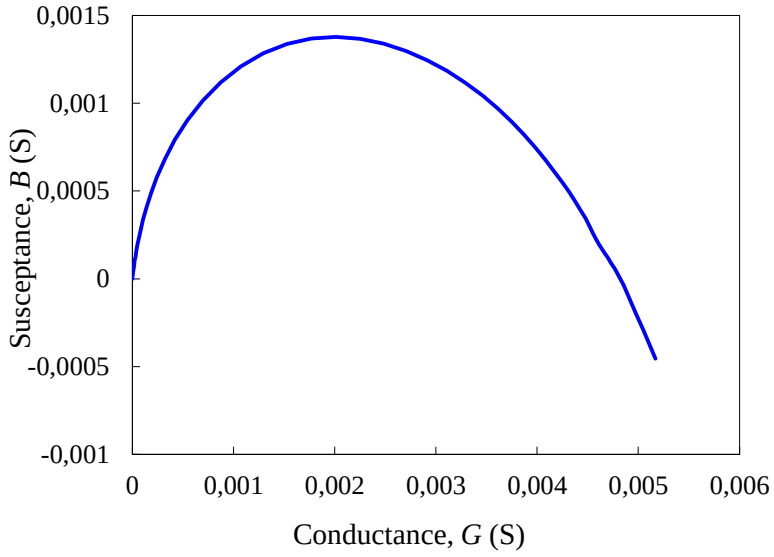

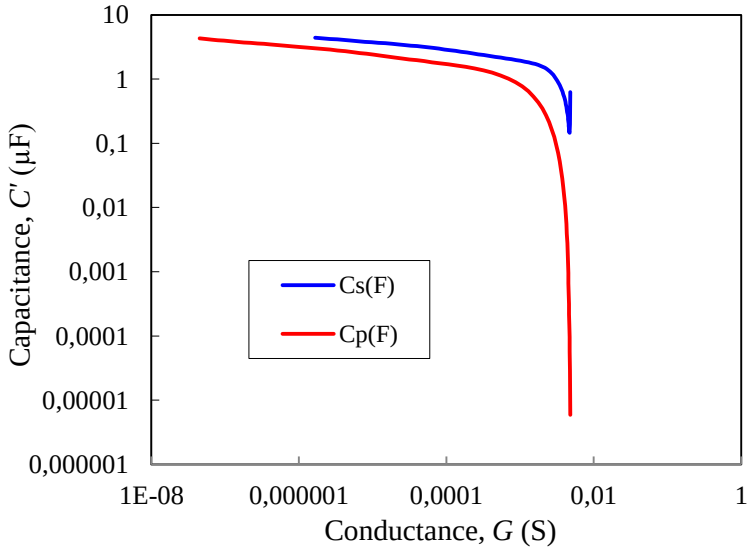

APPENDIX C: Impedance spectra of studied ILs

Ionic liquid: 1-ethyl-3-methylimidazolium hydrogen sulfate [C_2mim][HSO_4]

Electrode system: D3.3/125/FV350V – stainless steel plate

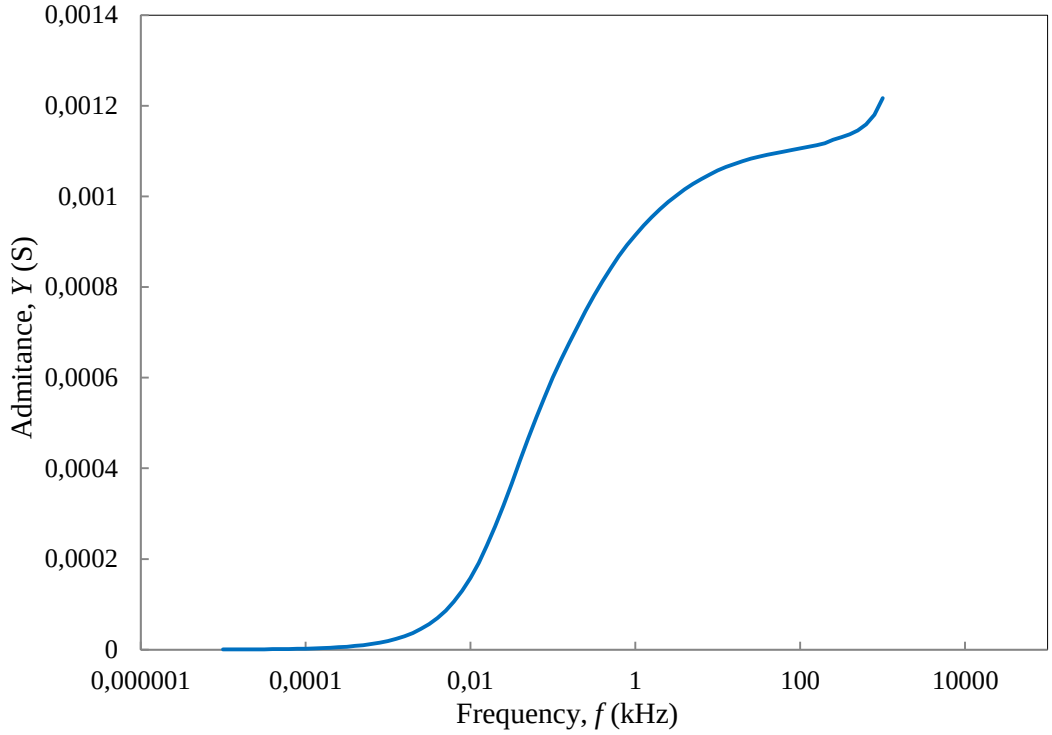

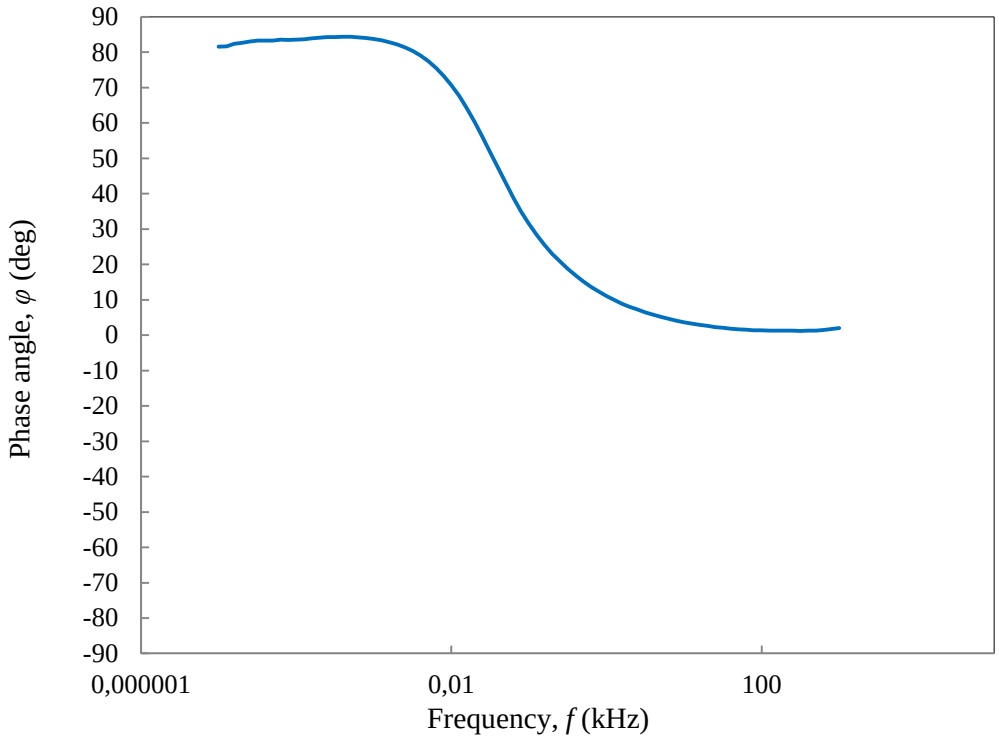

APPENDIX C: Impedance spectra of studied ILs

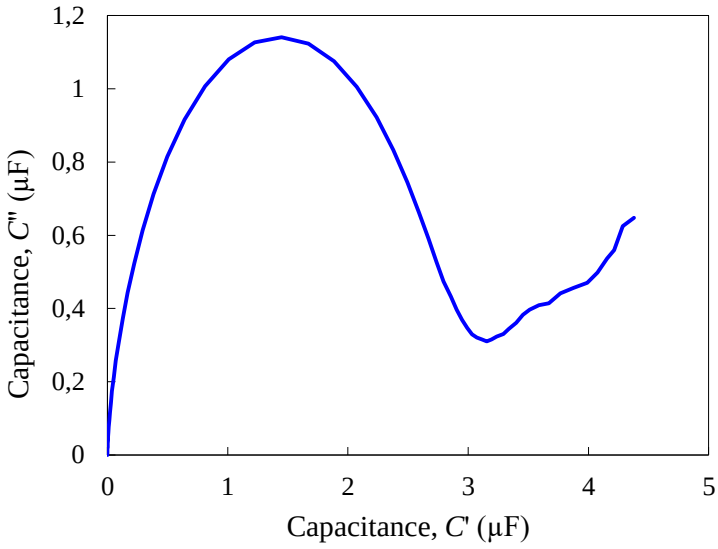

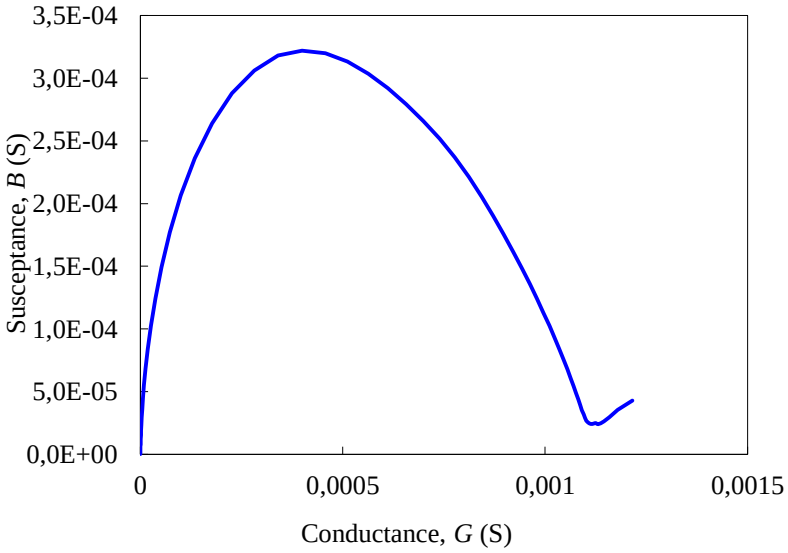

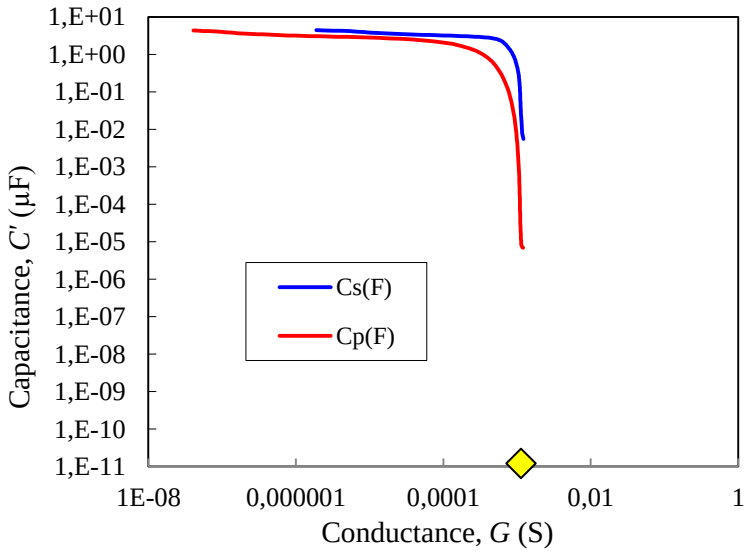

APPENDIX C: Impedance spectra of studied ILs

Ionic liquid: 1-butyl-3-methylimidazolium trifluoromethanesulfonate [C_4mim][OTf]

Electrode system: D3.3/125/FV350V – stainless steel plate

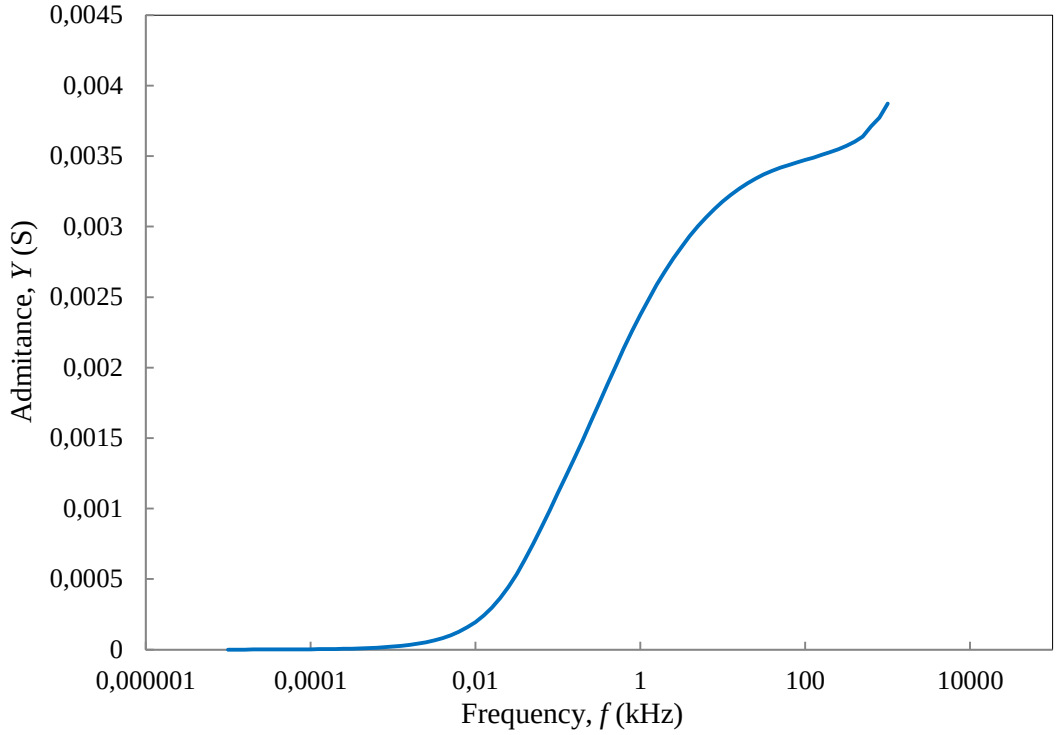

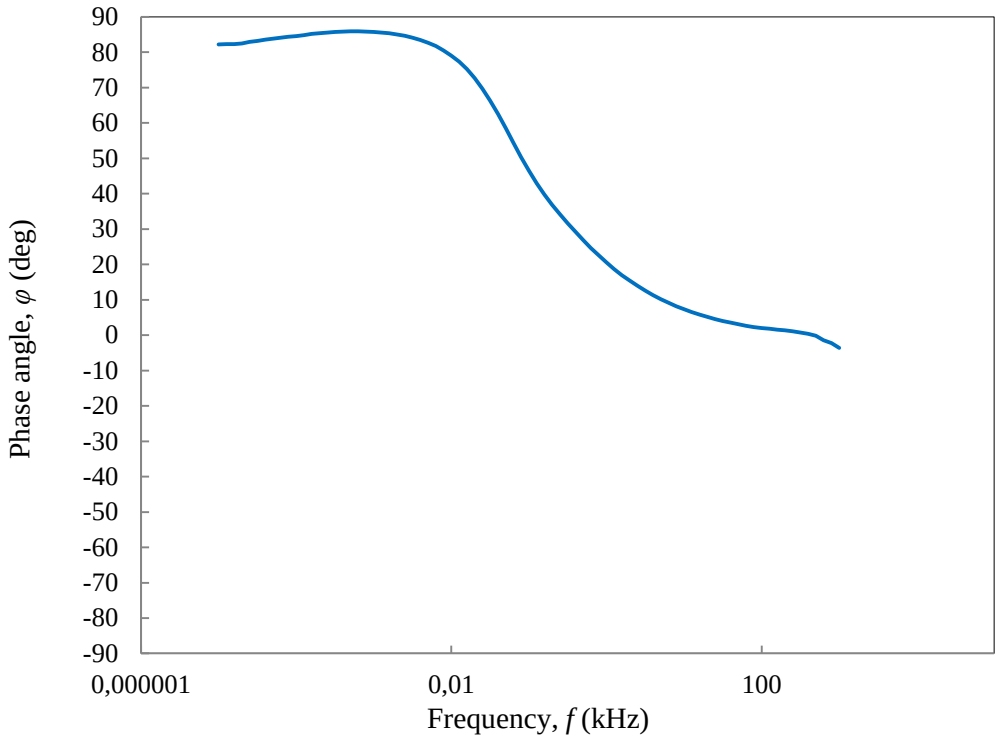

APPENDIX C: Impedance spectra of studied ILs

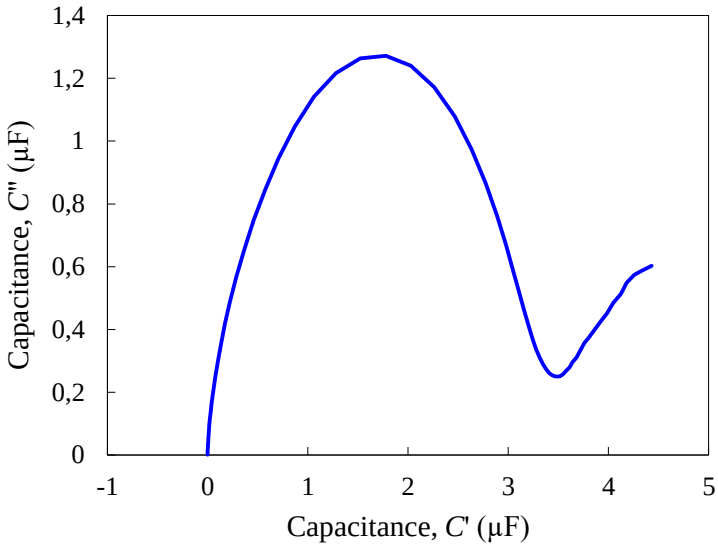

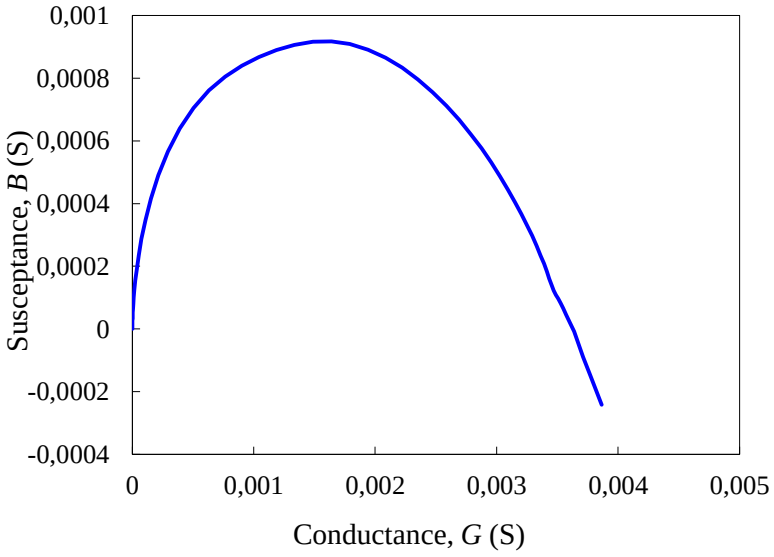

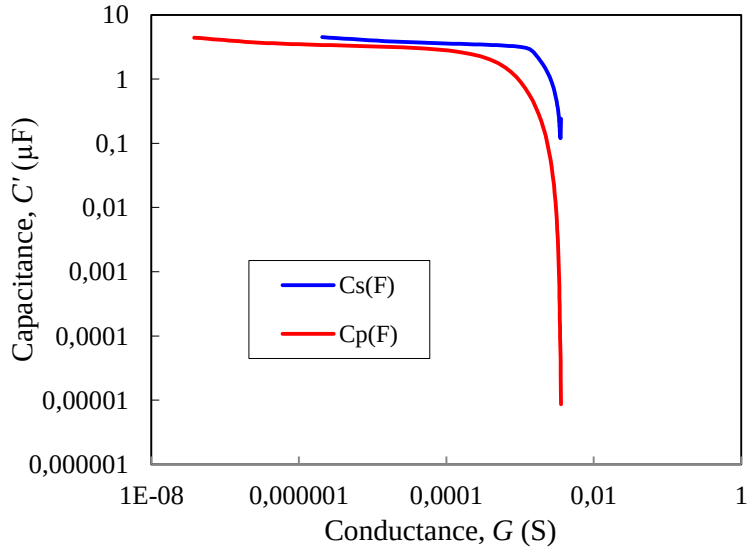

APPENDIX C: Impedance spectra of studied ILs

Ionic liquid: 1-butyl-1-methylpyrrolidinium bis(trifluoromethylsulfonyl)imide [C_4mpyrr][NTf_2]

Electrode system: D3.3/125/FV350V – stainless steel plate

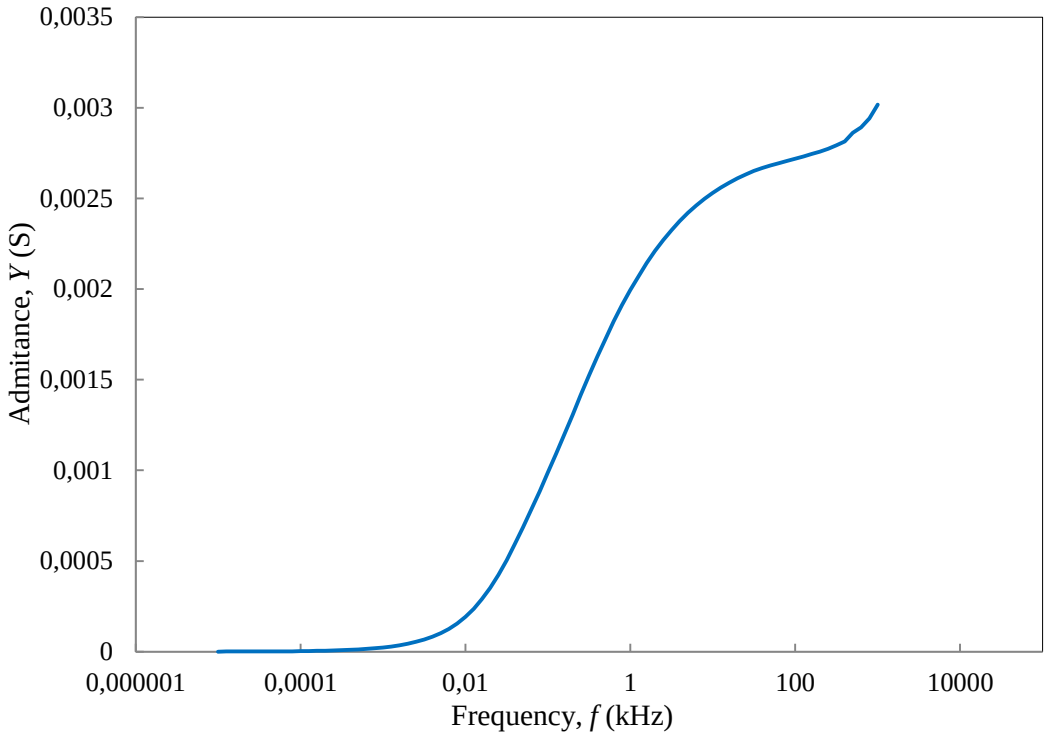

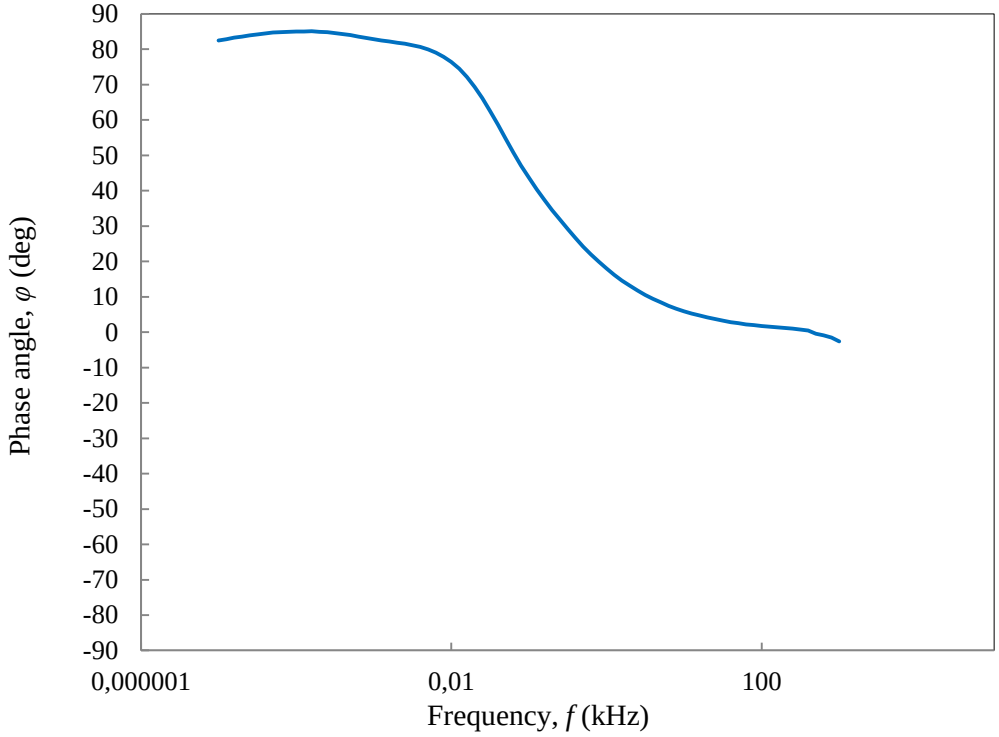

APPENDIX C: Impedance spectra of studied ILs

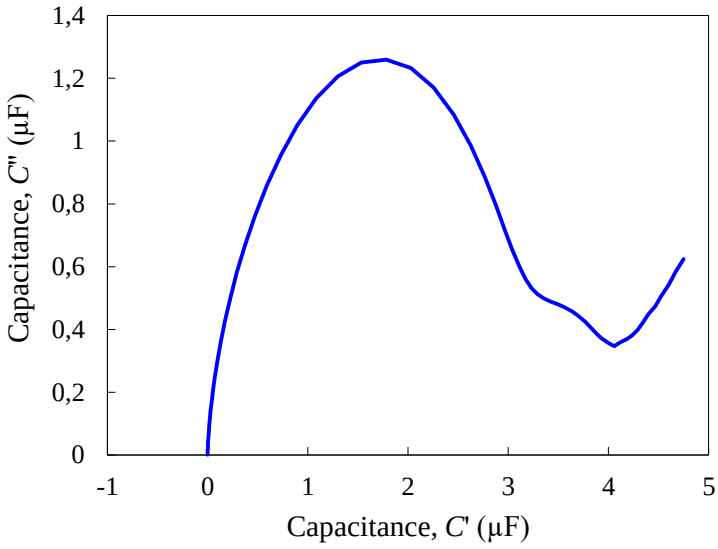

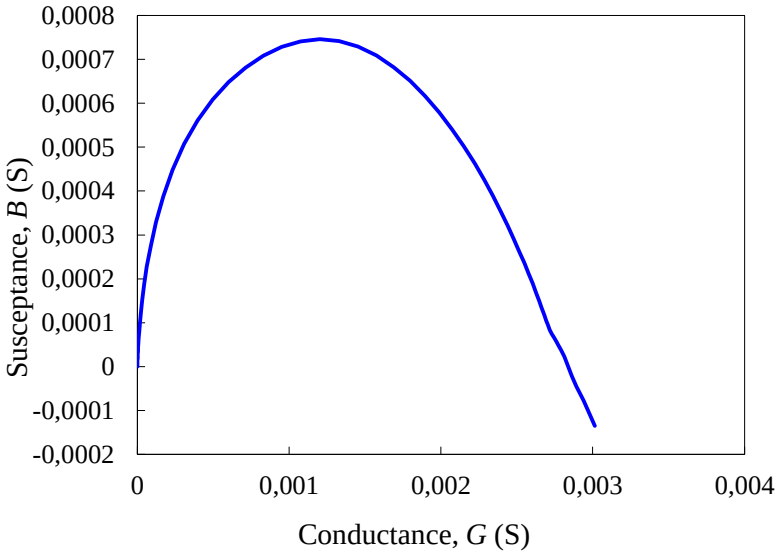

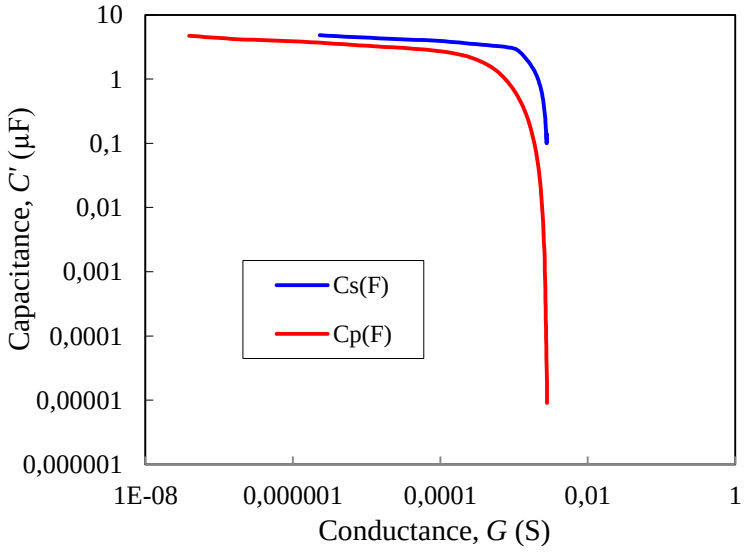

APPENDIX C: Impedance spectra of studied ILs

Ionic liquid: 1-hexyl-3-methylimidazolium bis(trifluoromethylsulfonyl)imide [C_6mim][NTf_2]

Electrode system: D3.3/125/FV350V – stainless steel plate

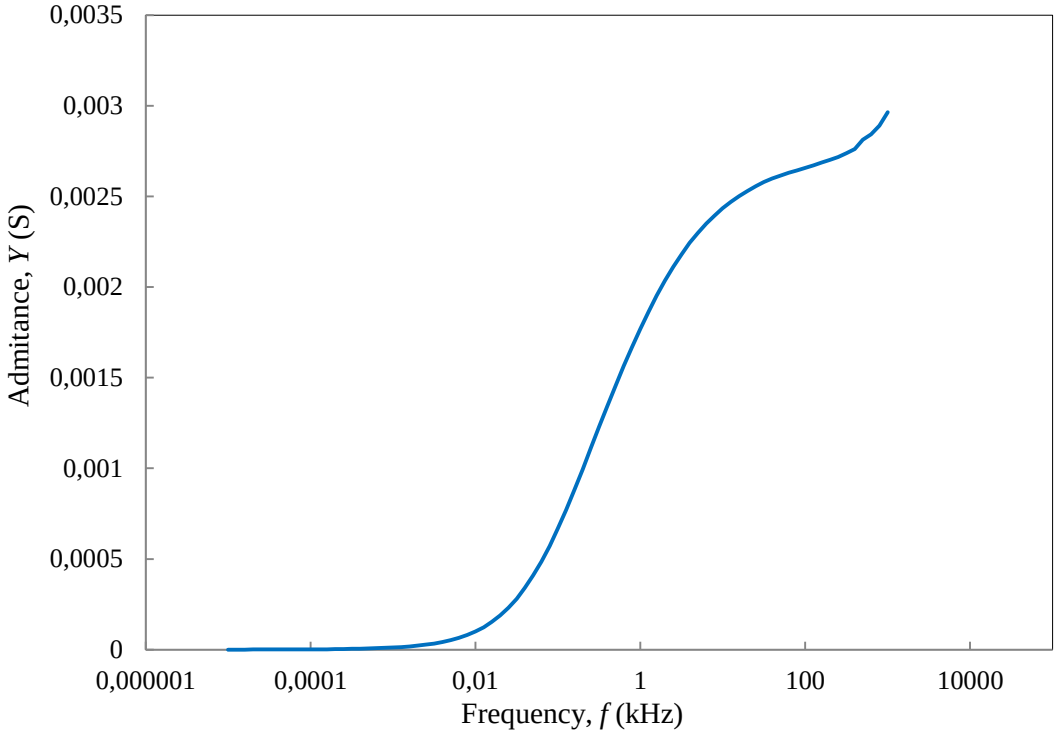

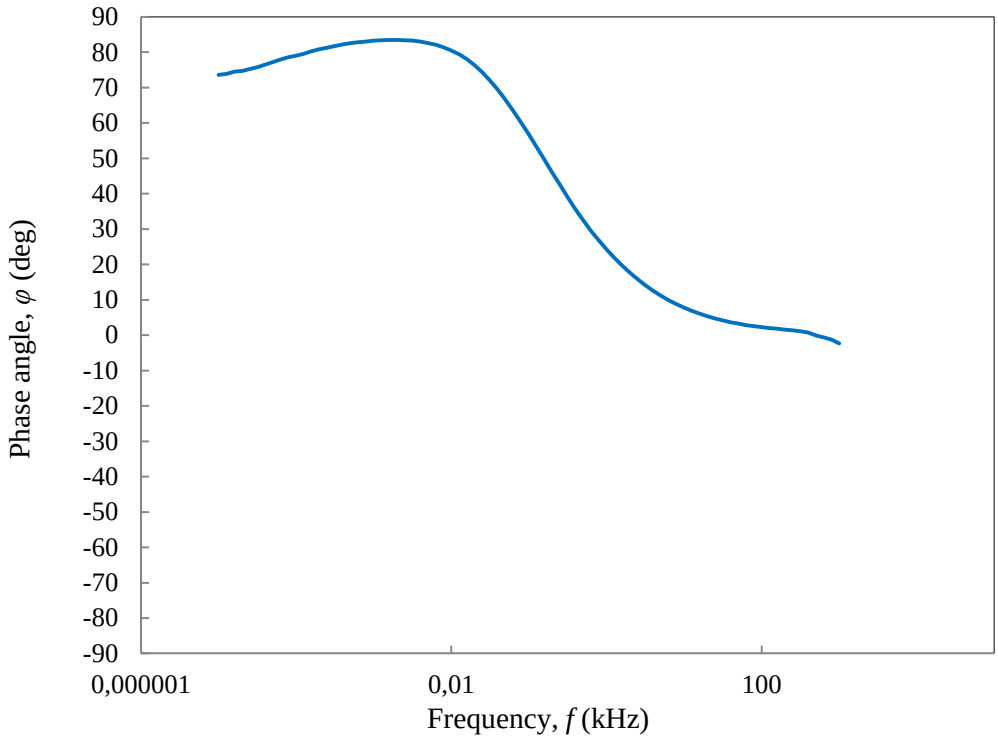

APPENDIX C: Impedance spectra of studied ILs

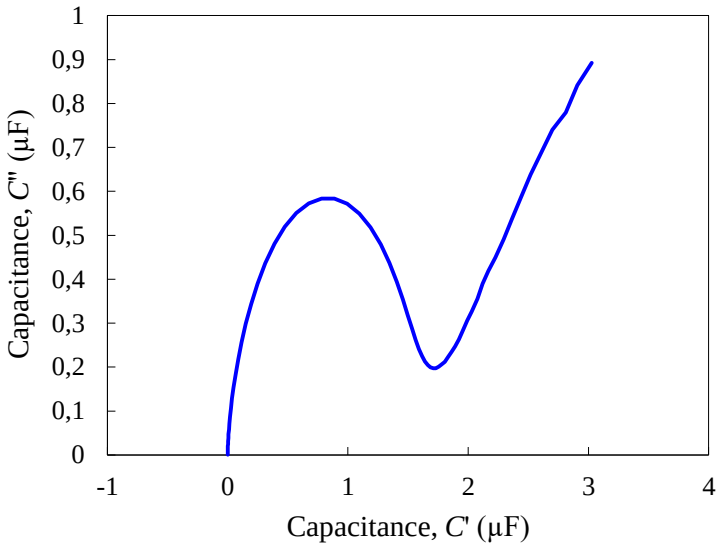

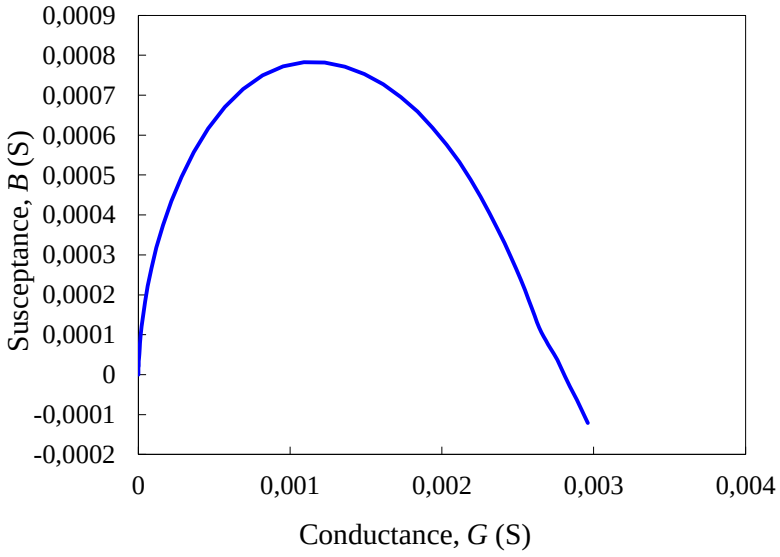

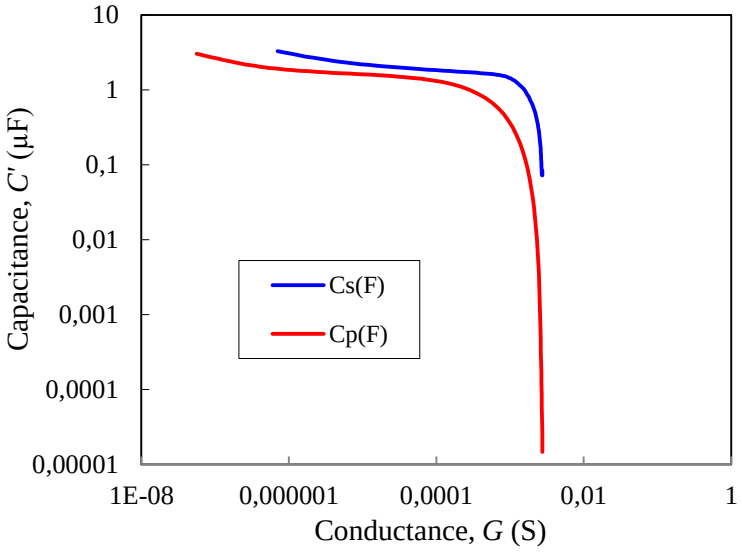

APPENDIX C: Impedance spectra of studied ILs

Ionic liquid: 1-butyl-3-methylimidazolium trifluoroacetate [C_4mim][CF_3CO_2]

Electrode system: V68 W15311WC – Pt plate

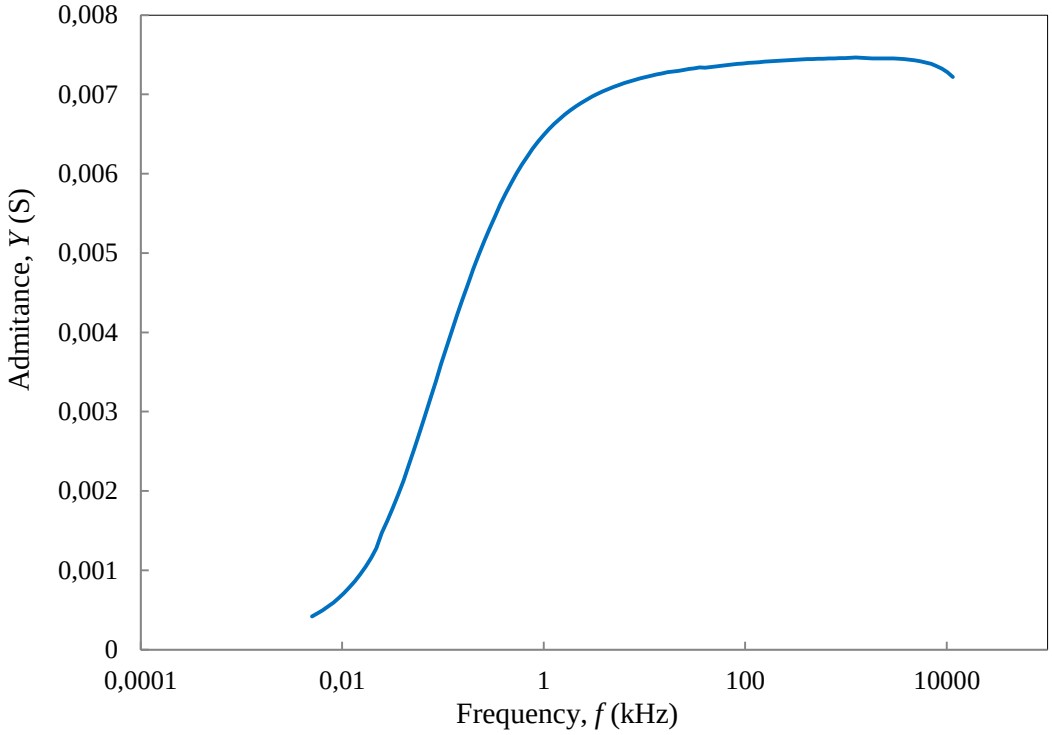

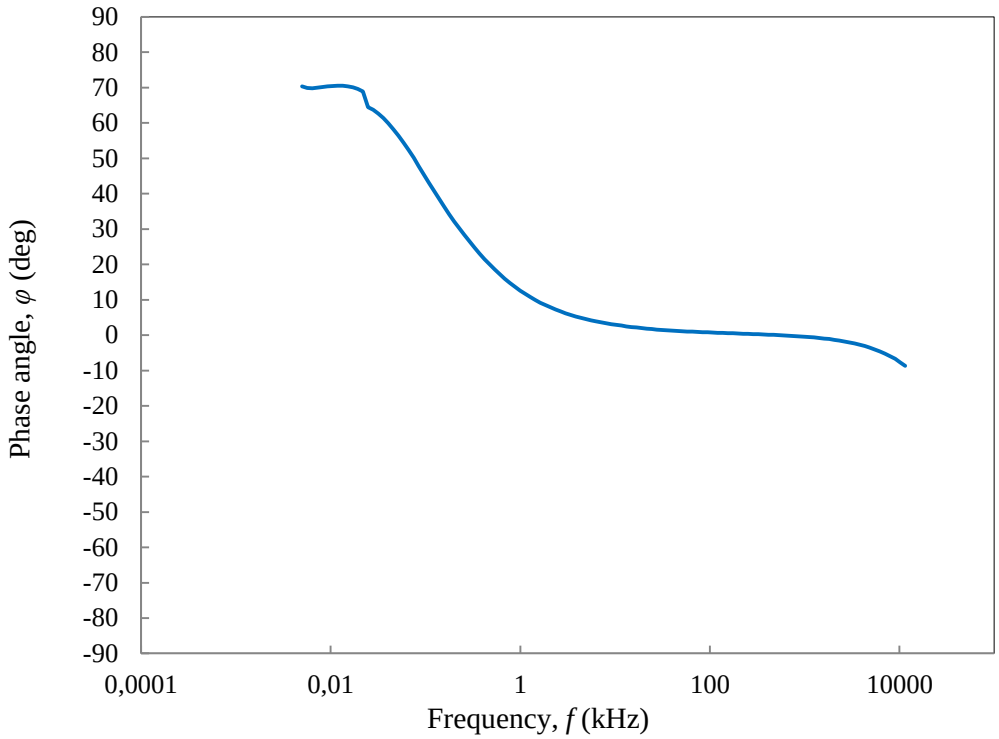

APPENDIX C: Impedance spectra of studied ILs

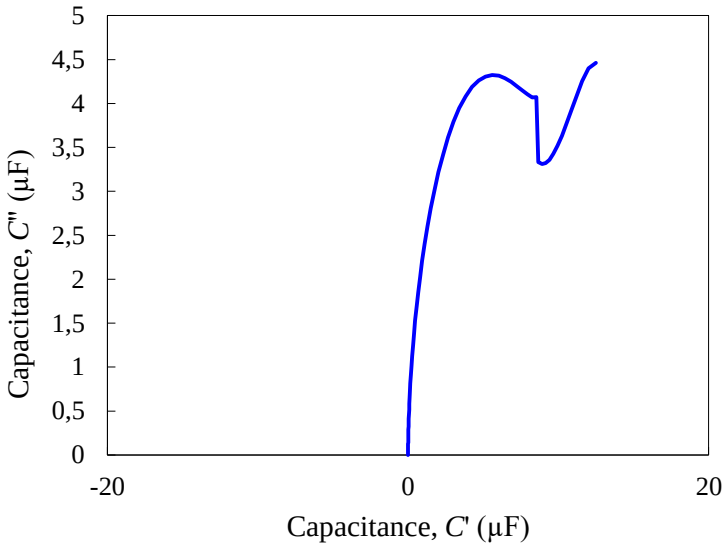

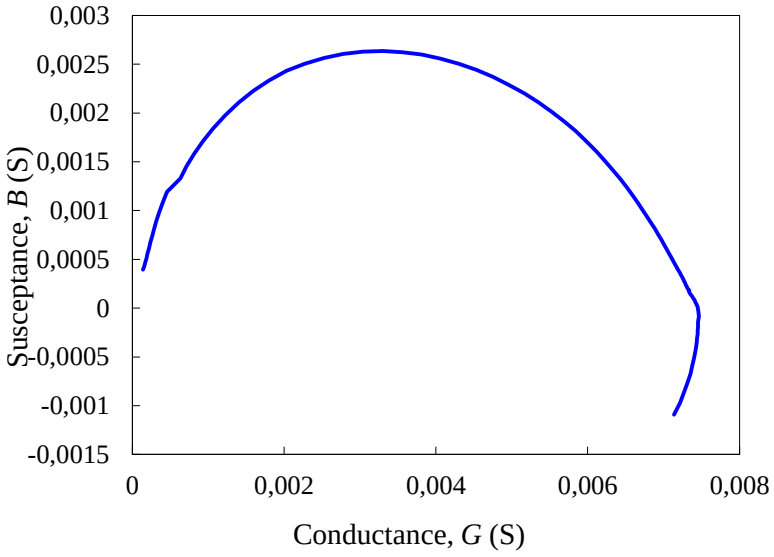

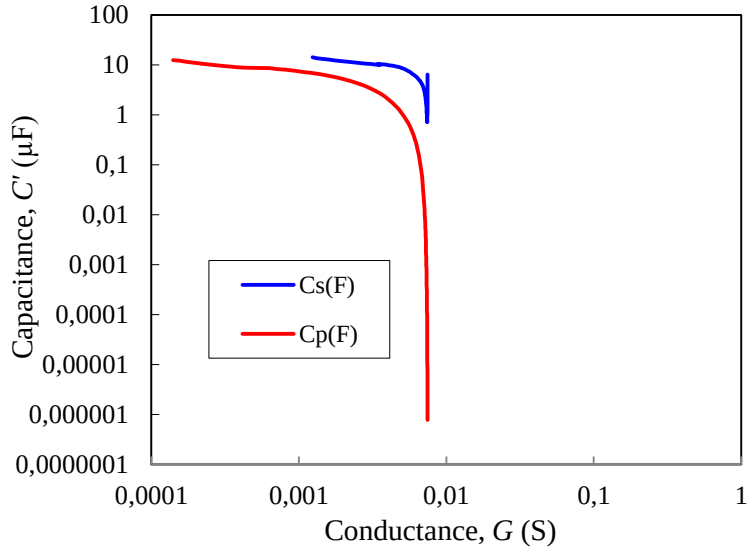

APPENDIX C: Impedance spectra of studied ILs

Ionic liquid: 1-ethyl-3-methylimidazolium tetrafluoroborate [Emim][BF4]

Electrode system: V68 W15311WC – Pt plate

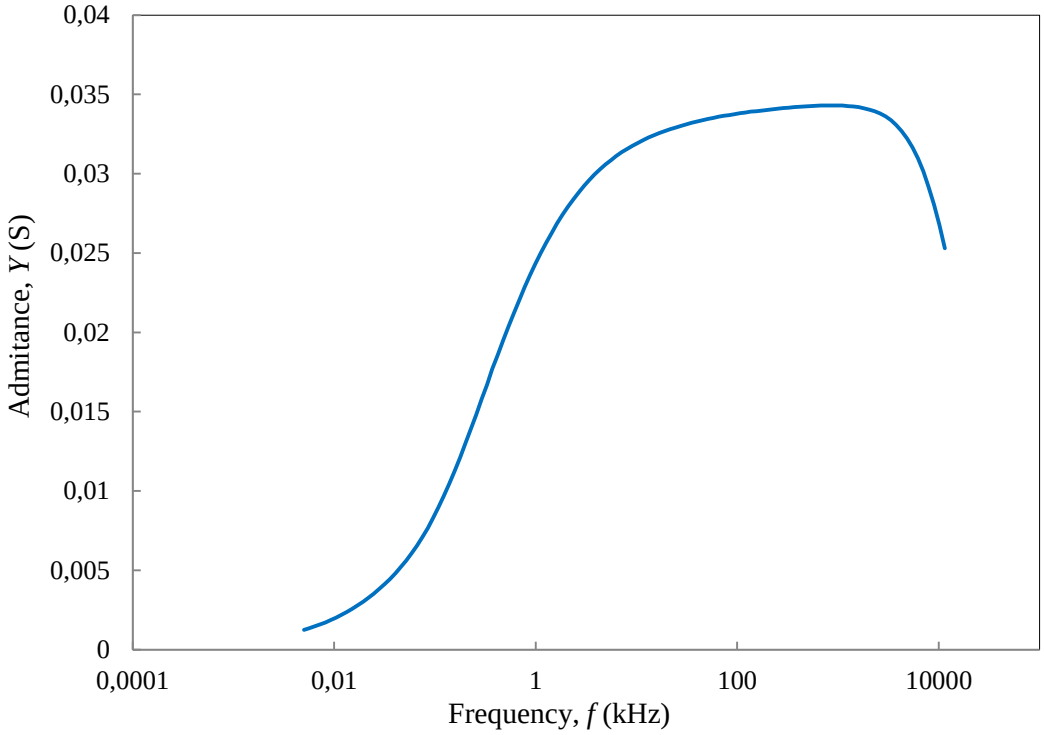

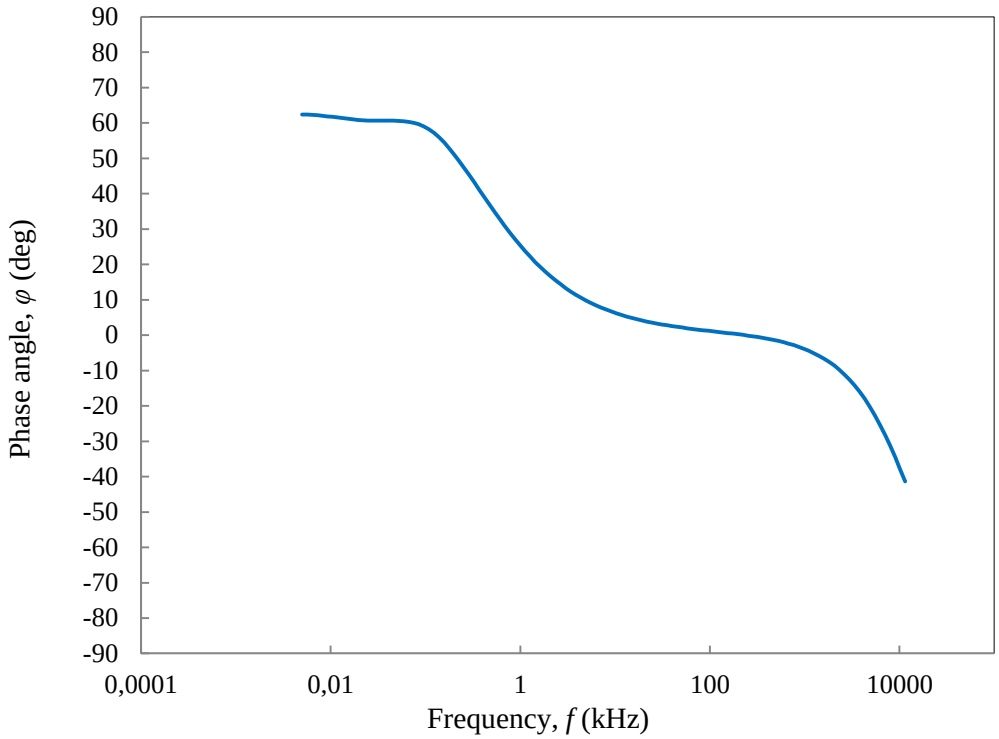

APPENDIX C: Impedance spectra of studied ILs

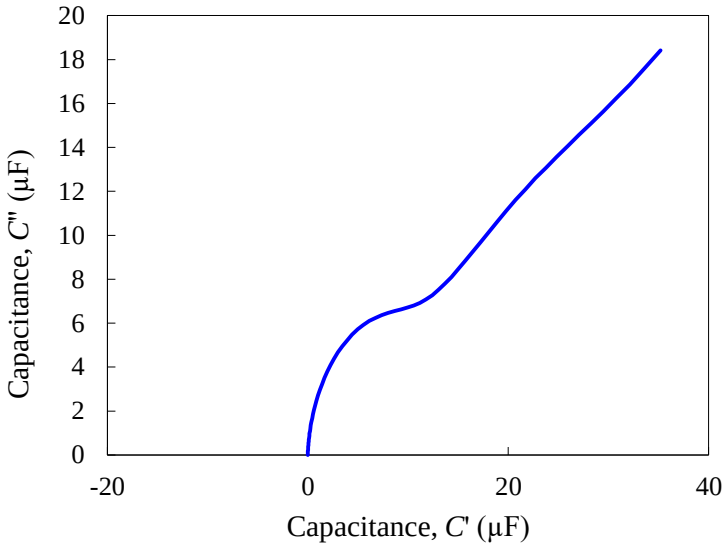

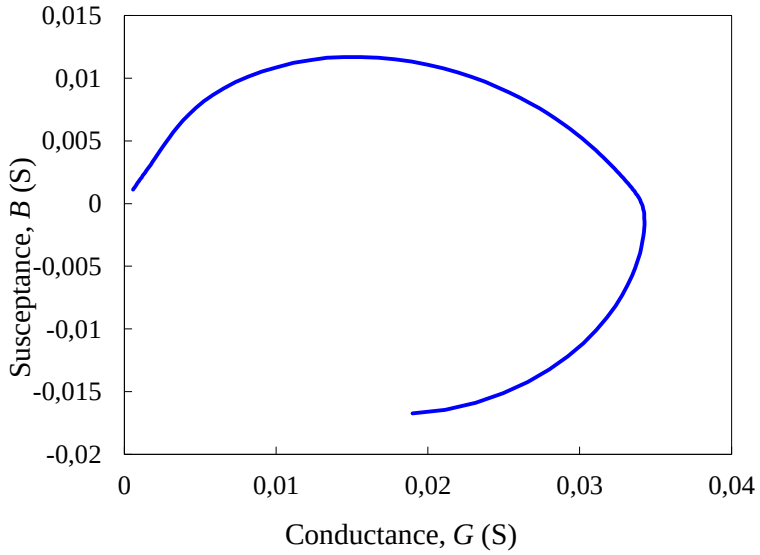

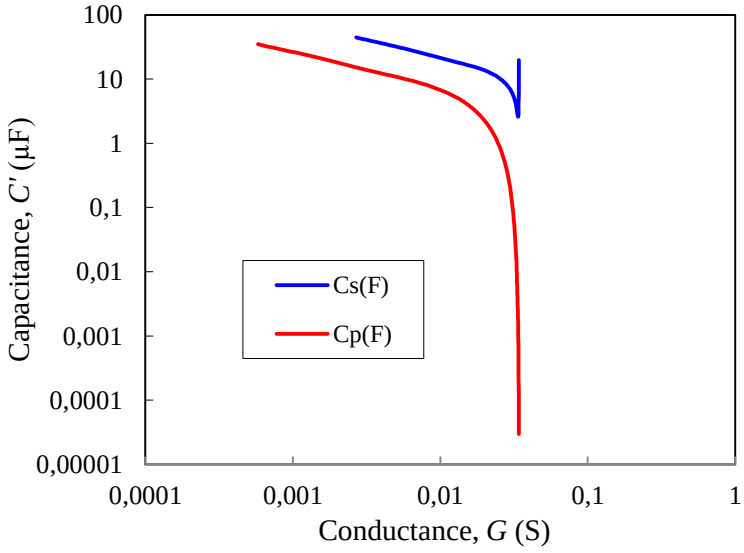

APPENDIX C: Impedance spectra of studied ILs

Parameters of capacitors with ionic liquids as electrolytes measured at 123 Hz

Ionic liquid	G_p [mS]	B_p [mS]	C_p [µF]	C_s [µF]
$[C_2mim][NTf_2]$	3.91	6.01	7.79	11.10
$[C_2mim][EtSO_4]$	3.70	3.60	4.67	9.61
$[C_2mim][HSO_4]$	1.38	0.94	1.22	3.84
$[C_4mim][OTf]$	3.16	2.83	3.67	8.24
$[C_4mpyrr][NTf_2]$	2.39	1.42	1.84	7.07
$[C_6mim][NTf_2]$	2.97	2.09	2.72	8.18
$[C_4mim][CF_3CO_2]$	3.04	2.63	3.41	7.98
[Emim][BF4]	5.25	8.15	10.60	15.00